Nonlinear Model-Based Friction Compensation in Control Systems: Theory and Experiment

by

Gina Miller

A thesis submitted to the Department of Mathematics and Statistics

in conformity with the requirements

for the degree of Master of Science (Engineering)

Department of Mathematics and Statistics

Queen's University

Kingston, Ontario, Canada

April 1997

Canada

Abstract

In this work, two control strategies that include model-based friction compensation are introduced. These strategies are useful for eliminating steady state error and stick-slip motion in precision control problems at low velocity. The state variable friction model used for compensation is found to capture frictional lag, the Stribeck effect, presliding displacement, and stick-slip motion. The first control strategy uses a friction observer whose state estimation error converges to zero. It was found to be accurate but slow. A second control strategy is developed to allow faster error dynamics. In this strategy, a more complex dynamic feedback is introduced. The theoretical properties of both controllers are investigated and verified experimentally. These model-based friction compensation schemes are shown to be superior to standard PD controllers in low-velocity regimes.

Acknowledgments

Contents

List of Figures

Chapter 1

Introduction

Friction is a phenomenon that is not yet thoroughly understood. However, understanding and compensating for its effects becomes very important in precision control problems; particularly when velocity is low or there are velocity reversals. With proportional and derivative feedback control, unmodeled nonlinear friction effects can lead to steady state errors and stick-slip motion. Integral action can reduce steady state error, but with friction, it can also induce limit cycles or hunting [25]. An alternative is to employ friction compensation within the control law to "cancel" nonlinear friction effects. This requires an accurate model of the friction forces present in the mechanical system [8].

Classical linear friction models have traditionally been used by the controls community. Among these models are Coulomb (kinetic) friction, which is independent of velocity; viscous friction, which arises in lubricated systems and is proportional to velocity; and static friction, which is the friction force at zero velocity, and is known to be greater than kinetic friction. Combinations of these three friction types are usually used by control engineers, often with PD or PID control. The classical friction models are adequate for many applications, but do not capture the nonlinear nature of friction near zero velocity. Thus tribologists and control engineers are motivated to develop nonlinear models for friction. A state variable friction model is proposed in [7] for the purposes of friction compensation.

The purpose of this work is to study model-based friction compensation in simple positioning and tracking problems, using the state variable friction model from [7]. Experiments are conducted using a high precision tracking device, with one degree of freedom. The simplicity of the test equipment allows us to isolate friction effects.

The overall value of friction compensation for high-precision tracking will be ex-

amined in this thesis. Theory indicates that, with a good model for friction, model-based compensation can eliminate tracking errors and result in a stable, smooth performance. However, experimental implementation will determine how friction compensation performs with an inexact model, and in the presence of disturbances. Two model-based friction compensation controllers will be tested. The first was proposed in [7]. The second is developed here. Both combine proportional and derivative control with friction compensation, which is achieved via dynamic output feedback. The performance of each will be assessed in comparison to that of a linear PD feedback controller. Experimental results should indicate whether these controllers are practical, and if they are preferable to standard linear feedback techniques.

Chapter 2 includes a discussion of known friction characteristics, and reviews some friction models and compensation techniques used by the controls community. Chapter 3 describes the experimental apparatus. Chapter 4 reviews the state variable friction model of [7], discussing the properties of the model, and the friction characteristics it captures. Chapter 5 outlines the off-line model identification techniques used with the experimental servo apparatus. Results are presented to validate the adopted model. Chapters 6 and 7 introduce two model-based friction compensation controllers, and present experimental results for tracking and positioning. In Chapter 6 the control strategy of [7] is presented, and experimental issues pertaining to friction compensation on the servo system are discussed. The controller of [7] is compared to a PD controller, which is introduced as a baseline experiment. Finally, in chapter 7 a new dynamic feedback control law with friction compensation is developed for a more general class of systems. An explicit controller is derived for the experimental servo apparatus, and tested in positioning and tracking tasks. The performance of the new dynamic feedback controller is compared to that of a PD controller, and to the friction compensation control strategy of [7].

Chapter 2

Friction, Models, and Compensation Techniques

In 1994, B. Armstrong-Helouvry, P. Dupont, and C. Canudas de Wit published a comprehensive survey of friction models, analysis tools and friction compensation techniques as applied to control systems [4]. This was apparently the first survey of its kind, and the authors combined information about friction from the fields of tribology, lubrication engineering, physics, acoustics, and control systems engineering. The publication begins with a discussion of friction characteristics, then surveys studies of friction dynamics over the past 50 years, focusing on control systems applications.

Since the survey of Armstrong-Helouvry *et al.* was published, further studies have emerged that tackle the issue of friction compensation in control systems. Techniques for parameter identification have been introduced, and new models for friction compensation proposed. This chapter outlines some of the concepts discussed by Armstrong-Helouvry *et al.* including: characteristics of frictional behaviour from the perspective of tribology; a brief history of friction models; and some compensation techniques for friction in control systems. In addition, it includes a survey of recent friction compensation techniques as applied to high precision control and tracking problems.

2.1 Friction and Friction Models

Friction has been studied in one form or another for centuries. One of the early recorded studies of the subject was done by Leonardo Da Vinci during the fifteenth cen-

tury. Classical models for friction have been devised to predict its most notable behaviour. Coulomb's model captures a force independent of velocity, but proportional to normal load. This model is often referred to as kinetic friction. Static friction, which prevents slipping at zero velocity, has also been modeled as proportional to normal load. Traditionally, the friction coefficient for static friction, μ_s, is higher than that of kinetic friction, μ_k. Viscous friction, another classical model, is proportional to velocity and notably goes to zero when motion stops.

The linear nature of Coulomb and viscous friction models makes them an attractive choice for many engineering problems. Often, the simple linear model for viscous friction will suffice. The most common model for friction used in engineering applications is a combination of static friction, coulomb (kinetic) friction, and viscous friction [4]. However, nonlinearities exist in the friction-velocity relationship. In recent years, the source of these nonlinearities has been explored and attempts have been made to account for them in friction models.

Tribology is the study of rubbing contact surfaces. Research in this area has done much to broaden the understanding of the mechanisms of friction. Tribology studies have usually been motivated by the need to reduce wear in machines, thereby prolonging machine life. However, a theoretically motivated model for friction, arising from tribology studies, would have wide applications in control theory.

The mechanisms of friction can best be described by considering rubbing surfaces on the microscopic level. All surfaces, even those that appear to be smooth, have tiny asperities. Contact between the two surfaces occurs where asperities come together [4]. There is a degree of deformation of these asperities under load [4], and friction is a function of shear strength at the asperity junctions. This motivates the need for lubrication to reduce friction forces. A fluid lubricant will form a barrier between surfaces, supporting the load. The shear strength of a fluid depends on its viscosity, but is generally much lower than that of a solid. Hence friction is reduced.

Armstrong-Helouvry *et al.* present a lengthy discussion of the four dynamic regimes of friction within a lubricated system. These four regimes are: static friction; boundary lubrication; partial fluid lubrication; and full fluid lubrication. During the static friction phase, no sliding occurs and force is entirely a result of interaction between surface asperities. In the boundary lubrication regime, sliding begins and some fluid is drawn into the contact area. At this point, the fluid layer is thinner than the height of the asperities,

and does not support any part of the load. Thus the source of friction remains metal-on-metal contact. The third regime is partial fluid lubrication, in which the layer of lubricant between the opposing surfaces thickens with increased speed. As this layer becomes thicker, pockets of fluid begin to share the load with the asperities, which usually means a drop in friction. The final regime is full fluid lubrication in which the full load is supported by a fluid layer and viscous friction dominates. It should be noted that in systems that are not lubricated, oxide films will form on the surface of steel and other engineering materials to produce a boundary layer [4].

Static friction occurs when the relative velocity between opposing surfaces is zero, so it is not a consequence of sliding. As a tangential load is applied to the contacts, the asperity junctions deform both elastically and plastically [4]. The elastic deformation implies that, for small movements, the asperity junctions exhibit spring-like behaviour. The range of motion of this elastic deformation before sliding occurs is classified as presliding displacement. As in a spring, the force induced by the presliding displacement (static friction) is approximately linear with respect to the deflection x [3]. The relationship is governed by $F_S = Kx$, where K is the stiffness of the asperity junction. The magnitude of presliding displacement is minute; deflections of 2-5 microns have been measured in steel [3]. Presliding displacement has become important to the controls community. A number of models have been introduced that account for the spring-like behaviour of the asperity junctions at the onset of motion [9]. The first of these was proposed by Dahl in 1968, based on observations of small rotations of ball bearings [4]. The spring-like behaviour associated with presliding displacement is referred to as the Dahl effect [3]. The asperity junctions will deflect until the applied force exceeds the break-away force and sliding begins.

Consider the sliding mass in figure 2.1. The mass is subject to an applied force, produced by a spring deflecting at a constant rate, v. The force applied by the spring increases linearly with time until it exceeds the break-away force and the mass slides. When sliding commences, there is a drop in friction force, velocity increases and viscous friction rises. Furthermore, the spring relaxes and the applied force decreases. The mass slows to a stop, and the cycle begins again. This type of motion is classified as stick-slip. For a constant rate of spring deflection, v, the stick-slip motion is a stable limit cycle [4]. Stick-slip motion is a result of many contributing friction factors including: stiction or static friction; rising static friction; and the Stribeck effect.

Studies indicate that the break-away force can increase when the rate of change
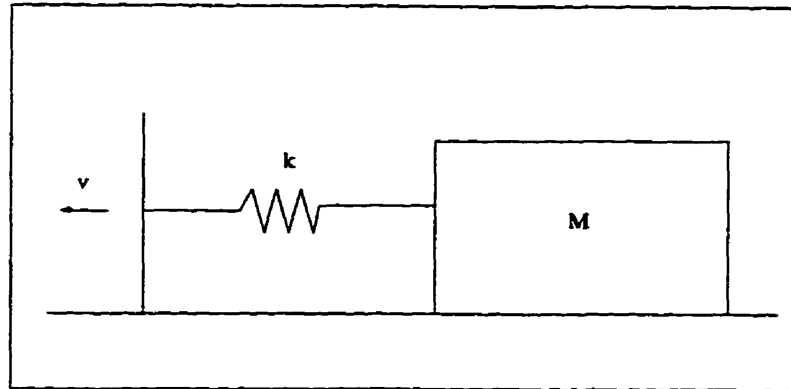
Figure 2.1: Mass-Spring system. The applied force on the mass increases at a constant rate.

of the applied force is decreased [7]. This phenomenon, known as rising static friction, has also been attributed to an increase in dwell time, or time spent "stuck" [4]. In either case, the break-away force will vary up to a maximum value, which is static friction for the mass when it has been at rest for a prolonged period of time.

Another characteristic of frictional behaviour is the tendency for friction to drop shortly after sliding begins. This effect is known as the Stribeck effect. The generalized Stribeck curve, figure 2.2, displays what is widely accepted as the shape of the steady-state friction-velocity curve (c.f. [3], [9], [11]). It is often used to illustrate the four dynamic regimes. The Stribeck effect, shown in region B of figure 2.2, occurs during the period of partial fluid lubrication. At this time, some of the load is taken up by the fluid layer, which has a lower shear strength than the asperity junctions and reduces friction. This drop in friction can have destabilizing effects in control applications and can lead to limit cycling or unstable responses [9]. The general shape of the Stribeck curve clearly indicates the dependence of friction upon velocity. It should be noted that the Stribeck curve is a plot of *steady state* friction versus velocity and does not display transient behaviour.

Stick-slip motion can destabilize a control system. Haessig and Friedland simulated a series of different friction models to see how they represent stick-slip motion [11]. They define static friction to be greater than friction during slip, and account for the fact that static friction is a function of position. The spring of figure 2.1 is a physical realization of a proportional controller. Adding a dash-pot includes damping in the system, which corresponds to a PD controller. Dupont determined that for systems with friction linearized
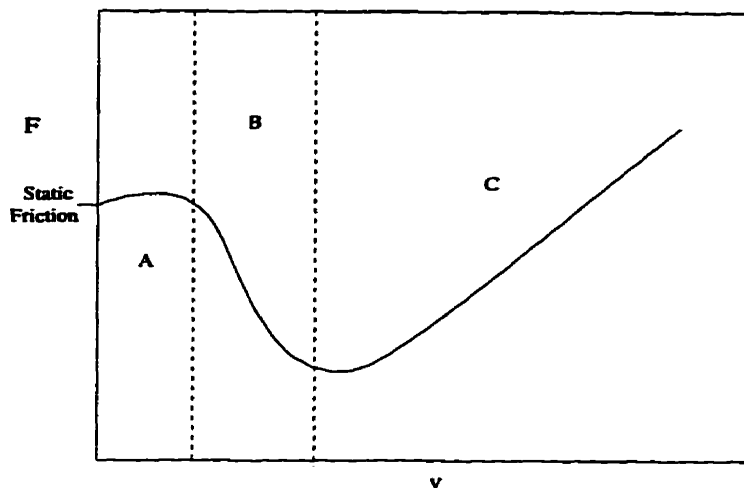
Figure 2.2: Generalized Stribeck curve, F_{SS} versus velocity

about a velocity V_0, stick-slip can be eliminated by stiffer control [9].

In addition to stick-slip behaviour, many systems exhibit frictional memory. This is prevalent in the partial boundary lubrication regime. It implies that there is a lag between a change in velocity, and a response to that change in friction force. Dupont noted that friction is dependent on the history of motion [9]. Similar observations have been made by Rice and Ruina [22]. Frictional memory delays the onset of the drop in friction described as the Stribeck effect.

Hess and Soom [12] conducted various experiments to examine friction under unsteady sliding velocities in "no-stick" motion. Their experiments use different normal loads and lubricants with oscillating velocity above the critical velocity for sticking. The frequency of the velocity oscillations is varied to study the effect on the friction coefficient. Their experimental results show evidence of frictional memory. A hysteresis loop is observed in the curve of friction coefficient versus velocity. The higher the frequency, the wider the loop. They attribute this behaviour to changes in friction lagging a change in velocity. Hess and Soom propose that modeling this lag as a constant time lag, captures this phenomenon.

It is difficult to derive an analytical model that captures all friction behaviour for all regimes. A number of friction models have been proposed to capture specific properties, at least under a restricted range of conditions. The Dahl model depicts friction as a stiff nonlinear spring [4], the form of which is, from [7],

$$\dot{F} = \sigma_0 v \left(1 - \frac{F}{F_C} sgn(v) \right),$$

where v represents sliding velocity, F_C represents Coulomb friction and σ_0 represents spring stiffness. Frictional memory is captured by the Dahl model but the only steady state characteristic predicted is Coulomb friction, which is independent of velocity. Extensions of the Dahl model have since been proposed. One such model is introduced by Canudas de Wit, Olssen, Aström and Lischinksy for control applications [7]. It extends the Dahl model to capture the dependence of steady state friction on velocity: the Stribeck effect. This model will be explored in more depth in subsequent chapters.

Hess and Soom propose a model that includes a pure time lag to capture the phenomenon of frictional memory [12]. Their model is largely dependent on surface material, and lubricant properties [4]. An alternative type is the state variable model, which includes an internal "state" describing the behaviour of the contact surface. State variable models have been proposed by members of the rock community [22] to capture the mechanisms of slip as applied to movements in the earth's crust. Rice and Ruina discuss the behaviour of their state variable model in experiments on stick-slip motion [22]. The state variable model outlines a relationship between the shear force opposing sliding and the sliding velocity. The shear force depends on the "state" which depends on slip history [22]. The model, in general, reflects a dependence on instantaneous velocity and on prior velocity. It appears that the internal state evolves, via exponential decay, to a value dependent only on the current velocity. This implies that the the "state" tends toward a steady state value, delayed by transient effects, which are dependent on slip history [22]. The Dahl model is an example of a state variable model, as is the model of Canudas de Wit *et al.*

Deriving a model for steady-state friction as a function of velocity is also important. This relationship generates the generalized Stribeck curve, the shape of which will vary with loading and lubrication properties. From papers surveyed in [4], a steady state friction model of the form

$$F(v) = F_C + (F_S - F_C)e^{-(v/v_s)^{\delta}} + F_v v$$

is presented, where F_S represents the maximum level of static friction, F_C represents the minimum level of Coulomb friction, F_v represents the viscous friction coefficient, and v_s, δ are empirical values. The viscous term was added by the authors.

Armstrong-Helouvry proposes a seven parameter general friction model that captures several different friction phenomena [4]. This model is actually a composite of two different models. The first represents non-sliding characteristics such as stiction and presliding displacement. The other captures sliding characteristics such as the Stribeck effect; Coulomb and viscous friction; and frictional memory. A full description of the model and the parameter ranges is presented in [4].

It should be noted that in mechanical systems, contributions to the total friction are made by various different mechanisms. Transmission elements are often the dominant contributors [9]. It is usually impossible to isolate the contributions made from each element so friction models are identified to encompass the total friction within the mechanical system.

2.2 Compensation Techniques

The control community uses friction studies to predict when slip will occur, to predict and compensate for stick-slip motion, and to compensate for friction and reduce steady-state error in positioning and tracking applications. This knowledge has been applied to studies of robotic manipulators (c.f. [3], [2], [8], [6]). In these cases, friction compensation is used for precise motion control. Other applications include servo-valve control [10], AC servo motor position control [15], and high precision positioning tables [18].

The literature available on friction compensation and control systems is vast. Research in the area covers a wide range of mechanisms, control tasks, friction models, analysis techniques and compensation techniques. Armstrong-Helouvry *et al.* condense this extensive body of work, and discuss widely-used compensation techniques as applied to control systems [4]. Four types of control tasks in which friction compensation is useful include: the regulator, tracking with velocity reversals, tracking at low velocities, and high speed tracking. Some methods of friction compensation include: high gain PD and PID feedback, dither, impulsive control, and model-based friction compensation.

At this time, both PD and PID feedback control are widely used in industrial applications (c.f. [18], [4], [9]). These controllers are relatively simple to implement, and assume a linear system model. A PD controller is known to exhibit stable behaviour in point-to-point positioning and tracking, but may result in a large steady state error [24]. In tracking problems, if the feedback gains are too low, PD control may also result in stick-slip

motion [9]. This can be eliminated by increasing the damping and stiffness in the system [9]. Unfortunately, studies have noted oscillatory motion associated with high proportional gain in real systems [1]. Integral control is generally used to reduce steady state error in positioning, but is not effective in tracking problems [18]. In addition, limit cycles, or hunting, can arise due to stiction effects [24], [25].

Stiction effects can be reduced with dither or impulsive control [25]. Dither involves the addition of a high frequency signal to the control input, which is introduced to modify system behaviour. This method can prevent the system from entering the static friction regime. However, the motion never actually stops, and wear may be accelerated [25]. Alternatively, static friction may be overcome by impulsive control, wherein a series of high magnitude impulses, of very short duration, are applied to a system at rest. Implicit in this method is the requirement that system be in the "stuck" phase when the pulse is applied [4]. Here the impulses themselves carry out the desired motion, and must be calibrated accordingly [4]. An example of impulsive control was presented by Yang and Tomizuka [25]. They experiment with an adaptive pulse width controller for precise point-to-point positioning. The method of [25] is a variable structure control. The pulse width controller is designed for fine motion control only, and a conventional controller is used for coarse control. Impulsive control was also employed by Armstrong-Helouvry [3] in the control of a PUMA robot arm. There it is used in combination with feedforward control and position-dependent friction compensation.

An alternative method of compensation is to "cancel" friction forces. With model-based friction compensation, a term is added to the control law that applies a force equal and opposite to the friction within a system [4]. This requires accurate knowledge of system friction [8]. An appropriate model can be identified off-line, prior to use, or on-line, by adaptive means. The primary differences in model-based friction compensation techniques are found in the source of velocity used to compute friction, and in the complexity of the friction model [4]. All studies surveyed by Armstrong-Helouvry *et al.* include a component of Coulomb friction in the model.

When on-line identification is employed during friction compensation, the result is adaptive control [4]. One example is suggested by Canudas de Wit *et al.* [8], where a model that captures static, Coulomb, and viscous friction, as well as the Stribeck effect, is introduced. Here, adaptive friction compensation is used in the control of a robot manipulator. Canudas de Wit *et al.* actually employ a combination of on-line and off-line

identification. Preidentification is used to identify constant values for mass and moment of inertia to simplify on-line computations. A similar example of adaptive control is found in [18], where it is used for precise control of a positioning table. Here, the model for friction is discontinuous and includes static and Coulomb friction. The structure of the control law combines proportional and derivative control with inertial and friction compensation. Experimental results show superior performance of the compensated system, when compared to PD control.

Although on-line identification detects variations in the friction force, it add complexity in implementation [4]. An alternative is fixed friction compensation, based on a model that has been identified by off-line methods. Off-line identification determines parameter values using data collected from the experimental open-loop response of the mechanical system. The inputs must be carefully chosen, in order to isolate different model parameters [4]. Difficulties arise with off-line experiments because a good estimate for acceleration may be needed. However, some techniques use long, steady glides, so do not require acceleration information [3]. Publications surveyed by Armstrong-Helouvry *et al.* suggest a variety of techniques [4]. If the parameters enter the friction model linearly, standard identification techniques can be applied [4].

Bona and Indri explore fixed friction compensation with a model that captures the negative slope of friction at low velocities, but is simply Coulomb friction at higher velocities [6]. Their primary interest is in maintaining stability when friction arises between the end effector of a robot manipulator and the contact surface. Their results show that stability can be maintained if care is taken not to over-compensate for friction in the model.

Tataryn *et al.* [24] experimentally compare friction compensation techniques, using a robot manipulator. They examine modified integral action in combination with PD control, and PD feedback with nonlinear friction compensation. Two nonlinear friction models are tested; both contain static and Coulomb friction. Their results show that smooth nonlinear compensation is more accurate in both regulator and tracking problems than integral action and discontinuous compensation.

Because friction depends on velocity, the source velocity estimate used to compute the friction force is important. A natural choice is measured velocity. However, the quality of friction compensation is affected by the resolution and noise of the sensors used [6]. For model-based friction compensation, different combinations of linear and nonlinear friction models have been employed (c.f. [18], [8], [1], [24]). Studies show that performance is

enhanced with a more complete model [4].

2.2.1 A brief word about analysis and simulation

Control systems are usually analyzed mathematically, by techniques such as phase plane analysis, functional analysis, and algebraic analysis [4]. Armstrong-Helouvry *et al.* discuss these techniques in [4]. In addition, valuable insight about system behaviour can often be gained from simulation, helping to bridge the gap between theoretical analysis and real system behaviour. It is also a valuable tool for validating identified models [4].

For discontinuous friction models, implementation problems can arise. Discontinuities are present in the system of differential equations, which must be accounted for when integrating the equations. One solution is to approximate the discontinuity at zero velocity with a function of finite slope. Another solution, proposed by Karnopp [16], models friction as a function of velocity everywhere except in a neighborhood about zero-velocity. There it is determined by other factors. This type of modeling can capture the multi-valued nature of friction at zero velocity.

An alternative solution is to model friction as a function of position at zero velocity. The state variable models of Dahl and Canudas de Wit *et al.* [7] have this property. Although state variable models require that a stable observer be constructed for the unmeasurable internal state, they seem better adapted for friction compensation with low velocity [4]. This is the approach used in this thesis.

Chapter 3

Experimental Apparatus

3.1 Laboratory Hardware
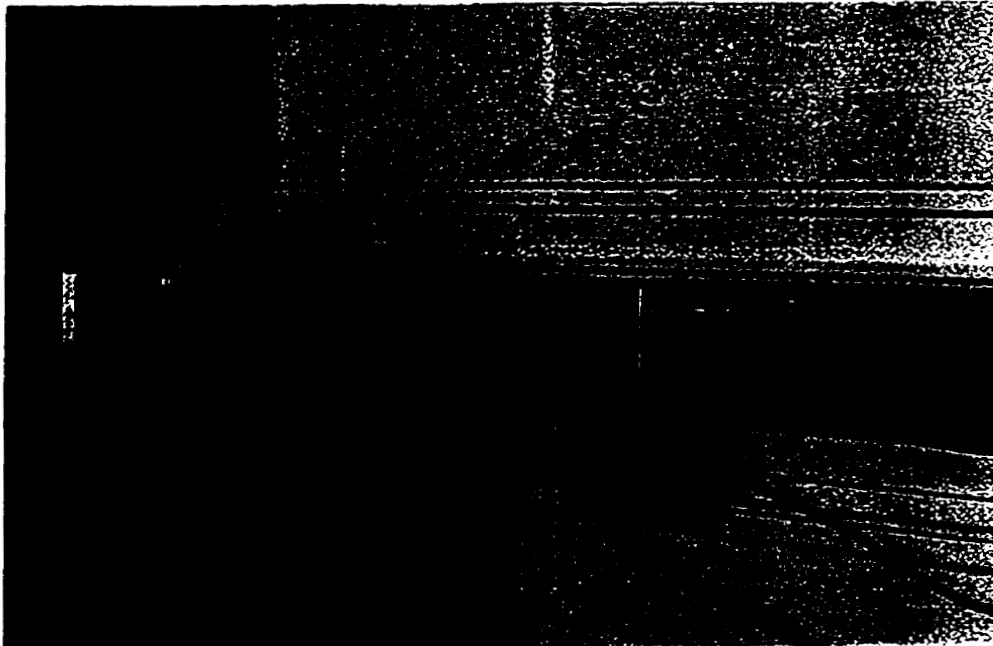
Figure 3.1: Photo of cart and track assembly

The laboratory apparatus consists of a cart and track assembly as seen in figure 3.1. The track, approximately 2 m in length, has two carts that move on recirculating ball bearings. A DC servo motor is connected to *cart 1* by a cable and pulley system. The motor
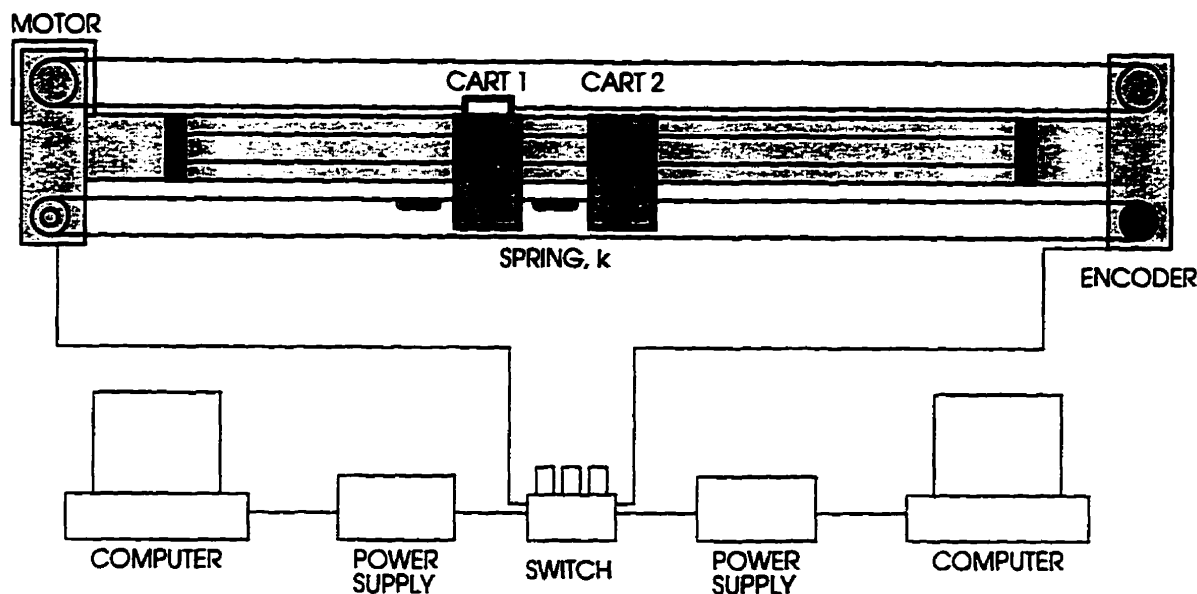
Figure 3.2: Schematic diagram of hardware set-up

contains a built-in optical encoder that measures the position of *cart 1*. A second encoder is mounted at the opposite end of the assembly. It records the position of *cart 2*. Wires from both encoders carry position data signals to a motion controller board within a Pentium 133 personal computer. The computer outputs a voltage signal to a PWM amplifier which drives the DC servo motor. This can be seen in figure 3.2.

3.1.1 Linear Bearing System

The cart and track assembly is a Techno/Isel Double Rail Linear Bearing System. The double rail is composed of two parallel hardened and ground steel shafts, 12 *mm* in diameter. The steel shafts are secured into an aluminum extrusion which acts as a frame holding the components together. These components make up the track. The system is machined and designed for high precision and low friction. Each linear bearing is a single core with two circulating ball bearing circuits of 3.5 *mm* diameter balls. Two bearing cores are mounted on a machined plate to make up one carriage or cart.

3.1.2 DC Servo Motor

The motor used to drive the carts is a Yaskawa Minertia J series permanent magnet 24V DC servo motor. It is a brush type motor with terminal resistance of 10 *Ohms*. It has

a built-in optical encoder with 2 channel quadrature output. The encoder has a resolution of 3600 quadrature counts per revolution. At 24 volts, with no load, the speed of the motor is 1275 *rpm*.

3.2 Computer and Interface Board

A Pentium 133 computer equipped with an Omnitech Robotics MC-1000 interface board is used to compute and output the control voltage to the servo motor. The MC-1000 motion controller board has an 8 bit DAC (Digital to Analog Converter), and two digital input channels that allow constant measurement of position data from the encoders. The board is also equipped with a counter that allows measurements of motor position at speeds up to 9000 *rad/s*.

3.3 Software

3.3.1 The Motor Programming Interface - MPI

The MPI is a series of Borland C files that provide menu driven access to motor control commands and an interface of interrupt driven control routines. It is able to monitor position signals from the MC-1000 interface board, record data, and output control voltage signals as specified by a control subroutine. The MPI was written by Serge Mister for Mathematics and Engineering Control Robotics lab in the department of Mathematics and Statistic, Queen's University.

The control subroutine is developed by the user and requires the modification of only one Borland C file. The user has the freedom to declare any variables, initialize variables as desired, program calculations, and record data from any declared variable.

The MPI may be used within a DOS or Windows environment.

3.3.2 Velocity Estimates

To increase nonlinear friction, and to simplify the mathematical model, the carts were locked together and behaved as one. Position data was read from the built-in the motor encoder, attached to *cart 1*.

The velocity of the carts is estimated by

$$\frac{\Delta(position)}{\Delta(time)}$$

Since position measurements are quantized, high sampling frequency results in a noisy estimate for velocity. There are several ways to handle this problem. Lowering the sampling frequency reduces noise in the velocity estimate. Unfortunately, some applications require a high sampling frequency, and the velocity estimate must be filtered to produce a smooth signal. Because of the nonlinear nature of our model, the construction of a Leuenberger observer to estimate velocity is extremely difficult.

3.3.3   Simulation Programs

Real time simulations can be conducted with the MPI. The simulations are coded in Borland C and can be run as part of the MPI subroutine. Results can be plotted with recorded data for comparison. However, to examine the characteristics of an unknown, and possibly unstable, dynamical system, there are more appropriate simulation packages.

Simulations were also conducted using Simnon/PCW 2.0, a Windows version package for the simulation of the nonlinear systems. It is a product of SSPA, Göteborg, Sweden, with a 1995 copyright by SSPA Systems. The version is 2.01.0000/Regular, student version.

Chapter 4

The Friction Model

Classical friction models such as Coulomb and viscous friction are often used in control applications, but do not capture the nonlinear nature of friction about zero velocity. Friction is not completely understood and its behaviour changes for different loading and lubrication conditions. It would be useful to obtain an analytic model for friction that captures nonlinear effects, at least within a range of conditions.
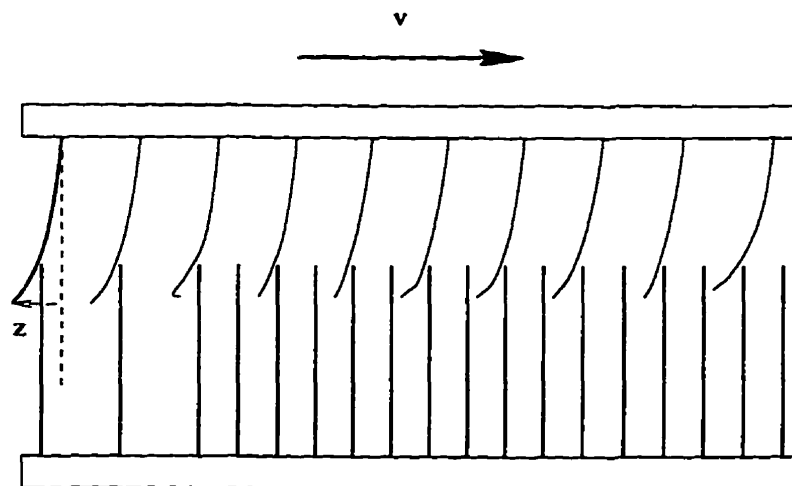
Figure 4.1: Schematic of bristle interactions. For simplicity, one set of bristles has been depicted as rigid.

For low velocity, high precision positioning systems, one should consider the effects of stiction, stick-slip motion, the Stribeck effect, presliding displacement and frictional

memory. Canudas de Wit, Olssen, Aström and Lischinsky propose a dynamic model for friction in control systems that incorporates the spring-like behaviour of the Dahl effect, while including the destabilizing drop in friction of the Stribeck effect [7].

Friction at low velocities is a product of contact between asperities on opposing surfaces. It is reasonable to idealize these asperities as flexible bristles that deform as they interact, as in figure 4.1. When the tangential force upon the bristles is sufficiently high, the bristles deflect to a degree that allows slip to occur.

Canudas de Wit *et al.* propose a model that is based on the notion of bristle deflection [7]. Denoting average bristle deflection as z, their model is

$$\dot{z} = v - \frac{|v|}{g(v)} z \tag{4.1}$$

where v is the relative sliding velocity. The total sliding friction between the surfaces is then given by

$$F = \sigma_0 z + \sigma_1 \dot{z} + \sigma_2 v. \tag{4.2}$$

The model of equations (4.1) and (4.2) is an example of a state variable model, where z represents the internal state. The total friction force in equation (4.2) depends on both the instantaneous velocity, v, and on the state z. We note from the first term of equation (4.1) that z is proportional to the integral of v. Thus the model captures the dependence of friction on the history of motion.

One can also consider the steady state characteristics of the model. From equation (4.1), it can be shown that z approaches a steady state value given by

$$z_{ss} = g(v)sgn(v).$$

A proposed parameterization for $g(v)$ that captures the Stribeck effect is

$$\sigma_0 g(v) = F_C + (F_S - F_C)e^{-(v/v_s)^2}, \tag{4.3}$$

where F_C represents the Coulomb friction, and F_S the resting static friction. This is similar to the exponential model of steady state friction discussed in [4] with $\gamma = 2$. The characteristic Stribeck velocity, v_s, represents the velocity at which the system changes from static to kinetic friction. This velocity marks the change from dominant metal-on-metal friction to fluid lubrication, and is usually determined empirically.

The expression for total friction given by (4.2), is composed of a nonlinear friction part, dependent on z, and a linear viscous friction part that is proportional to sliding

velocity. We expect the viscous friction term to be dominant at high velocities. The nonlinear deflection terms should contribute more for low velocities, where nonlinear effects come into play. Nonlinear friction is given by

$$F = \sigma_0 z + \sigma_1 \dot{z},$$

which accounts for the spring-like behaviour of friction at zero velocity, the Dahl effect. The stiffness of the bristles is represented by σ_0 and the damping by σ_1. Note that σ_0 represents the stiffness of the asperities, not the bulk material.

4.1 Properties of the Model

4.1.1 Finite Deflection

Because z represents bristle deflection, intuition leads one to believe that z is finite.

Property 1 *Assume* $0 < g(v) \le a$; $g(v)$ *is positive and bounded above. If* $|z(0)| < a$, *then* $|z(t)| \le a \ \forall \ t \ge 0$.

Property 1 can be proven by Lyapunov-like analysis, the details of which can be found in [7]. Property 1 implies that z is bounded, assuming that $g(v)$ is bounded and that z has a sufficiently small initial value. Furthermore, the maximum magnitude for z is no greater than that of $g(v)$. Consider the parameterization of $g(v)$ from equation (4.3). Clearly, if $F_S > F_C$, then $g(v)$ is decreasing for all v. It is also evident that $g(v) > 0$ for $F_S > 0, F_C > 0$. Therefore, $g(v)$ of equation (4.3) is bounded. In the case where static friction exceeds Coulomb friction, i.e. $F_S > F_C$, $g(v) \le \frac{F_S}{\sigma_0}$. Then, Property 1 implies that $|z(t)| \le \frac{F_S}{\sigma_0}$ for all $t \ge 0$, if $F_S > F_C$.

4.1.2 Dissipativity

One would also expect friction to dissipate energy. Canudas de Wit *et al.* claim in [7], that equations (4.1) and (4.2) describe a dissipative system. Dissipativity is best described in terms of system energy. In general, the rate of change of energy of any system is the sum of net energy input and internal energy generation. The net internal energy generation of a *dissipative* system is negative. Define the mapping: $\psi : u \to y$, where u is

the input and y is the output of a system. The mapping, ψ, is *passive* with respect to an energy function V, if V is lower bounded and the time derivative of V verifies

$$\dot{V} = y^T u - g(t),$$

where $g(t) \geq 0$ and represents the internal energy change [23]. With no external input or output, the energy change within the system relies solely on the internal energy dissipation, and $\dot{V} \leq 0$ for all t. Hence the internal energy in a *passive* system is non-increasing.

Slotine and Li [23] define a *dissipative* system as one that is passive and has the property that

$$\int y^T u dt \neq 0 \qquad \Rightarrow \qquad \int g(t) dt > 0.$$

Consider, as an example, equation (4.1);

$$\dot{z} = v(t) - \frac{|v|}{g(v)} z.$$

Define energy as $V = \frac{z^2}{2}$. Taking the time derivative of V along solution curves of (4.1) yields

$$
\begin{aligned}
\dot{V} &= z\dot{z}, \\
\dot{V} &= vz - \frac{|v|}{g(v)} z^2.
\end{aligned}
$$

The input, in this case, is velocity and the output is average bristle deflection, z. Clearly V is bounded below by zero. From equation (4.3), we know that $g(v)$ is positive, so $\frac{|v|}{g(v)} z^2 \geq 0$ and equation (4.1) describes a passive system. Integrating both sides from 0 to t yields

$$V(t) - V(0) = \int_0^t v(\tau) z(\tau) d\tau - \int_0^t \frac{|v|}{g(v)} z^2. \tag{4.4}$$

If equation (4.1) is dissipative, then the last term in (4.4) is strictly positive, which implies that

$$\int_0^t v(\tau) z(\tau) d\tau > V(t) - V(0).$$

Therefore, a sufficient condition for this system to be dissipative is that

$$\int_0^t v(\tau) z(\tau) d\tau > V(t) - V(0),$$

for all $z, v \neq 0$.

Property 2 *The map $\psi : v \to z$, as defined by equation (4.1), is dissipative with respect to the function $V(t) = \frac{1}{2}z^2$ i.e.,*

$$\int_0^t v(\tau)z(\tau)d\tau > V(t) - V(0).$$

The proof of property 2 can also be found in [7].

4.2 Friction Characteristics Captured

Canudas de Wit *et al.* conducted a series of simulations, using their friction model, to determine whether it accurately depicts presliding displacement, frictional memory, stick-slip motion, and varying break-away force (rising static friction) [7]. Their results show a qualitative agreement with documented experiments.

The bending bristle interpretation of the model suggests that it predicts presliding displacement. The bristle model is an extension of the Dahl model, which is known to capture this phenomenon [7]. Simulations show that, for forces smaller than the resting static friction (F_S) the bristles behave as a nonlinear spring.

To test for frictional memory prediction, simulations were conducted in a manner similar to the experiments of Hess and Soom [12]. While operating outside of the stiction regime, hysteresis appears in the friction-velocity curve for simulations of the response to increasing and decreasing velocity. Increased rates of acceleration and deceleration widen the hysteresis loop in Hess and Soom's experiments, and a similar result is predicted by the model from equations (4.1) and (4.2).

Canudas de Wit *et al.* simulated the spring-mass system of figure 2.1 to test for stick-slip motion. The model predicts a cycle of sticking and sliding. Irregular behaviour in the friction force around the point where sliding stops is noted, and the simulated motion of the mass behaves as expected. Stick-slip motion simulations were then used to determine if the break-away force remains constant, or if it varies with the rate of change of the applied force. The model predicts that the break-away force decreases with an increase in force rate of change. This also agrees with experimental results.

Finally, the model was used to simulate a PID feedback control regulator. It is well known that nonlinear friction can lead to unstable behaviour or limit cycling (hunting) when a PID controller is used [25], [24]. This is because static friction is greater than slip friction [11]. The controller integrates the error until the control output is sufficient

to overcome static friction forces [25]. Sliding commences and the friction drops, which can result in overshoot. For some PID gains, a stable limit cycle can result. Simulating a closed-loop system with PID feedback control and their friction model, Canudas de Wit *et al.* show that hunting results for some choices of controller gains.

4.3   Summary

Canudas de Wit *et al.* present a state variable model for friction where the internal state corresponds to the average deflection of bristles on opposing contact surfaces [7]. They performed simulations using their model and found that it captures presliding displacement, frictional memory, rising static friction and stick-slip motion. Furthermore, the steady state friction-velocity relationship captures the Stribeck effect. These characteristics of friction are important in control systems, for low velocity, high precision positioning and tracking. Thus it is a good model for use in fixed friction compensation for low velocity control.

Chapter 5

Model Identification

Our model for the motion of the servo motor-cart system that was described in Chapter 3, is

$$m\ddot{x} = Ku - F, \tag{5.1}$$

where u is the control voltage signal output to the motor, and the K is the motor torque constant. The position of the cart is represented by x and the total mass of the cart-motor system is denoted by m. The total friction force is represented by F. The motor torque constant is known to be $K = 0.667\ N/V$.

Here, F models the friction within the entire mechanical system. Thus F includes brush and bearing friction in the motor, friction between bearing elements on the carts, and friction between the cart elements and the track. It is impossible to isolate individual sources of friction and model each separately. However, it has been found that a generalized model, when identified using empirical data, is appropriate to model the combined friction effects within the system [4]. Thus the parameters identified for the cart and track system model of equation (5.1) encompass the friction effects from all moving parts, and approximate the total friction in the mechanical system.

5.1 The Friction Model

The dynamic bristle model from [7] describes the nonlinear dynamics of friction at low velocities. Equations (4.1) and (4.2) model the average bristle deflection, z, via the

nonlinear differential equation

$$\dot{z} = v - \frac{|v|}{g(v)}z,$$

and the total friction between the sliding surfaces by

$$F = \sigma_0 z + \sigma_1 \dot{z} + \sigma_2 v.$$

Recall also that the steady state bristle deflection, z_{ss}, is given by

$$z_{ss} = g(v)sgn(v).$$

This follows from setting $\dot{z} = 0$ in equation (4.1). With the parameterization for $g(v)$ from equation (4.3), the steady state friction force can be described by

$$F_{ss} = (F_C + (F_S + F_C)e^{-(v/v_s)^2})sgn(v) + \sigma_2 v, \tag{5.2}$$

where F_C represents Coulomb friction, F_S represents static friction, and v_s represents the characteristic Stribeck velocity. This means that there are 6 parameters, $\sigma_0, \sigma_1, \sigma_2, F_S, F_C$, and v_s, to be identified for our friction model.

5.2 Least Squares Estimation

Because equation (5.2) is linear in all parameters except v_s, it lends itself to least squared error parameter estimation. Given a reasonable estimate for v_s, and a suitable number of observed values for F_{ss}, a preliminary estimate for the system parameters can be found by least squares methods.

The aim of least squares estimation is to minimize the sum of the squares of the difference between actual observations, and values calculated from a model. From [5], any model of the form

$$
\begin{aligned}
y(t) &= \phi_1(t)\theta_1 + \phi_2(t)\theta_2 + ... + \phi_n(t)\theta_n \tag{5.3} \\
&= \phi(t)^T\Theta \tag{5.4}
\end{aligned}
$$

is a candidate for least squares estimation, where $y(t)$ represents the observation at time t. The set $\{\theta_1, ..., \theta_n\}$, is the set of unknown parameters, and is denoted by Θ in vector form. For each observed variable there is a corresponding regressor, $\phi(t)^T = [\phi_1(t), ..., \phi_n(t)]$: a

known vector containing measured experimental values. Given m discrete observations, a system of m linear equations arises, which can be expressed as the matrix equation

$$Y = \Phi\Theta. \tag{5.5}$$

Here Y is the vector of m observed variables, and Φ is an $m \times n$ coefficient matrix. The $i'th$ row of Φ, denoted $\phi(t_i)$, contains the coefficients for $\{\theta_1, ..., \theta_n\}$ corresponding to the observed value of y at $t = t_i$. The n-vector Θ remains the set of parameters to be identified. If $\Phi^T\Phi$ is invertible, then the value of Θ that minimizes

$$\|Y - \Phi\Theta\|^2$$

is

$$\hat{\Theta} = (\Phi^T\Phi)^{-1}\Phi^T Y.$$

A proof of this well-known fact can be found in [5].

Recall equation (5.2) and, for simplicity, assume positive velocity. It follows that steady state friction is given by

$$F_{ss} = F_C + (F_S + F_C)e^{-(v_{ss}/v_s)^2} + \sigma_2 v. \tag{5.6}$$

In vector form this can be expressed as

$$F_{ss} = \mathbf{a}^T\mathbf{x},$$

where

$$\mathbf{a} = \begin{pmatrix} 1 - e^{-(v_{ss}/v_s)^2} \\ e^{-(v_{ss}/v_s)^2} \\ v_{ss} \end{pmatrix}, \quad \mathbf{x} = \begin{pmatrix} F_C \\ F_S \\ \sigma_2 \end{pmatrix}.$$

With n observed values for steady state friction, the column vector $\mathbf{F_{ss}}$ can be constructed. Since F_{ss} is a function of steady state velocity, each component of $\mathbf{F_{ss}}$ corresponds to a particular value of v_{ss}. For $F_{ss}(t_i)$, and $v_{ss}(t_i)$, a vector $\mathbf{a}(v_{ss}(t_i))$ of coefficients exists. With n observed values of F_{ss}, the matrix equation that arises is

$$\mathbf{F_{ss}} = A\mathbf{x}, \tag{5.7}$$

where A is an $n \times 3$ coefficient matrix. The the least squares estimation of $\mathbf{x}$ is then given by

$$\mathbf{x_{opt}} = (A^T A)^{-1} A^T \mathbf{F_{ss}}. \tag{5.8}$$

5.3   Identification Procedure

Recall our cart-motor system model (equation (5.1))

$$m\ddot{x} = Ku - F.$$

It is clear from this equation that, for steady state velocity, the acceleration term becomes zero, and $Ku = F$. Thus the steady state friction can be determined from the constant voltage signal sent to the servo motor. Velocity is estimated by $\Delta Position/\Delta time$.

To identify the effective mass of the carts, linear viscous friction is included in the system model. High velocity data was used, so as to minimize the effects due to nonlinear friction. The linear system model is given by

$$m\ddot{x} + \beta\dot{x} = Ku,$$

or

$$m\dot{v} + \beta v = Ku, \tag{5.9}$$

where v is the velocity of the carts and β is the viscous friction coefficient. Taking the Laplace transform of (5.9) yields

$$\frac{V(s)}{U(s)} = \frac{K}{ms + \beta}, \tag{5.10}$$

which is of the form

$$\frac{V(s)}{U(s)} = \frac{c}{\tau s + 1}. \tag{5.11}$$

The time required for a system to achieve 95% of steady state is 3τ. An estimate of τ can be obtained from the velocity response of the cart to a step input. From equations (5.10) and (5.11), it is clear that $c = K/\beta$ and $\tau = m/\beta$. If the magnitude of the step input is A, then the velocity-time graph can be fit to the curve

$$v(t) = \frac{KA(1 - e^{t/\tau})}{\beta}. \tag{5.12}$$

For a step input, the dynamical system (5.9) will reach steady state for large t. Hence

$$v_{ss} = \frac{KA}{\beta}. \tag{5.13}$$

The steady state velocity can be approximated from recorded data; both K and A are known. Therefore, β can be calculated from equation (5.13), and mass can be determined

with the estimate of τ. A value of $m = 2.0$ kg was adopted for total equivalent mass in the servo motor-cart system.

With our servo system, steady glides can be achieved using constant voltage signals ranging from 4V to 13.5V. The steady state velocity can be approximated from the open-loop response. Twenty steady state data points were obtained from voltage signals in the necessary range. With measured values for F_{ss} and v_{ss}, a least squares estimate for the parameters F_C, F_S and σ_2 was computed using (5.8).

It is important to note the limitations of least squares estimation for this application. Although steady motion is easily achieved at high velocity, it is difficult to realize on the servo system at low velocity. Thus only high velocity data was used. The least squares approximation gives a good estimate for the viscous friction coefficient, σ_2, which is the predominant source of friction at higher velocity. However, the low velocity region of the steady state friction-velocity relationship was found by extrapolation. Therefore, only an initial estimate for F_S and F_C could be obtained by this method. These parameters were adjusted empirically to better represent system behaviour.

The characteristic Stribeck velocity, v_s, which appears in the equation (5.2), has a strong influence on the shape of the Stribeck curve. Friction changes from static to kinetic at $v = v_s$. The value of v_s depends on material and lubricant properties, and is usually determined empirically. A reasonable estimate for v_s was needed for the least squares estimation. The Stribeck velocity ranges from 0.00001 m/s to 0.1 m/s [4] so $v_s = 0.01$ m/s was used initially. Later, this value was modified to better match observed system behaviour.

The least squares method provides an estimate for parameters found in the steady state equation for friction. However, steady state friction data does not yield information about σ_0, which represents bristle stiffness, and σ_1, which is related to damping during friction transients. Examining the equations of motion in the stiction regime can yield appropriate choices for these parameters. Within this regime, there is presliding motion which is governed by

$$m\ddot{x} = \sigma_0 z + \sigma_1 \dot{z} + \sigma_2 \dot{x}.$$

Here x represents the displacement of the mass. The above equation can be linearized about $z = 0$ and $\dot{x} = 0$. Within a small operating range of this point, the total displacement can be attributed to the bending of the bristles. Therefore $x = z$, and $\dot{x} = \dot{z}$. It then follows

that

$$m\ddot{x} + (\sigma_1 + \sigma_2)\dot{x} + \sigma_0 x = 0, \tag{5.14}$$

which is a damped second order system with stiffness σ_0, and damping $(\sigma_1 + \sigma_2)$.

Simulations were conducted by Canudas de Wit *et al.* [7] using a stiffness value of $\sigma_0 = 10^5 \ N/m$. Adopting this value in the model for the servo motor and cart predicts an open-loop response that is comparable to the actual system response. Simulations also indicate that small variations in σ_0 do not affect the open-loop response. Hence $\sigma_0 = 10^5 \ N/m$ was adopted for all experiments.

To find a reasonable value for σ_1, one must consider damping in a second order system. Any second order spring-mass-damper system can be expressed in the frequency domain as

$$s^2 + 2\xi\omega_n s + \omega_n{}^2, \tag{5.15}$$

where ω_n is the natural frequency of the system and ξ is the damping factor. Taking the Laplace transform of equation (5.14) yields

$$ms^2 + (\sigma_1 + \sigma_2)s + \sigma_0.$$

It then follows that

$$\begin{aligned}
\sigma_0 &= m\omega_n{}^2, \\
(\sigma_1 + \sigma_2) &= 2m\xi\omega_n,
\end{aligned}$$

which yields $\omega_n = 250 \ rad/s$ for $m = 2 \ kg$. The choice of ξ is somewhat arbitrary and determines how quickly oscillations die away with changes in the system. For $\xi = 0.5$, moderate damping occurs in the linearized system of (5.14), which yields $\sigma_1 \approx 495 \ Ns/m$ for $\sigma_2 = 4.6 \ Ns/m$. Increasing the value of σ_1 results in more damping, but tests show that minor variations in σ_0 and σ_1 have little affect on the open loop response.

Variations in F_S and F_C influence the low velocity response. These parameters were adjusted by comparing the predicted response of the nonlinear system model, to an actual measured response. The test inputs used were a ramp input, and an input that decreases with time; both exhibit the effects of low velocity friction, but at different stages in the motion. Experiments and simulations show that higher values of F_S and F_C are required for the model to accurately predict the response to decreasing input, than are required to predict the response to a ramp. Parameters were adjusted to reach a somewhat

optimal compromise. The model cannot perfectly predict the response of the real servo system to all inputs. It is our hope that the model prediction can closely resemble the real behaviour, and capture the major effects of nonlinear friction.

5.4   Results and Model Validation

The final model parameters adopted were

$$\sigma_0 = 10^5\ N/m, \sigma_1 = 495\ Ns/m, \sigma_2 = 4.6\ Ns/m, F_C = 2.0\ N, F_S = 2.15\ N, v_s = 0.005\ m/s.$$

The steady state friction-velocity relationship for the adopted model is shown in figure 5.1. The curve has the desired characteristic Stribeck shape. One might note that the destabilizing friction drop is small, and that viscous friction quickly becomes the dominant friction force for this model.
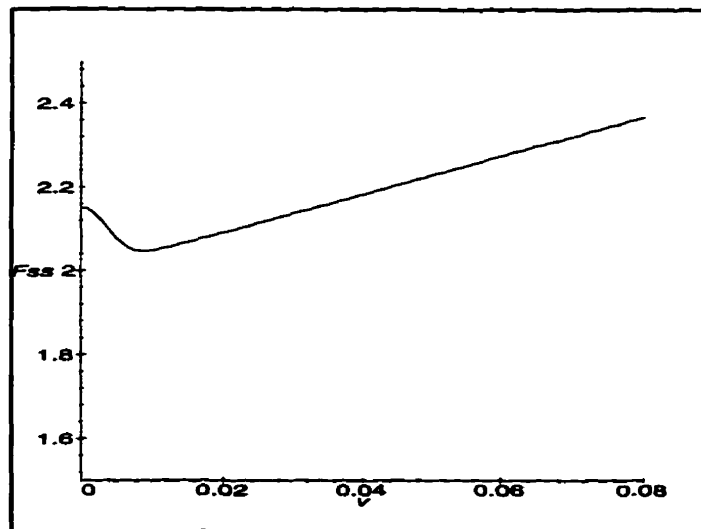
Figure 5.1: Steady state friction versus velocity.

The graphs in figures 5.2 to 5.3 indicate the system's open loop response to different inputs. The solid line, labeled "Actual System Response", shows the position of the cart as measured by the encoder. The two dashed lines show the simulated position of the cart generated by two different system models. The line labeled "Linear Model Prediction"
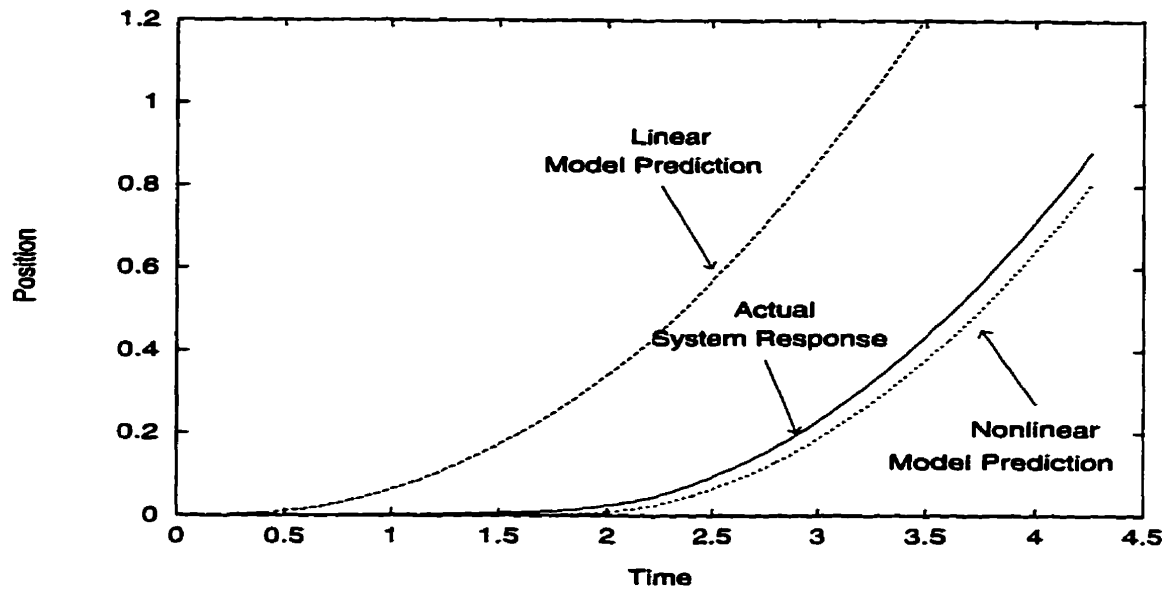
Figure 5.2: Response to ramp input of $u = 2t$

is the response predicted by a system model with linear friction; $F = \beta \dot{x}$. A viscous friction coefficient of $\beta = 5.5\ Ns/m$ has been identified for previous experiments with the servo system, and was adopted for these simulations. The line labeled "Nonlinear Model Prediction" indicates the response predicted by the system model with the friction given by equations (4.1) and (4.2).

The response to a ramp input is displayed in figure 5.2. The nonlinear prediction, unlike the linear one, follows the actual system performance closely. Here, the error in the nonlinear model prediction is within 10%. The linear model predicts the position of the cart to be more than 3 times greater than the actual position. The notable failing of the linear model prediction is that it exhibits no static friction effects. In the linear system simulation, motion begins as soon as a force is applied. This contradicts the behaviour of the real system and that of the nonlinear model prediction.

The system response to a decreasing input was also tested. The results are shown in figure 5.3. As observed in previous tests, the nonlinear model predicts the real response with less than 10% error. At $t = 1\ s$, the linear model prediction overestimates the cart position by about 100%; the error in this prediction increases with time. The position in both the nonlinear simulation and the actual system, tends to a constant value when the input is sufficiently low. The position in the linear simulation does not.
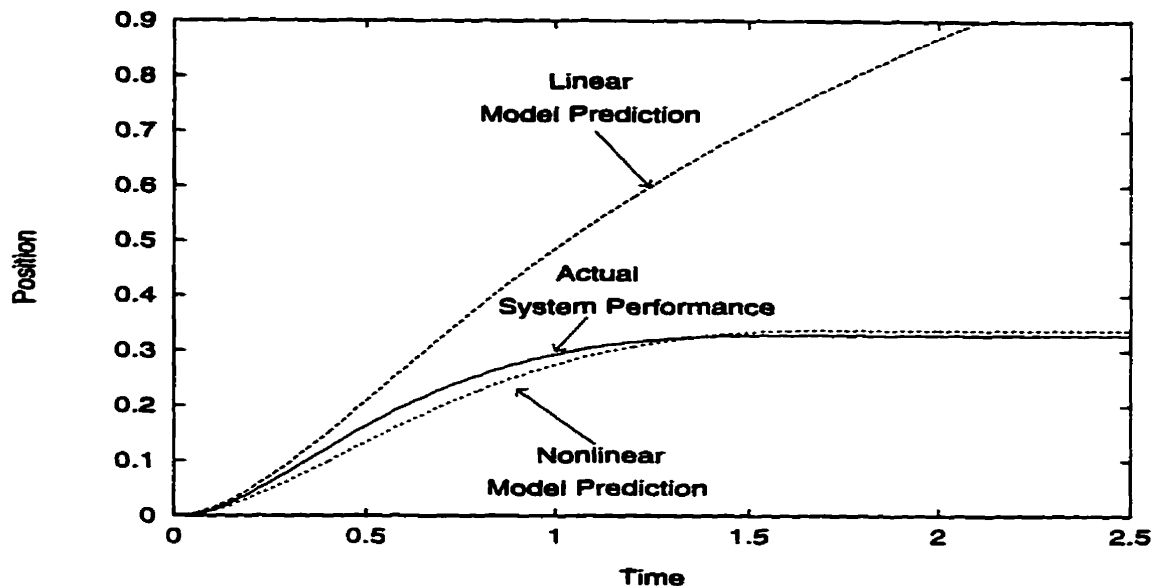
Figure 5.3: Response to decreasing input, $u = 10/(1 + 2t)$

The response to a sinusoidal voltage input is represented in figure 5.4. Once again, the prediction of the nonlinear model is within 10% of the actual cart position, the error increases when the direction of motion changes. It should be noted that the actual system response shows a tendency to move farther to the left than to the right, under the same magnitude of force applied. This indicates that the friction in the real system is direction dependent and is higher in the direction of positive motion. Neither simulation exhibits this asymmetric behaviour because the parameters of each model are constant. Nonetheless, the accuracy of the nonlinear model is much higher than that of the linear model which tends to underestimate friction entirely. Static friction is clearly a significant phenomenon at low velocities.

Canudas de Wit *et al.* tested their model to determine whether it captures frictional memory, presliding displacement and stick-slip motion. The results of similar simulations and experiments are included here. Figure 5.5 displays the simulated relationship between applied force and presliding displacement of the cart. The applied force was ramped slowly up to approximately 1.7 N, held constant for a short period of time, was slowly ramped down to -1.7 N, then back up to 1.7 N. The maximum force, 1.7 N, is less than the identified static friction. The shape of the curve in figure 5.5 is similar to that in [7], which indicates that our model predicts presliding displacement. Figure 5.6 shows
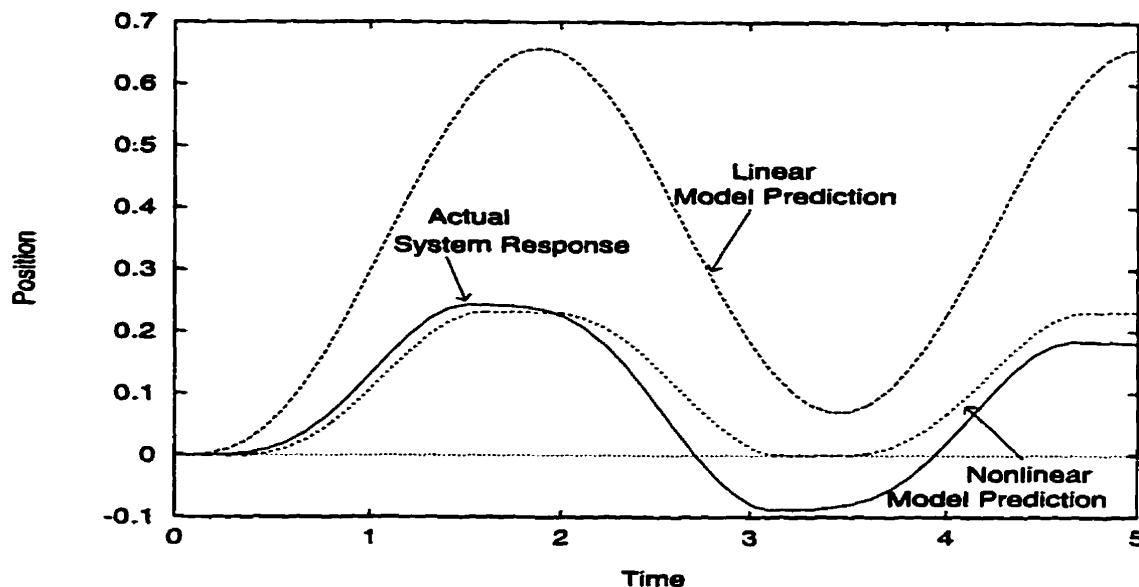
Figure 5.4: Response to sinusoidal input, $u = 6sin(2t)$

the simulated friction-displacement relationship from a slightly different perspective. Here both the positive and negative friction-displacement curves, from zero initial conditions, are displayed. Figure 5.6 clearly indicates that the simulated presliding displacement behaves like a nonlinear spring. The predicted position response, as a function of time, is shown in figure 5.7. The maximum predicted deflection is approximately 3.2×10^{-5}, corresponding to the maximum applied force of approximately 1.7 N.

It is natural to conduct similar tests with experimental hardware to determine whether the actual system exhibits the behaviour predicted by the model. Because we do not have a measured value of friction, an accurate friction-deflection curve (similar to figure 5.5) cannot be displayed for the real system. However, the position response is shown in figure 5.8. Clearly motion is detected, despite the fact that the applied force does not exceed the modeled F_S. Here the encoder records a deflection of approximately 1 mm, for an applied force of 1.7 N (figure 5.8), which is much greater than the predicted displacement (figure 5.7). The actual detected motion should probably be described as small scale unsteady sliding, instead of presliding displacement, because of its magnitude. Thus our model may overestimate static friction. One can also note from figure 5.8 that initially, there is no movement detected for very small applied forces.

Simulations were also conducted to determine if our model captures frictional lag.
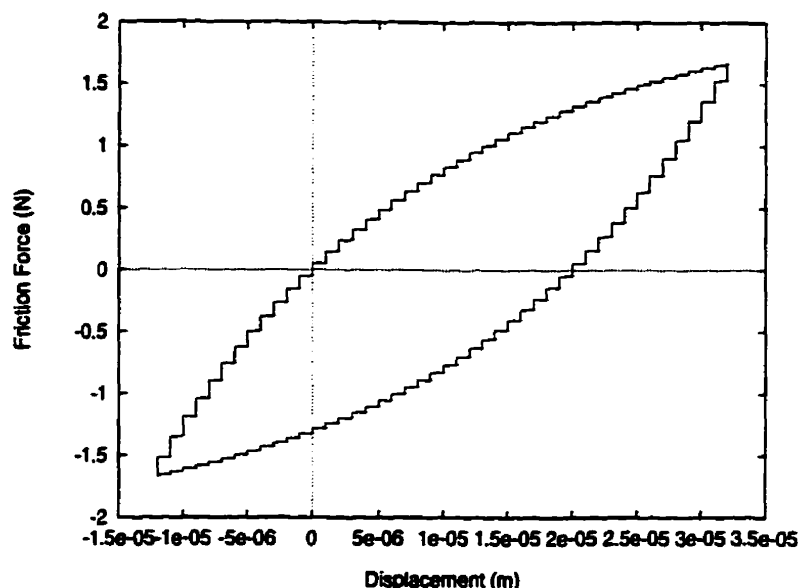
Figure 5.5: The model exhibits presliding displacement for applied forces lower than F_S.

Canudas de Wit *et al.* compared their simulation results to the experimental results of Hess and Soom [12]. Similarly, input used here produced a constant amplitude velocity oscillation with variable frequency, $v = Asin(\omega t)$ m/s. Figure 5.9 shows the relationship between velocity and friction force for $\omega = 10$ rad/s and $\omega = 25$ rad/s. Clearly hysteresis arises; the loop is wider for higher frequency. The behaviour exhibited in figure 5.9 is qualitatively similar to behaviour seen by Canudas de Wit *et al.* [7], and by Hess and Soom [12]. Therefore, our model predicts frictional memory. Unfortunately, the nature of servo motor-cart apparatus prohibits experimental testing for frictional lag because prolonged unidirectional motion is required.

Finally, the model was tested for predicting stick-slip motion. An applied force was generated by simulating the constant velocity deflection of a linear spring of stiffness k, as depicted in figure 2.1. Figure 5.10 shows the position of the cart, x, and the displacement of the end of the spring, y. The results in figure 5.10 show the response of the mass to forces applied by a stiff spring being slowly deflected; $k = 20$ N/m and $\dot{y} = 0.01$ m/s. The path of the mass, x, clearly indicates that stick-slip motion occurs. The position response of the real system, to the same input, is plotted with the predicted response in figure 5.11. Both exhibit stick-slip motion, although the motion of the actual system is less uniform than that
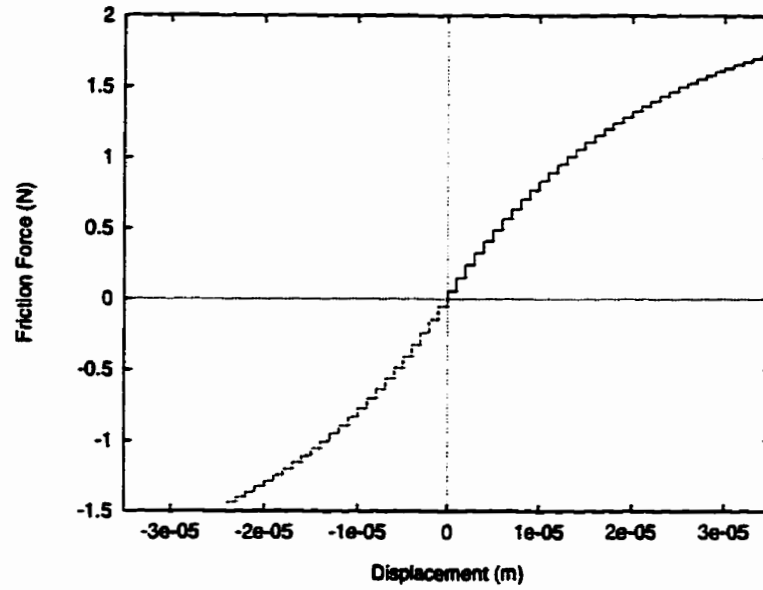
Figure 5.6: The friction force versus presliding displacement curve indicates behaviour similar to a nonlinear spring.

of the simulation. In this case, the break-away force is lower for the real system than for the simulation. Nevertheless, the predicted response is very close to that of the real system.
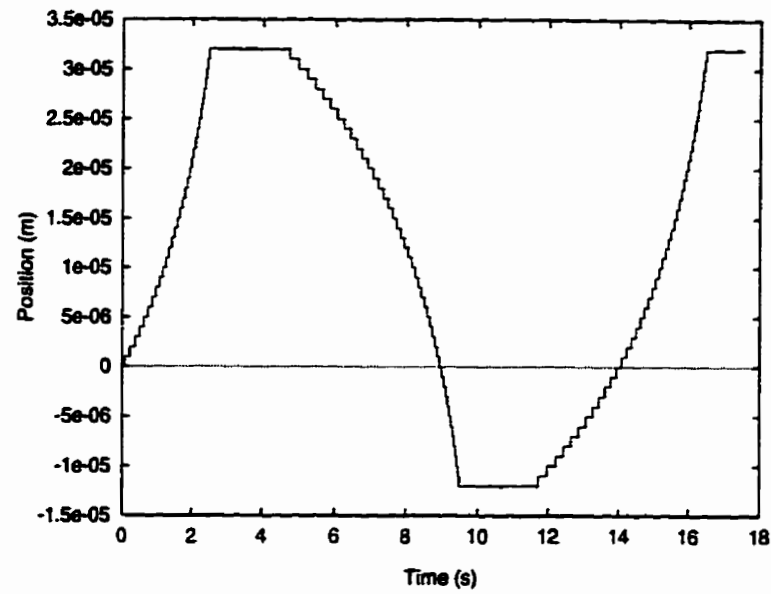
Figure 5.7: Simulated open-loop position response to an oscillating ramped input that does not exceed the modeled static friction, F_S.
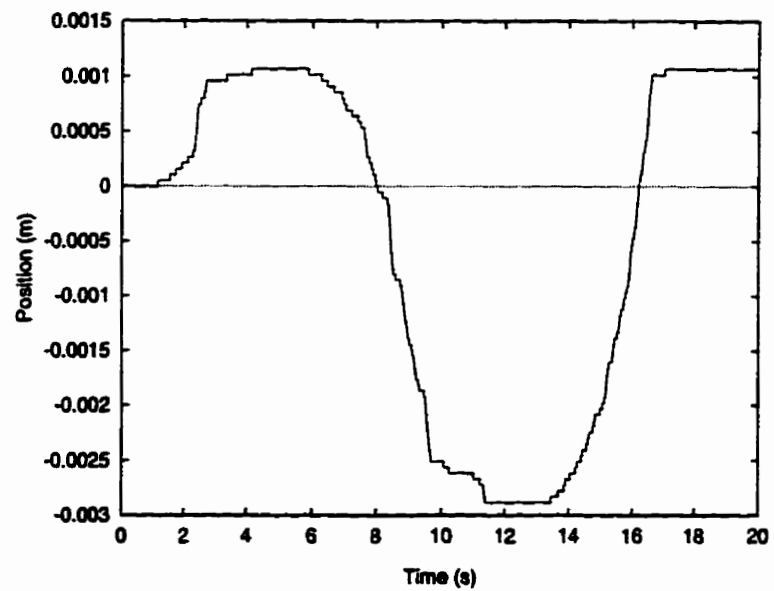
Figure 5.8: Actual open-loop position response to an oscillating ramped input that does not exceed the modeled static friction, F_S.
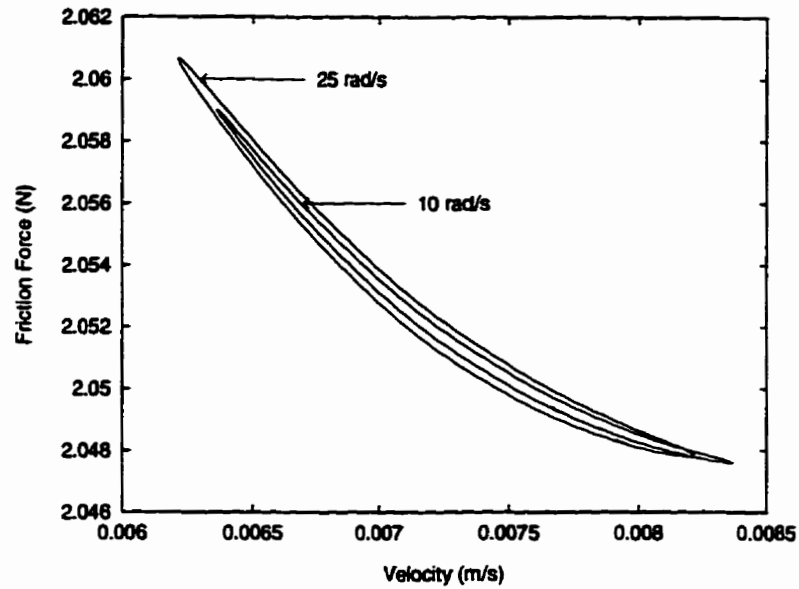
Figure 5.9: The model predicts frictional memory for oscillating velocity outside the stiction regime.
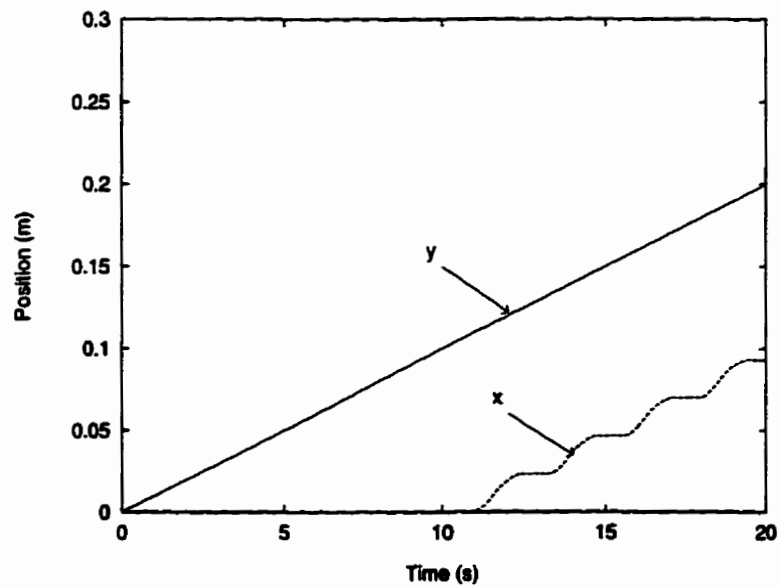
Figure 5.10: The model predicts stick-slip motion for a constant increase in applied force. Here y represents the displacement of the end of the spring and x represents the position of the cart.
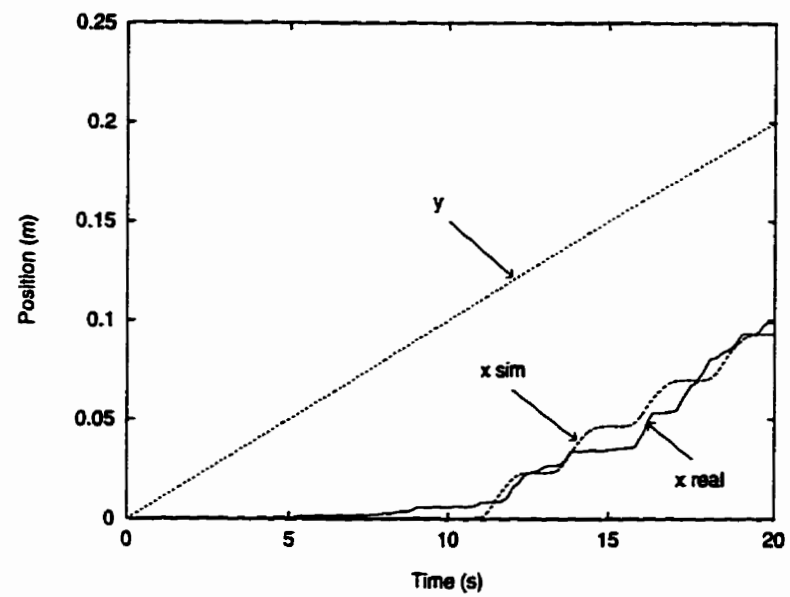
Figure 5.11: Simulated and real position response to a constant increase in applied force. Stick-slip motion appears in both the actual response and in the prediction of the model.

5.5 Summary

The results of this chapter clearly indicate that the nonlinear bristle friction model from equations (4.1) and (4.2) better represents the friction within the servo system than the linear viscous friction model. Simulations with both friction models were compared to the servo system's actual response, and the predictions of the nonlinear system closely resemble actual behaviour. Predictions of the linear system do not include stiction effects and tend to underestimate the total friction.

The nonlinear bristle model was also tested for dynamic friction behaviour. It was found to capture presliding displacement, frictional memory, and stick-slip motion, in simulation. Tests for presliding displacement and stick-slip motion were also conducted on the experimental hardware. Small displacements are detected for an applied force that is less than the identified static friction. The magnitude of these displacements was significantly larger than those predicted by the model, which may imply that the model overestimates static friction. Some displacements were not detected for very small applied forces because of quantization in the position encoder. Results also indicate that stick-slip motion occurs in the real system, under the same conditions as predicted by the model.

The bristle model, identified for the servo system, is not perfect. When included in the servo system model, the predicted response does not exactly fit the response of the real cart. This can be attributed to a number of causes. The interface between the cart and track is not uniform; other components that contribute to friction forces are also non-uniform. Minor variations in the surface of the track, the motor brushes and bearings, and in the ball bearings, can lead to inconsistent responses of the real system. It has also been noted that the responses to different inputs suit different sets of parameters. In order to capture such behaviour, a recursive parameter identification technique for time-varying parameters could be implemented. We chose not to pursue this avenue. With constant parameters, the system response using the nonlinear friction model of [7] gives a vast improvement over the standard linear model.

The fact that friction is asymmetric is evident in figure 5.4. Asymmetries can arise due to imperfections in the servo motor, and unbalances in the motor shaft [8]. The recirculating ball bearings may also contribute. In future work, it may be useful to identify a friction model in which parameters differ for each direction of motion.

Chapter 6

The C-O-A-L Dynamic Feedback Controller

6.1 Introduction

Regulator problems are those that involve positioning and pointing. Tracking control requires a trajectory to follow a desire path. In both cases, the goal is to drive the position error, $e = x - x_d$, to zero. Friction can compromise a system's performance in high precision, low velocity tracking problems. Tracking control with velocity reversals poses a particular challenge because of the nonlinear nature of friction near zero velocity.

Friction compensation can be achieved, given a reasonable friction model, by adding to a feedback controller, a term that cancels friction forces. The bristle model for friction discussed in Chapter 4 is a good candidate for friction compensation. Because the model of (4.1) and (4.2) is a state variable model, many difficulties associated with implementing a discontinuous friction model at zero velocity are overcome [4]. Unfortunately, the bristle deflection, z, is an unmeasurable internal state; an observer must be constructed to estimate z. Canudas de Wit, Olssen, Aström and Lischinsky propose an observer for z based on equation (4.1). In addition, they present a dynamic feedback controller with friction compensation [7]. Their control law shall be referred to in this work as the C-O-A-L controller.

In this chapter, the C-O-A-L controller is presented and conditions for stability are discussed. The C-O-A-L controller takes the general form of $u = u_1 + \hat{F}$, where $\hat{F}$ is the

model-based friction estimate, and u_1 is a feedback controller. In this work, u_1 represents proportional plus derivative feedback, so the performance of a PD controller is discussed, and used as a basis of comparison for the C-O-A-L controller. Experiments are conducted using the cart-motor servo system, to test the controller's proficiency at regulating the cart's position to a fixed point. The versatility of the controller is also explored to determine whether tuning is required for each task. In addition, the C-O-A-L controller is used to track a slow moving path. The experimental considerations for implementing model-based friction compensation on the servo system are also discussed.

6.2 Definitions

6.2.1 Strictly Positive Real Transfer Functions

Definition 6.1 ([23]) *A transfer function $G(s)$ is* **Positive Real (PR)** *if $Re[G(s)] \geq 0 \ \forall \ s|Re[s] \geq 0$. $G(s)$ is* **Strictly Positive Real (SPR)** *if $G(s - \varepsilon)$ is PR for some $\varepsilon > 0$*

.

Theorem 6.1 ([23]) *A transfer function $G(s)$ is strictly positive real (SPR) if an only if*

1. *$G(s)$ is a strictly stable transfer function*

2. *The real part of $G(s)$ is strictly positive along the $i\omega$ axis; $\forall \omega \geq 0$, $Re[G(i\omega)] > 0$*

Remark 6.1.1 *A set of necessary conditions for a transfer function $G(s)$ to be SPR are* [23]:

1. *$G(s)$ is strictly stable, i.e., all poles of $G(s)$ lie strictly in the left half of the complex plane.*

2. *The Nyquist plot of $G(s)$ lies entirely within the right half complex plane*

3. *$G(s)$ has relative degree of 0 or 1*

4. *$G(s)$ is strictly minimum phase, which implies that all the zeros of $G(s)$ lie strictly within the right half complex plane*

The following result provides a nice restatement of Theorem 6.1 in state space representation:

Lemma 6.1.1 (Kalman-Yakubovitch Lemma, [23])

Given the controllable linear system

$$\dot{x} = Ax + bu,$$

$$y = c^T x,$$

the transfer function

$$G(s) = c^T(Is - A)^{-1}b$$

is SPR if and only if there exist matrices $P > 0$ and $Q > 0$ such that

$$A^T P + PA = -Q$$

$$Pb = c^T.$$

6.3   The PD Controller

In linear control systems, a standard feedback controller for tracking problems is the proportional plus derivative (PD) controller. The general form of a PD controller is $u = k_v \dot{e} + k_p e$, where $e = x - x_d$ represents the tracking error in the system. For our servo system, x represents cart position. For many engineering applications, a linear viscous friction model is employed. Suppose $F = \beta \dot{x}$, where β represents the viscous friction coefficient. Then, following (5.1), the model governing the motion of the cart is

$$m\ddot{x} = Ku - \beta \dot{x}.$$

If a PD controller, $Ku = -k_v \dot{e} - k_p e$, is used to close the feedback loop, the resulting system is

$$m\ddot{x} + \beta \dot{x} = -k_v(x - x_d) - k_p(x - x_d). \tag{6.1}$$

Equation (6.1) resembles a damped spring-mass system. Both β and k_v contribute to the total damping and k_p determines the stiffness of the system. Thus, in the frequency domain, the transfer function between the desired path x_d and actual position x becomes

$$\frac{X(s)}{X_d(s)} = \frac{k_2 s + k_1}{ms^2 + (\beta + k_2)s + k_1}. \tag{6.2}$$

For optimal performance of a second order linear system, the poles of the transfer function should be placed on the 45 degree line in the left half of the complex plane. This gives a good trade-off between speed and accuracy.

It is also common to discuss second order systems in terms of their natural frequency ω_n, and damping ratio ξ. The characteristic equation for a second order system, given by the denominator of the transfer function, is of the form

$$s^2 + 2\xi\omega_n + \omega_n{}^2. \tag{6.3}$$

The pole placement, and subsequent choice of gains, uniquely determines the values of ω_n and ξ. Speed of response versus settling time is governed by damping in the system. Purely imaginary poles gives a value of $\xi = 0$, which indicates that no damping is present, and results in a marginally stable response. If $\xi < 1$, then the poles of the system are complex conjugates. Placing poles on the 45 degree line results in a damping ratio of approximately $\xi = 0.707$, which is widely accepted to be an optimal value. If the system has real poles, then $\xi > 1$; the system is over-damped, which produces a slow response and no overshoot.

The advantages of PD control are: a relatively simple closed-loop system, and the fact that theory exists to analyze stability and ensure optimal performance. In order to benefit from these advantages, a linear system model is required. Thus friction must be modeled linearly, which will fail to capture its dominant characteristics near zero velocity.

Experiments with a PD feedback controller were conducted using the servo controlled cart system. A linear viscous friction coefficient of 4.6 Ns/m has been identified in Chapter 5. Thus for equation (6.2), $\beta = 4.6\ Ns/m$ was adopted. A sampling frequency of 250 Hz was used for all experiments. This results in a relatively smooth velocity estimate and precludes the need for velocity filtering.

In regulator problems, the main deficiency associated with PD control is large steady state error. For a particular task, controller gains can be tuned to provide good performance. However, the controller lacks versatility. Re-tuning is required to achieve similar performance in other applications.

Figure 6.1 illustrates the steady state error associated with PD control. For this test, the poles of the system were placed on the 45 degree line at $-4 \pm 4i$. Although this pole placement should result in good performance, the gains are insufficient to overcome friction effects. The result is a steady state error of about 30%. Placing the poles further from the origin on the 45 degree line will increase the controller gains, and should produce a more accurate response. The response of the cart when the poles are place at $-13 \pm 13i$ is shown in figure 6.2. Clearly the response is more accurate with higher gains; the steady state error is less than 5%. This type of tuning can be effective, but is specific to the control
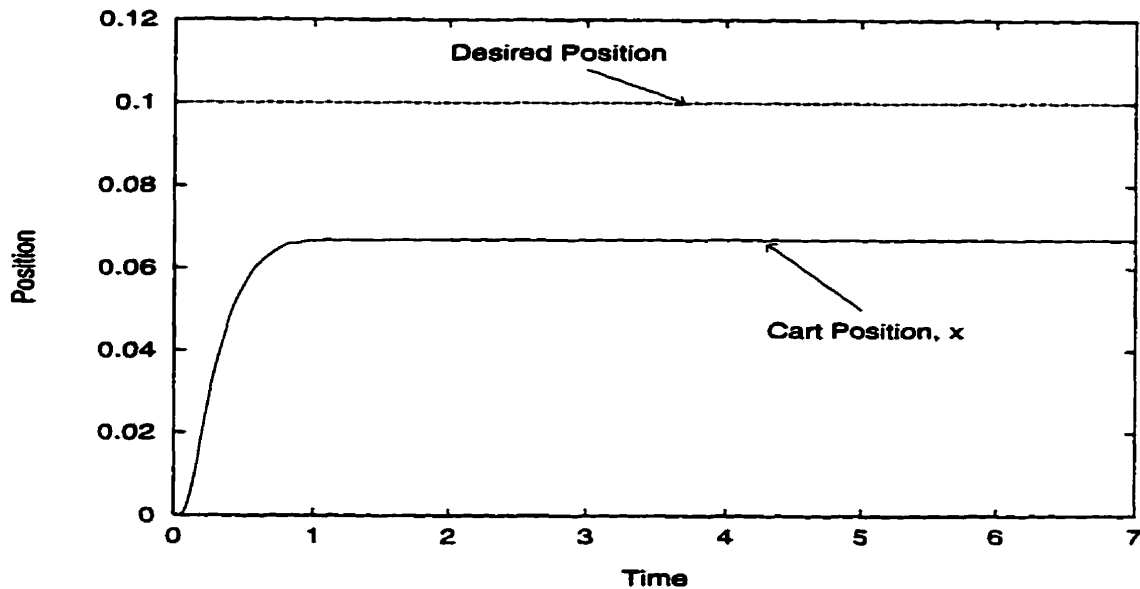
Figure 6.1: System response to $x_d = 10$ cm using a PD controller and linear friction model with poles at $-4 \pm 4i$

task. The need for re-tuning is displayed in figure 6.3, which shows the response of the PD controller to $x_d = 1$ cm with poles placed at $-13 \pm 13i$. This task requires fine control. With the adopted PD controller, the steady state error is almost 30%.

The PD gains can be increased again to improve the response to $x_d = 1$ cm, but a significant increase is necessary. Figure 6.4 shows improved accuracy with poles at $-20\pm20i$, but the control voltage output is truncated, as seen in figure 6.5. This illustrates one gap between theory and experimentation; one must take into account the physical limits of the system. For our system, a constraint is produced by the 24V output limit of the servo motor. When the control voltage is truncated by the limits of the motor, the system no longer behaves as the model predicts. In addition, high gain feedback amplifies noise and often stimulates high frequency unmodeled dynamics, which produce severe vibrations. In some cases, using high gains can destabilize the system. Thus an accurate controller that does not require high gains is desirable.

When a PD controller is used for tracking with low velocity or velocity reversals, stick-slip motion may occur. Figure 6.6 shows an example of this type of behaviour. Studies have shown that sufficiently large control gains will eliminate stick-slip motion [9]. However, steady state error and stiction effects at velocity reversals may still be present. The response
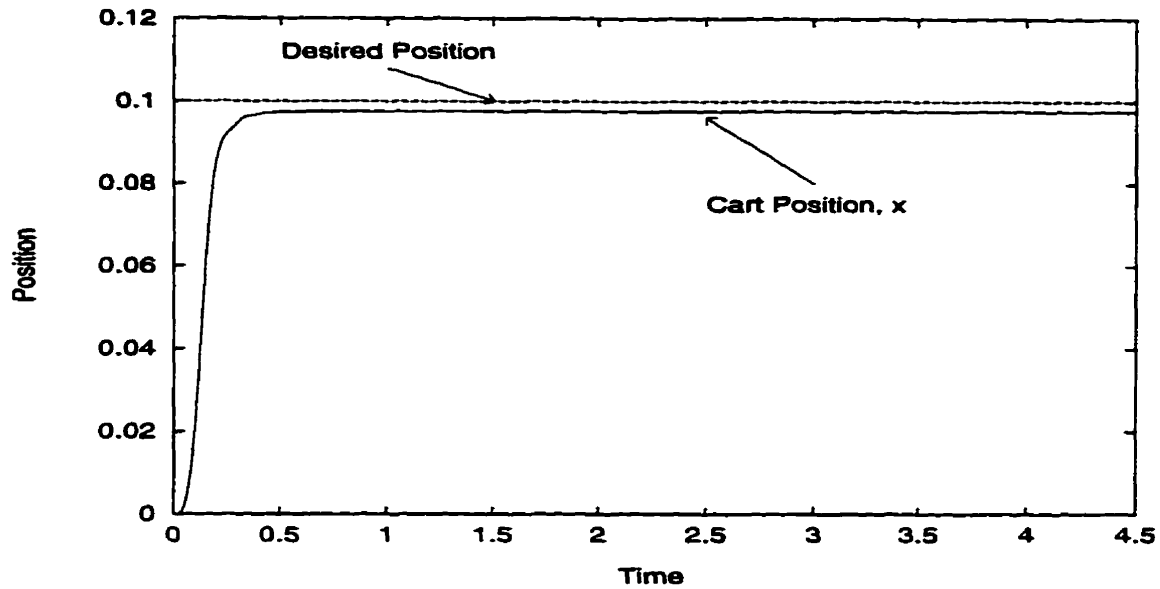
Figure 6.2: System response to $x_d = 10\ cm$ using a PD controller and linear friction model with poles at $-13 \pm 13i$

of a PD controller tracking $x_d = 0.1 sin(t)\ m$ is displayed in figures 6.7 and 6.8. From figure 6.7, it appears that the PD controller has performed this tracking task well. However, closer examination of the response in figure 6.8 shows that the cart's trajectory lags that of the desired path, indicating steady state error. There are also prolonged periods of zero velocity at direction changes, which can be attributed to unmodeled static friction.

It is clear that the PD controller does not overcome nonlinear friction effects. The addition of model-based friction compensation should improve the overall tracking performance.
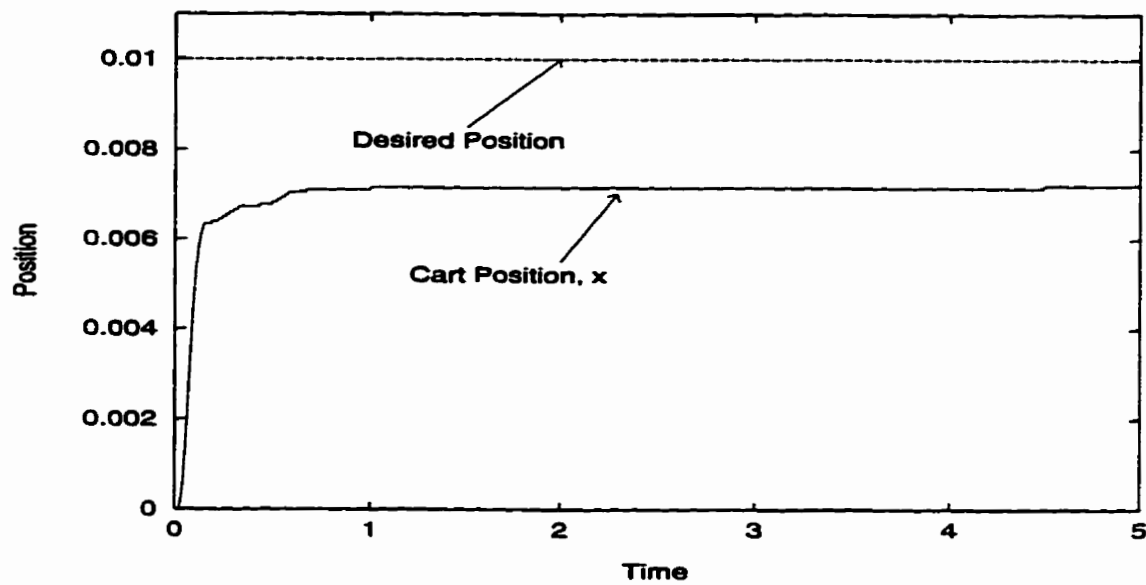
Figure 6.3: System response to $x_d = 1\ cm$ using a PD controller and linear friction model with poles at $-13 \pm 13i$
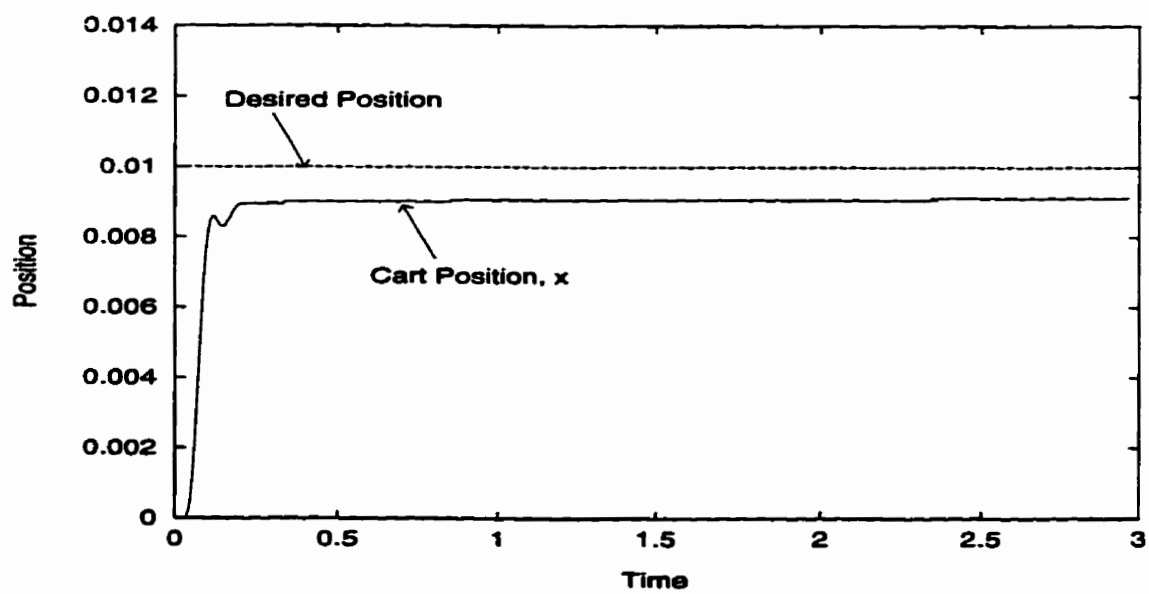
Figure 6.4: System response to $x_d = 1\ cm$ using a PD controller with poles at $-20 \pm 20i$
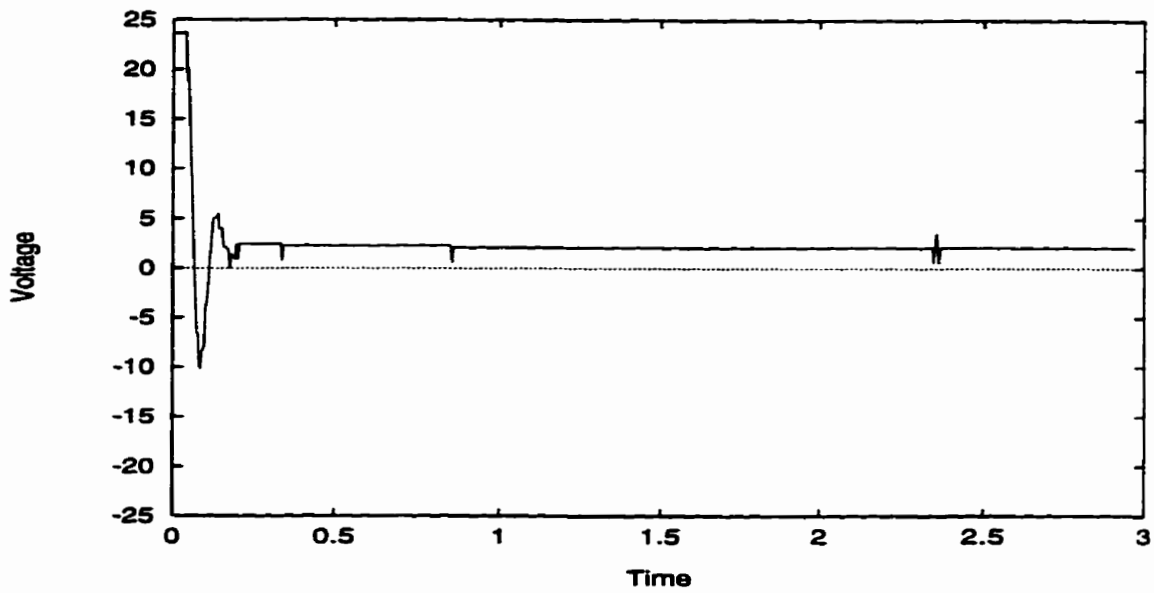
Figure 6.5: Control voltage output from a PD controller with poles at $-20 \pm 20i$ in response to $x_d = 1 \, cm$
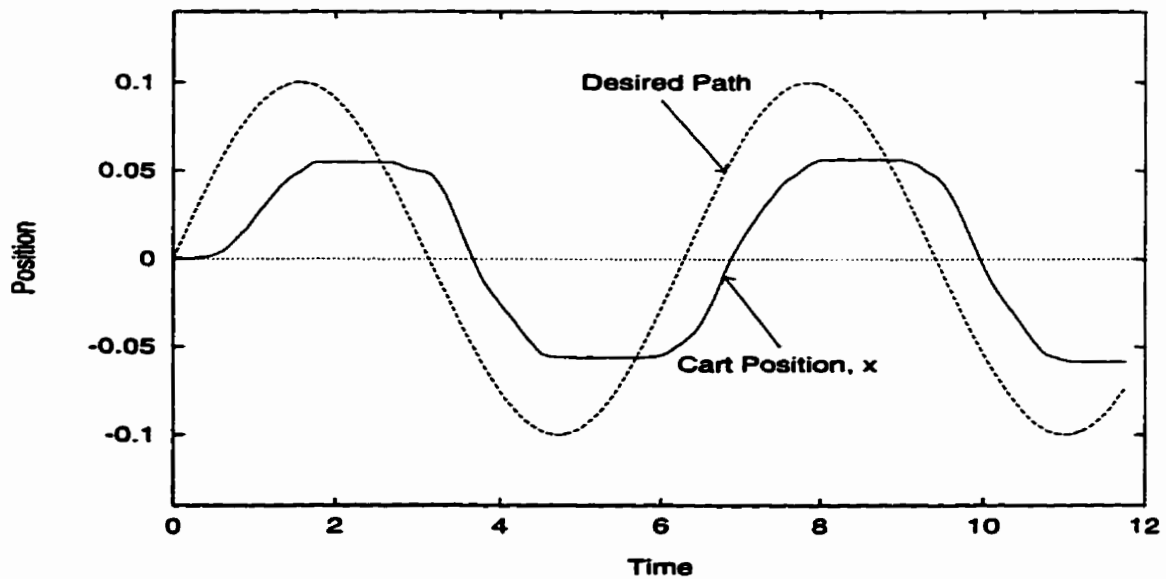
Figure 6.6: System response to tracking $x_d = 0.1 sin(t) \, m$ using a PD controller with poles at $-2 \pm 4i$
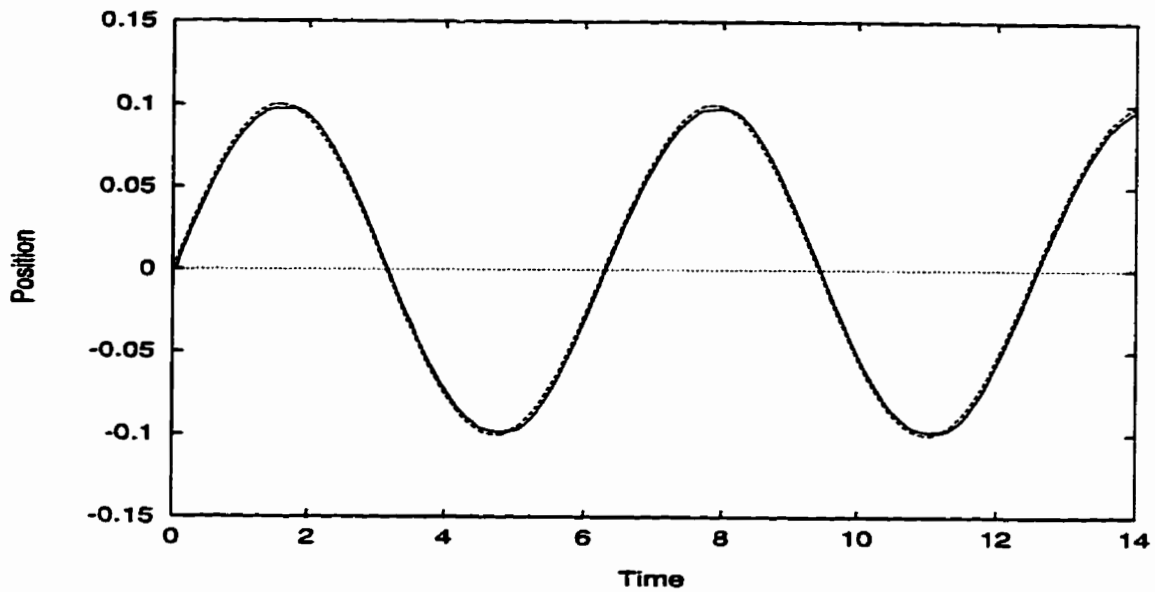
Figure 6.7: System response to tracking $x_d = 0.1sin(t)$ m using a PD controller with poles at $-13 \pm 13i$
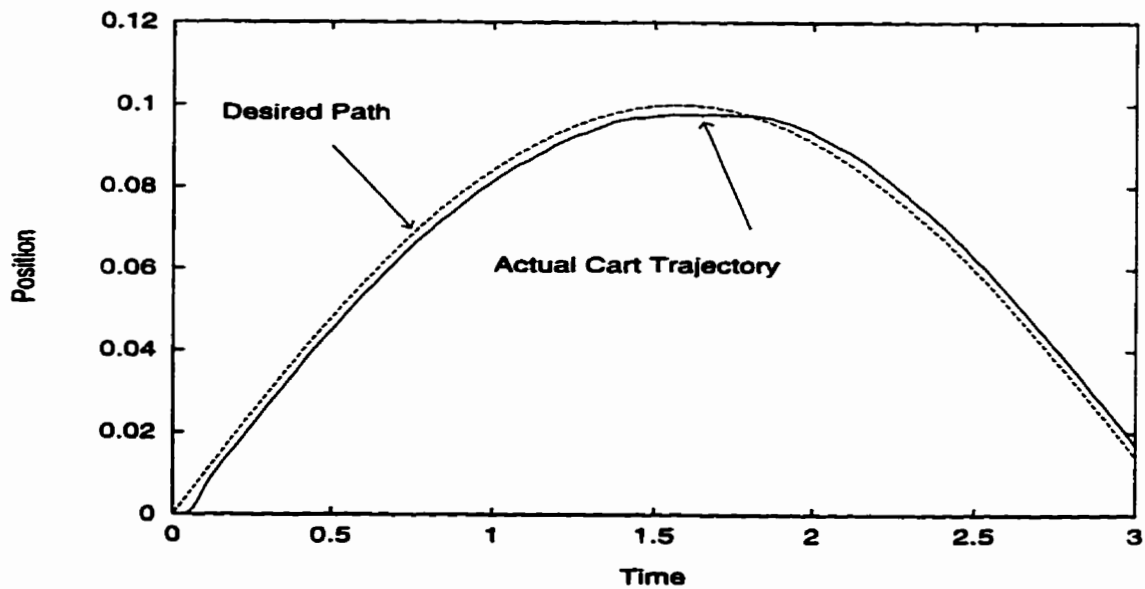
Figure 6.8: Segment of figure 6.7. System response to tracking $x_d = 0.1sin(t)$ m using a PD controller with poles at $-13 \pm 13i$

6.4 The C-O-A-L Dynamic Feedback Controller

The bristle model of equations (4.1) and (4.2) seems well suited to model-based friction compensation, but an observer is required to estimate the unmeasured internal state z. Canudas de Wit *et al.* developed an observer for z and a dynamic feedback controller with model-based friction [7].

Recall our model for the motion of the servo controlled cart of equation (5.1)

$$m\ddot{x} = Ku - F,$$

and the bristle model for friction of (4.1) and (4.2) proposed in [7]

$$\dot{z} = v - \frac{|v|}{g(v)}z,$$

$$F = \sigma_0 z + \sigma_1 \dot{z} + \sigma_2 v.$$

The friction observer proposed by Canudas de With *et al.* [7] is given by

$$\frac{d\hat{z}}{dt} = v - \frac{|v|}{g(v)}\hat{z} - ke, \quad k > 0, \tag{6.4}$$

$$\begin{aligned} \hat{F} &= \sigma_0\hat{z} + \sigma_1\frac{d\hat{z}}{dt} + \sigma_2 v, \\ &= \sigma_0\hat{z} + \sigma_1(v - \frac{|v|}{g(v)}\hat{z} - ke) + \sigma_2 v. \end{aligned} \tag{6.5}$$

The control law with friction compensation presented in [7] is given by

$$Ku = -h * e + \hat{F} + m\ddot{x}_d, \tag{6.6}$$

where $h = \mathcal{L}^{-1}[H(s)]$ and means convolution. The friction estimate is denoted $\hat{F}$ and x_d is the desired path or position of the cart. The term $H(s)$ is defined in the frequency domain and allows error feedback. An appropriate choice for $H(s)$ will yield a stable control system. The resulting closed-loop system is

$$m\ddot{e} = -h * e + \hat{F} - F \tag{6.7}$$

Canudas de Wit *et al.* present a theorem that, for certain $H(s)$, guarantees that both the observer error and position error tend to zero asymptotically if u satisfies (6.6).

Theorem 6.2 ([7]) *Using the system (5.1) with the friction model (4.1), (4.2), friction observer (6.4), (6.5), and the control (6.6), if $H(s)$ is chosen so that*

$$G(s) = \frac{\sigma_1 s + \sigma_0}{ms^2 + H(s)} \tag{6.8}$$

is strictly positive real (SPR), then $(F - \hat{F}) \to 0$ and $e \to 0$ asymptotically.

The proof of Theorem 6.2 can be found in [7]. Theorem 6.2 does not ensure fast convergence of e and $\tilde{F}$ to zero. The theorem also restricts $H(s)$ to guarantee that $G(s)$ is SPR. In our case, such restrictions lead to difficulties in experimental implementation.

6.4.1 Selection of H(s)

From equation (6.8) we have the transfer function,

$$G(s) = \frac{\sigma_1 s + \sigma_2}{ms^2 + H(s)}, \tag{6.9}$$

$$= \frac{e(s)}{\tilde{z}(s)}. \tag{6.10}$$

A natural choice for $H(s)$ is

$$H(s) = k_2 s + k_1, \tag{6.11}$$

which results in a control law (6.6) that combines proportional and derivative feedback with friction compensation. This choice of $H(s)$ satisfies the conditions that $G(s)$ have a relative degree of 1 and be strictly minimum phase. The definition of an SPR transfer function also requires that $G(s)$ be strictly stable. With $H(s)$ defined in (6.11) the poles of $G(s)$ are given by

$$s = \frac{-k_2 \pm \sqrt{k_2{}^2 - 4mk_1}}{2m}.$$

Note that, for $k_1 > 0, k_2 > 0$, we have $Re[s] < 0$.

Finally, for $G(s)$ to be SPR, the Nyquist plot must be strictly contained within the right half of the complex plane. This is essentially the result of Theorem 6.1 and is both a necessary and sufficient condition for $G(s)$ to be SPR. Assume Theorem 6.1 holds. Then for all ω we have

$$Re[G(i\omega)] \qquad > \qquad 0,$$

$$\Rightarrow \quad \frac{\sigma_0(-m\omega^2+k_1)+\sigma_1 k_2\omega^2}{(-m\omega^2+k_1)^2+k_2\omega^2} \quad > \quad 0,$$

$$\Rightarrow \quad \sigma_0(-m\omega^2+k_1)+\sigma_1 k_2\omega^2 \quad > \quad 0,$$

$$\Rightarrow \quad \omega^2(\sigma_1 k_2 - \sigma_0 m) + \sigma_0 k_1 \quad > \quad 0.$$

When $\omega = 0$, we need $\sigma_0 k_1 > 0$, and hence $k_1 > 0$. When $\omega \neq 0$, we require that

$$\sigma_1 k_2 - \sigma_0 m \quad > \quad 0,$$

$$\Rightarrow \quad \sigma_1 k_2 \quad > \quad \sigma_0 m,$$

$$\Rightarrow \quad k_2 \quad > \quad \frac{\sigma_0 m}{\sigma_1}.$$

Therefore, the restrictions on $G(s)$ which imply SPR via Theorem 6.1 are

$$k_1 > 0, \quad k_2 > \frac{\sigma_0 m}{\sigma_1}.$$

The parameters for the servo system have been identified as $m = 2.0\ kg$, $\sigma_0 = 10^5\ N/m$ and $\sigma_1 = 495\ Ns/m$. Thus the restrictions placed on k_1 and k_2 for our servo system are

$$k_1 > 0\ kg/s^2, \quad k_2 > 404\ kg/s.$$

A controller that combines PD feedback with friction compensation should allow us to take advantage of linear theory in choosing the proportional and derivative gains, as long as choices remain within the limits set by Theorem 6.2. Correct placement of the poles of $G(s)$ predicts the values of k_1 and k_2 that result in optimal performance for a system without friction. Therefore, placing the poles of $G(s)$ on the 45 degree line is the natural choice to achieve a fast and accurate response. Unfortunately, the strong SPR restrictions on k_1 and k_2 prohibit the use of reasonable complex poles. Because k_2 must be at least 400, k_1 must be approximately 20 000 in order for the poles to be complex, and approximately 40 000 for the poles to be on the 45 degree line. Clearly these values are unrealistically large. Thus PD gains that place the poles of $G(s)$ on the real axis must be employed, which results in over-damping.

A value of $k_2 = 450\ kg/s$ was adopted for experimental purposes. Choosing a "best" value for k_1 depends on the nature of the test. Larger k_1 should increase the speed of response. However, high gains coupled with large error result in mechanical problems and voltage truncation. Ideally, a large k_1 that avoids control saturation should be used

6.4.2 Friction Observer

The choice of k in the observer (6.4) is left unrestricted except that $k > 0$. Consider the case where $x_2 = 0$ but $e \neq 0$, i.e. the cart has stopped, but not at the desired position. Then

$$\dot{\hat{z}} = -ke,$$

and

$$Ku = -k_1 e + \sigma_0 \hat{z} + \sigma_1(-ke) + m\ddot{x}_d. \tag{6.12}$$

When the cart is in the stiction regime, the term $\sigma_0 \hat{z}$ provides integral action to the controller. This raises the question of whether hunting, often associated with integral action and uncompensated stiction [25], might occur. At zero velocity, the integrator gain, $\sigma_0 k$, is large unless k is very small. In addition, we noted in Chapter 4 that $|\hat{z}| \leq F_s/\sigma_0$. With $F_s = 2.15\ N$ and $\sigma_0 = 10^5\ N/m$, $|z|$ is approximately 2×10^{-5}. With a small value for k, ke will not dominate the equation governing $\dot{\hat{z}}$. The term $-ke$ is also included in the control law, and contributes to the gain associated with position error. For this reason, it is difficult to isolate the effect that increasing or decreasing $\dot{\hat{z}}$, by altering k, has on the overall system's performance.

A Lyapunov function for the linear system with transfer function $G(s)$ is defined as $V = \xi^T P \xi + \frac{\tilde{z}^2}{k}$ [7]. The derivative is

$$\dot{V} = -\xi^T Q \xi - \frac{2|v|}{kg(v)}\tilde{z}^2. \tag{6.13}$$

Here the change in control energy associated with observer error $\tilde{z}$ is inversely proportional to k. Therefore, it follows from (6.13) that a small magnitude for k should lead to a faster convergence of $\tilde{z}$ to zero; a small value for k is desirable.

It appears that there is no lower limit on k. However, a very small value of k implies that there is little error in the observer, which is not realistic. Figure 6.9 shows the simulated C-O-A-L controller response to $x_d = 10\ cm$, for different values of k. The simulations indicate that for $k = 0.001\ s^{-1}$ and $k = 0.00001\ s^{-1}$, the response of the system is the same. A value of $k = 0.001\ s^{-1}$ was adopted for all experiments. In this case, the integrator gain is approximately 100, which is smaller than the proportional and derivative gains used.
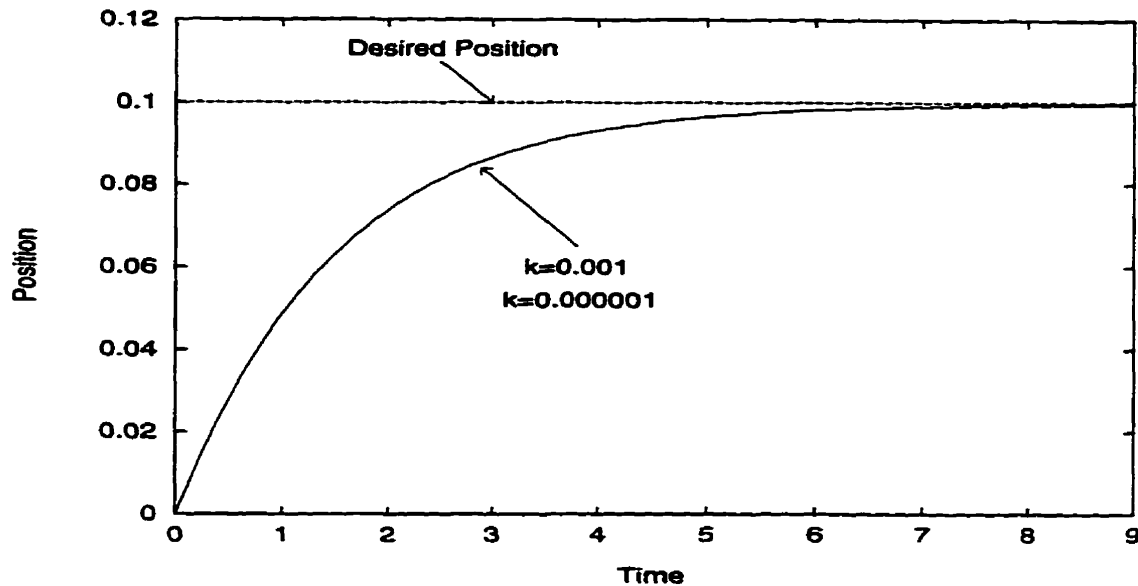
Figure 6.9: Simulated response of C-O-A-L controller while varying the observer constant k. ($k_1 = 350\ kg/s^2$, $k_2 = 450\ kg/s$)

6.4.3   Experimental Implementation

The C-O-A-L control law was tested using the servo motor system. The observer estimate was calculated using Euler's method to integrate the ordinary differential equation governing z. Euler's method requires a small step-size to achieve accuracy in approximating a derivative. The estimate for bristle deflection, $\hat{z}$, changes very quickly and has a very low magnitude. Therefore, a high sampling frequency was necessary to accurately model rapid dynamics, and to keep error small relative to the magnitude of $\hat{z}$. Unfortunately, a high sampling frequency produces a noisy estimate for velocity. This is due to the method of computing velocity, and the quantized nature of the position data. With a very high sampling rate and low velocity motion, there can be periods of time where the encoder does not record movement. When motion is detected, it is perceived as a very large change in position over a small time interval. The result is noise in the velocity estimate, which is fed back by the PD controller. This discretization noise also introduces considerable error into our estimation of $\hat{z}$. Figure 6.10 shows $\hat{z}$ computed with simulated velocity data for changes in direction of motion. It is evident from the graph that the change in bristle deflection is very rapid through a velocity reversal. For this reason, $\hat{z}$ is particularly sensitive to noise when the velocity of the cart is close to zero. Figure 6.11 depicts the observed value of $\hat{z}$
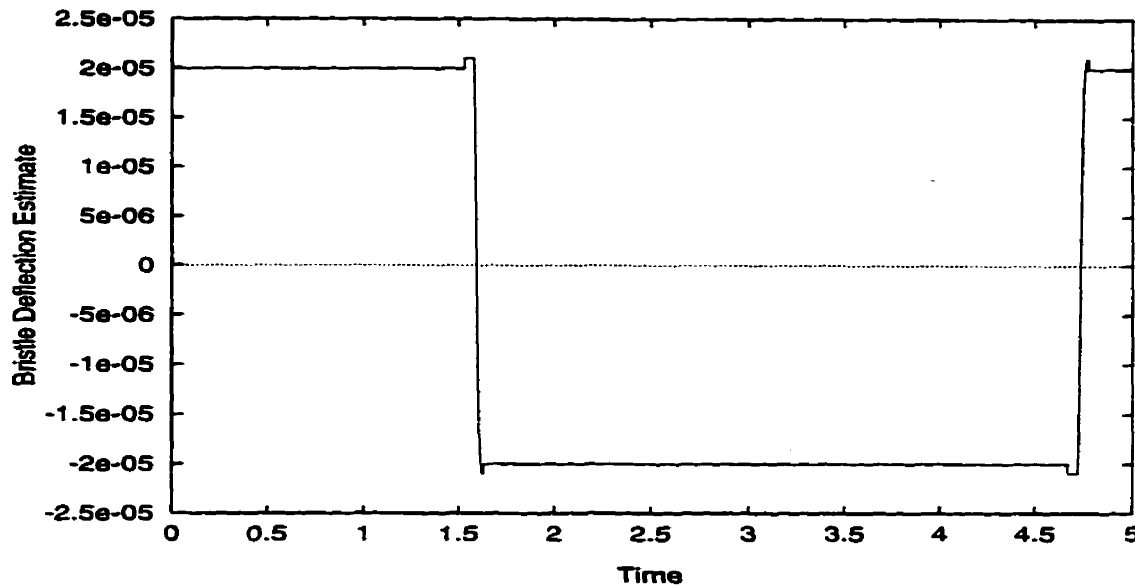
Figure 6.10: Simulated value of $\hat{z}$ in response to tracking a $x_d = 0.1 sin(t)$ m. ($k_1 = 300 \, kg/s^2$, $k_2 = 450 \, kg/s$)

computed with real velocity data. Notice the large fluctuations when the observer changes sign. Thus a trade-off between high sampling frequency for derivative calculation, and low frequency to reduce noise, is required.

The unfiltered velocity estimate for a sampling frequency of $f = 2500$ Hz, in response to step input, is shown in figure 6.12. Open loop experiments were used to determine the best method of reducing the noise present in this velocity estimate. One method is to average the velocity over several sampling intervals. Using this method provides a velocity estimator with a larger Δt, and a larger change in position over that time interval. Figure 6.13 shows the velocity estimate for $f = 2500$ Hz, calculated every 10 cycles. A vast improvement in the signal can be seen, and no large lags are introduced.

Additional smoothing may be achieved by filtering the velocity signal. The simplest smoothing filter that can be used to reduce noise is the first order filter

$$v_{smooth} = \delta t(a v_{noisy} - a v_{smooth}) + v_{noisy}. \tag{6.14}$$

The choice of smoothing constant, a, is critical. Larger values for a result in less smoothing so that v_{smooth} closely follows v_{noisy}. If a is too large the filter is ineffective. However, if a is too small, lag is introduced into the system. This negatively affects system performance and stability. Figure 6.14 shows the smoothed velocity estimate for $a = 120$ at $f = 2500$
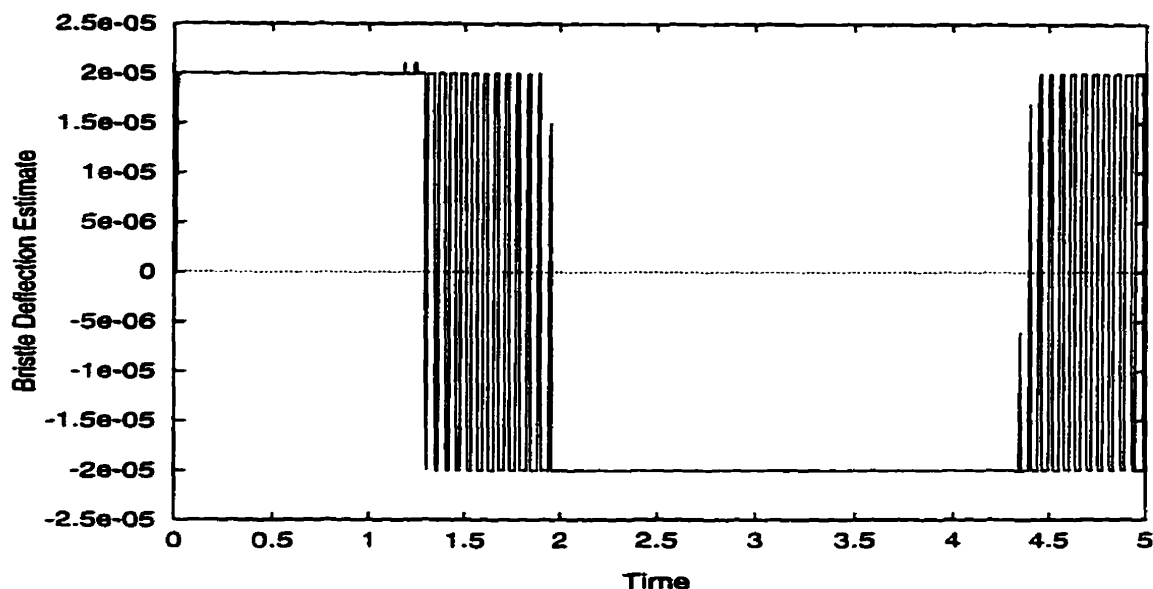
Figure 6.11: Observed value of $\hat{z}$ in response to tracking a $x_d = 0.1 sin(t)$ m. ($k_1 = 300\ kg/s^2$, $k_2 = 450\ kg/s$)

Hz. There is improvement over the unfiltered data of figure 6.12, but noise is still present at higher velocities. For $f = 1000$ Hz the smoothed velocity with $a = 30$ is compared to the unfiltered velocity in figure 6.15. The filtered signal is clearly better than the unfiltered one. However, for this value of a the smoothed velocity estimate lags the original one.

Sensor noise problems may also be solved by constructing an observer to predict velocity. Unfortunately, the nonlinear nature of our system model makes constructing a stable velocity observer extremely difficult. Another standard approach is to add a tachometer to our motor and a D to A converter to the computer. This would let us measure velocity more directly, although sensor noise and resolution issues also arise with direct velocity measurement.

Experimentation determined that a frequency of at least 3000 Hz is needed to overcome problems associated with fast dynamics of $\hat{z}$. In other words, to guarantee convergence of the Euler's method algorithm, which was used to integrate the $\hat{z}$ equation, we need to sample at least 3000 times per second. To smooth the velocity estimate, the filter of (6.14) was used with $a = 80$. Velocity was estimated and smoothed every 10 cycles.

To avoid large errors in $\hat{z}$ at high velocity, and to reduce computation, $\hat{z}$ was set to a steady state value for velocity above a designated cutoff velocity. Recall from Chapter
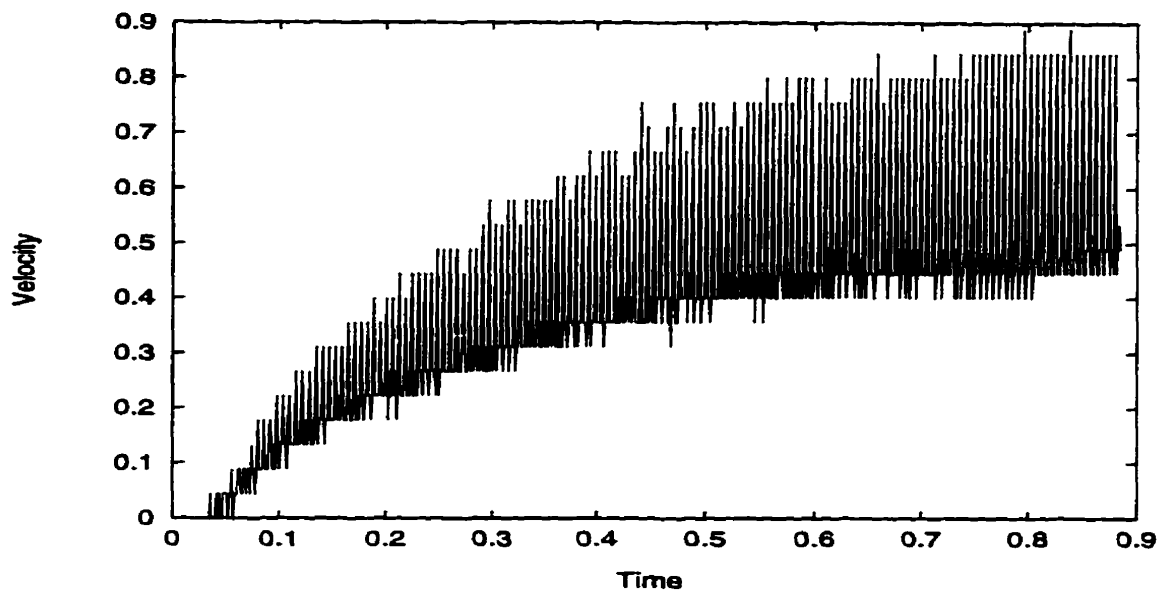
Figure 6.12: Unfiltered velocity at $f = 2500$ Hz sampling frequency.

4 that z tends to a steady state value; $z_{ss} = g(v)sgn(v)$. Simulations show that z reaches a steady state for $v > 0.04\ m/s$. Thus, for $v > 0.1\ m/s$, we let $\hat{z} = g(v)sgn(v)$.
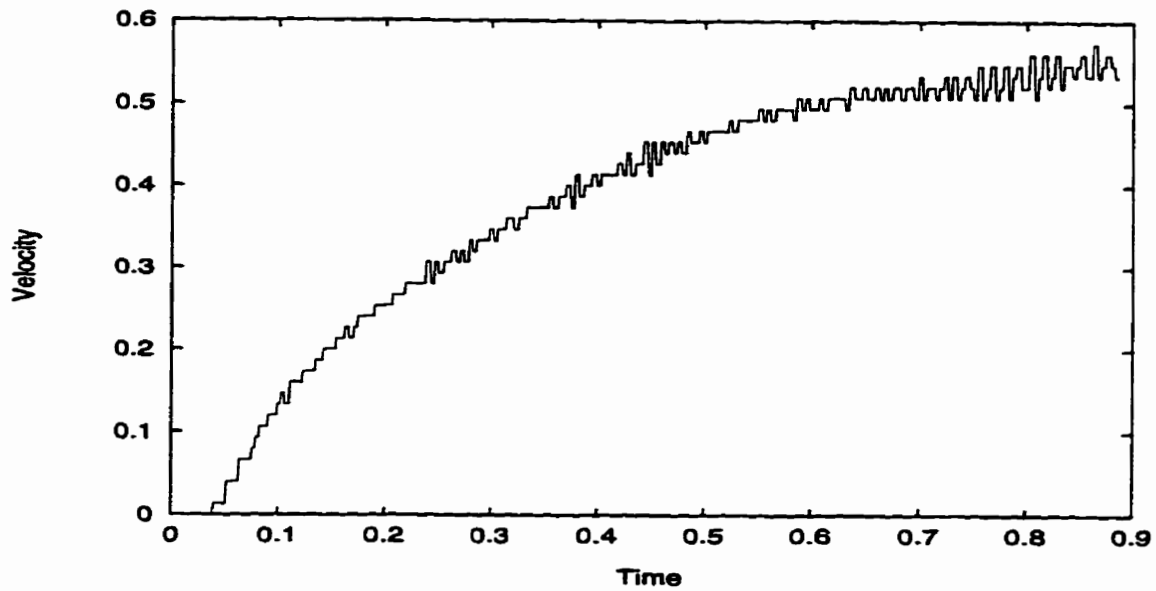
Figure 6.13: Unfiltered, frequency reduced, velocity estimate. Sampling frequency, $f = 2500$ Hz with velocity estimated every 10 cycles.
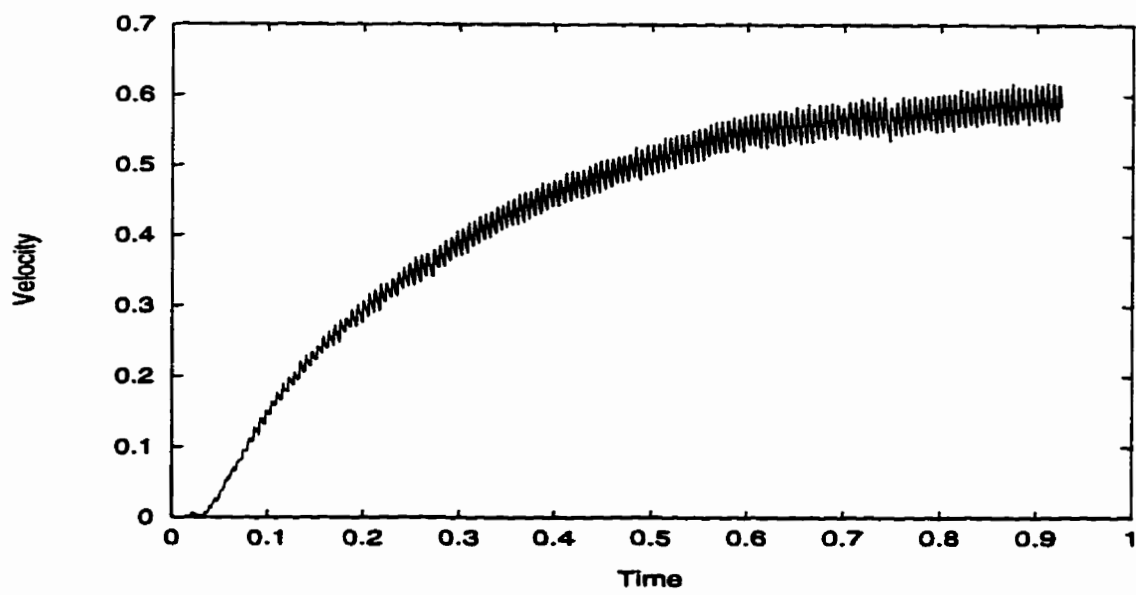
Figure 6.14: Filtered velocity estimate with $a = 120$ and $f = 2500$ Hz.
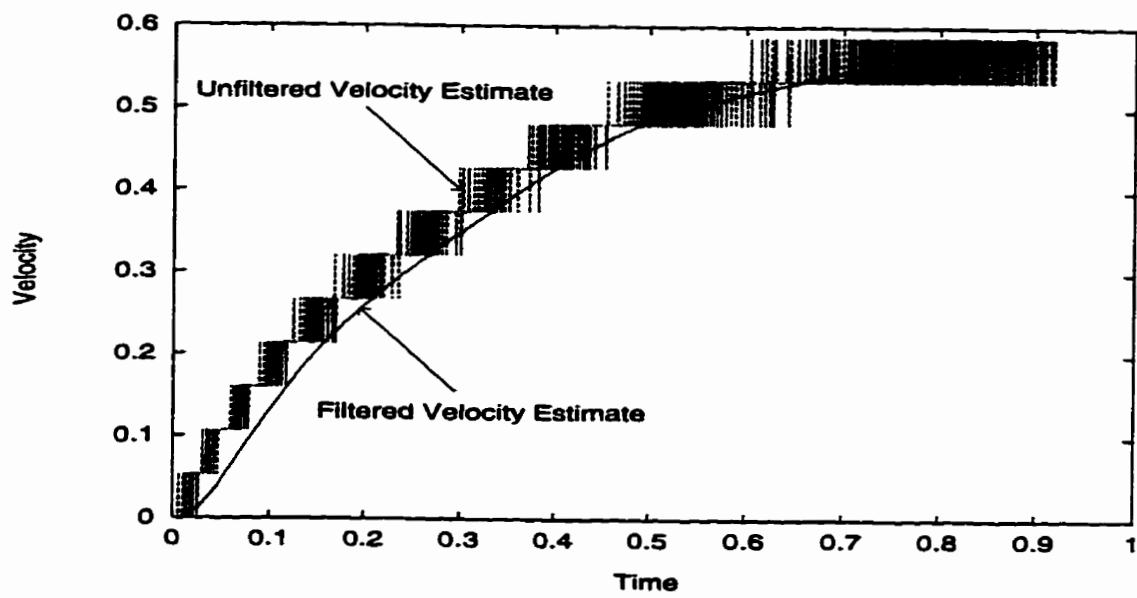
Figure 6.15: Filtered velocity estimate with $a = 30$ and $f = 1000$ Hz

6.5 Experimental Results Using the C-O-A-L Controller
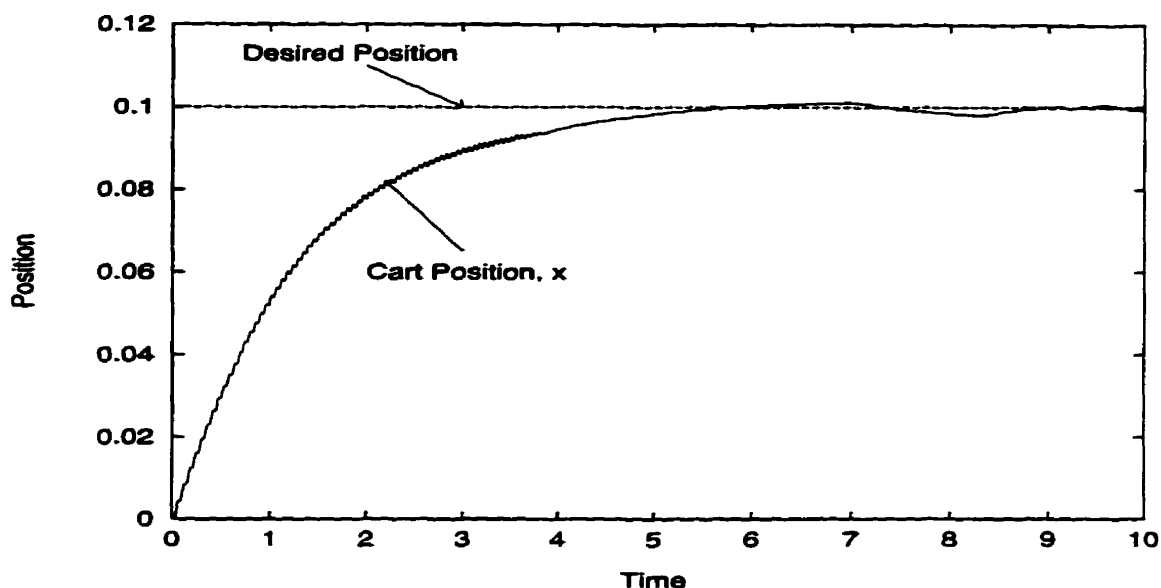
Figure 6.16: Response of the to C-O-A-L controller using $k_1 = 350\,kg/s^2$, $k_2 = 450\,kg/s$ to $x_d = 10\,cm$.

The C-O-A-L control law was used experimentally to track a step, and then a sinusoidal path. Figure 6.16 shows the closed-loop response of the cart required to move 10 *cm*. The proportional and derivative gains used were $k_1 = 350\,kg/s^2$ and $k_2 = 450\,kg/s$. The line labeled "Cart Position" indicates the recorded motion of the cart over time. Note that this line is not smooth, which implies vibration, particularly when the tracking error is large. The cart reaches the desired position, but begins hunting.

The C-O-A-L controller performance displayed in figure 6.16 is reasonably good, except for some undesirable vibration. Direct comparison to the performance of a PD controller under the same conditions is difficult because of the high feedback gains necessary with the C-O-A-L controller. The PD controller with gains of $k_p = 350\,kg/s^2$ and $k_v = 450\,kg/s$ responds with severe vibration due to unmodeled dynamics that are stimulated by high gain feedback. Thus it is not a good basis for comparison. However, the results of figure 6.16 can be compared to the response of a PD controller with $x_d = 10\,cm$ and with poles at $-13 \pm 13i$. Figure 6.17 shows this comparison. The C-O-A-L controller is slightly more accurate, but exhibits oscillatory motion. It is clear that the response of the PD controller is much faster with relatively low steady state error.

Figure 6.17: Comparison of the responses of a PD controller with poles at $-13 \pm 13i$ and the C-O-A-L controller with $k_1 = 350 \ kg/s^2$ and $k_2 = 450 \ kg/s$ to $x_d = 10 \ cm$

The response of the C-O-A-L controller with $k_1 = 350 \ kg/s^2$ for $x_d = 1 \ cm$ is displayed in figure 6.18. Here small vibrations are present, although they are less significant than those present in the response to $x_d = 10 \ cm$ (figure 6.16). Significant hunting occurs near the desired position. The results in figure are 6.18 are compared to the performance of a PD controller for the same task, with poles at $-13 \pm 13i$; both are displayed in figure 6.19. The C-O-A-L controller responds more slowly than the PD controller, but is much more accurate.

There are two obvious problems associated with implementing the C-O-A-L controller: there are vibrations present, and there is hunting near the steady state equilibrium position. The vibrations can be attributed to high feedback gains. Consider the output voltage from the C-O-A-L controller with $x_d = 10 \ cm$ (Figure 6.20). With $k_2 = 450$, noise in the velocity estimate is amplified in the voltage signal. Furthermore, $k_1 = 350$ results in control saturation, even with small error.

In order to avoid control saturation, we reduced k_1. Figure 6.21 displays the voltage output by the C-O-A-L controller with $x_d = 10 \ cm$, $k_1 = 100 \ kg/s^2$, and $k_2 = 450 \ kg/s$. The voltage signal is still very noisy, but no truncation occurs. Figure 6.22 graphs the position versus time of the cart in response to the C-O-A-L controller with $k_1 = 100 \ kg/s^2$
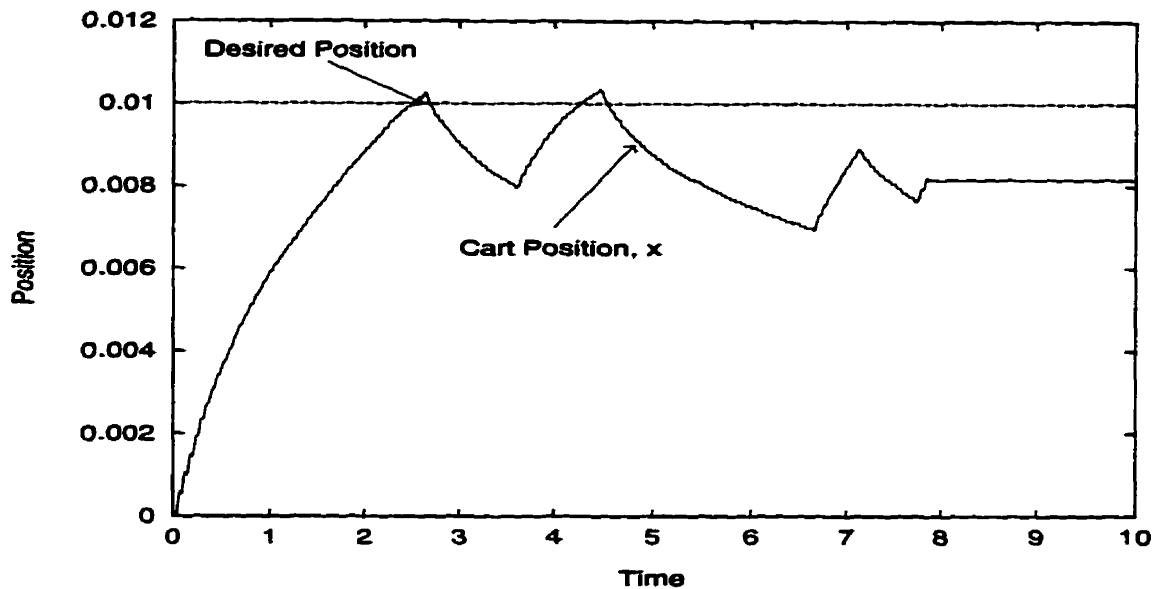
Figure 6.18: Position response of the C-O-A-L Controller with $k_1 = 350\ kg/s^2$, $k_2 = 450\ kg/s$ to $x_d = 1\ cm$

and $x_d = 10\ cm$. Here there is less vibration in the system. The response is reasonably accurate *but very slow*.

The second problem noted is that hunting occurs as the cart nears the desired position. Noise in the velocity signal near zero velocity may cause a sign change in $\hat{z}$ when the desired direction for friction compensation has not changed. In addition, a model that overestimates friction can result in overshoot [8], [6]. Our model is inexact and, amplified by high gains, the modeling errors may lead to hunting.

The C-O-A-L controller was also used to track a slow moving sinusoidal path, $x_d = 0.1sin(t)\ m$. Figure 6.24 displays the position response of the C-O-A-L with $k_1 = 350\ kg/s^2$ and $k_2 = 450\ kg/s$. Initially, a small position error can be noted, but over time the actual cart position becomes very close to the desired path. Figure 6.25 is a magnified segment of the graph in figure 6.24. It is evident from this picture that the cart continues to vibrate; higher amplitude vibrations occur at higher velocity. Nevertheless, the tracking is accurate. The actual path of the cart converges quickly to the desired path and there is no evidence of stiction effects at velocity reversals.

The fact that the compensated system does not exhibit stiction effects during direction changes could be due to the vibration in the cart's motion. Because the cart is
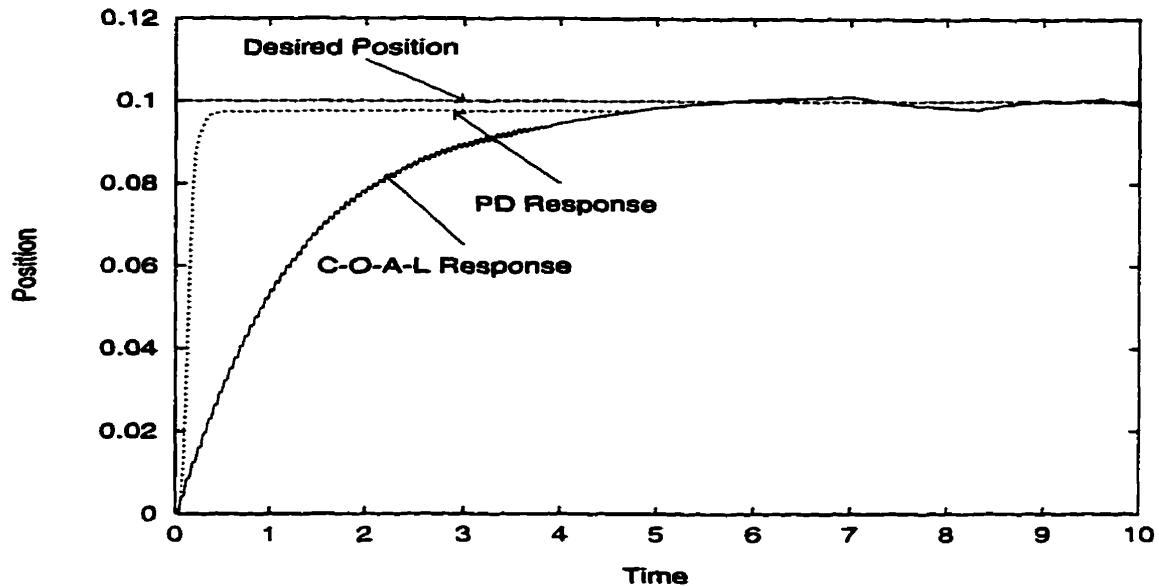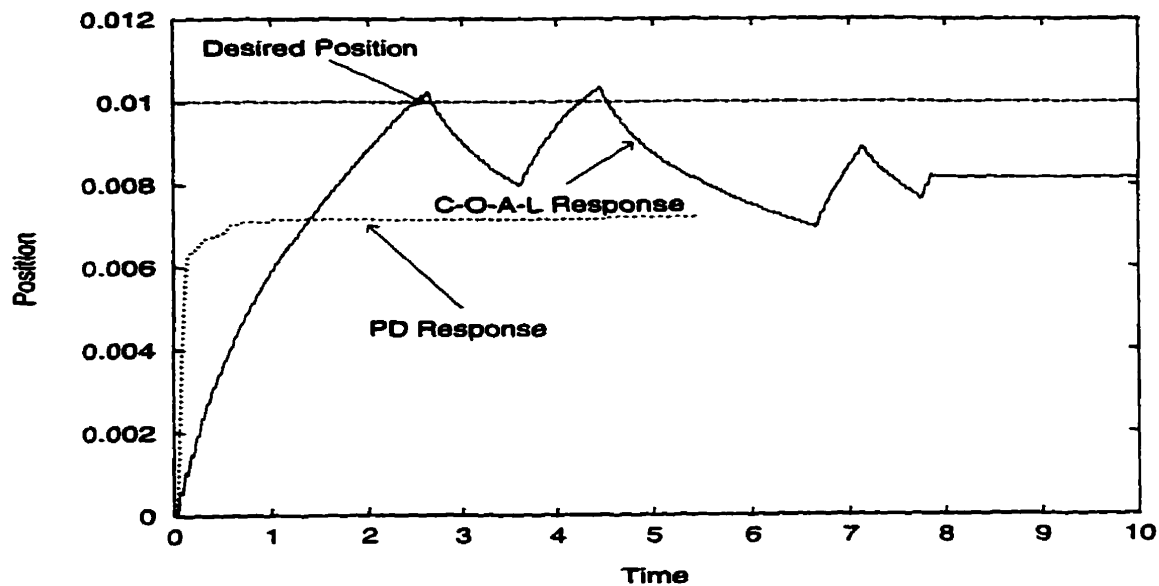
Figure 6.19: Comparison of the response of a PD controller with poles at $-13\pm13i$ and the C-O-A-L controller with $k_1 = 350\ kg/s^2$ and $k_2 = 450\ kg/s$ to $x_d = 1\ cm$

vibrating, friction is modified. In this way, the vibration may behave somewhat like dither and prevent the motion of the cart from entering the static friction regime.
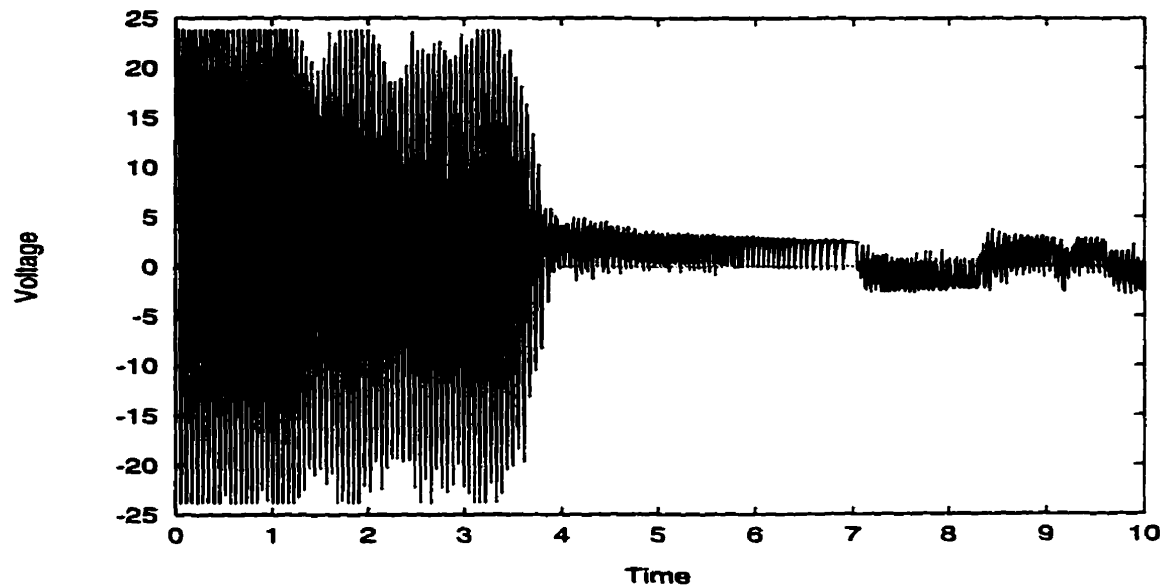
Figure 6.20: Output voltage of the C-O-A-L Controller with $k_1 = 350\ kg/s^2$, $k_2 = 450\ kg/s$ to $x_d = 10\ cm$
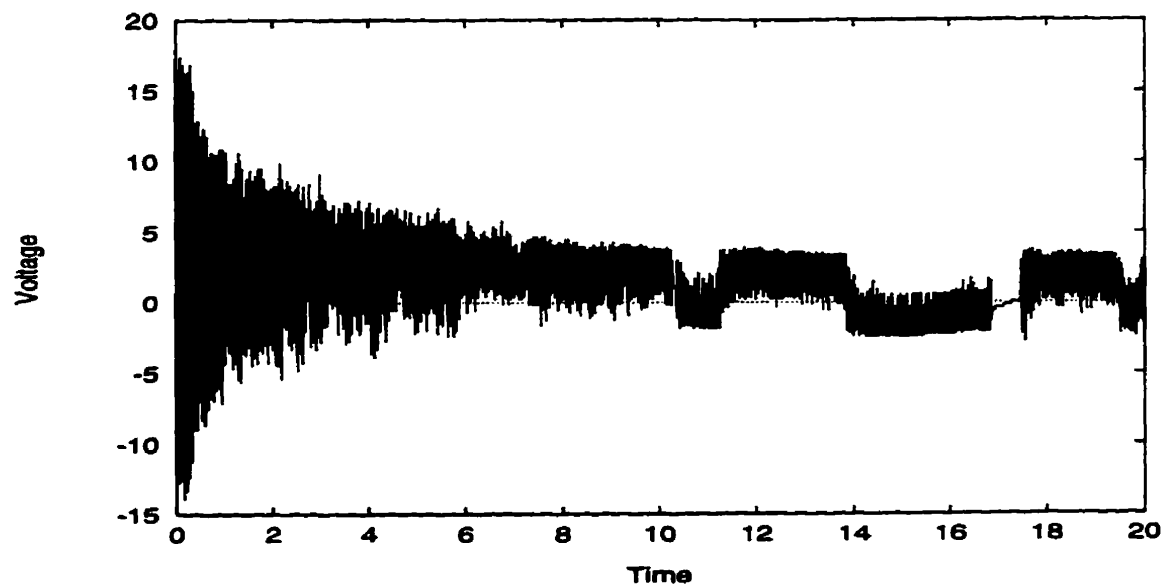
Figure 6.21: Voltage output from the C-O-A-L controller for $k_1 = 100\ kg/s^2$, $k_2 = 450\ kg/s$ with $x_d = 10\ cm$
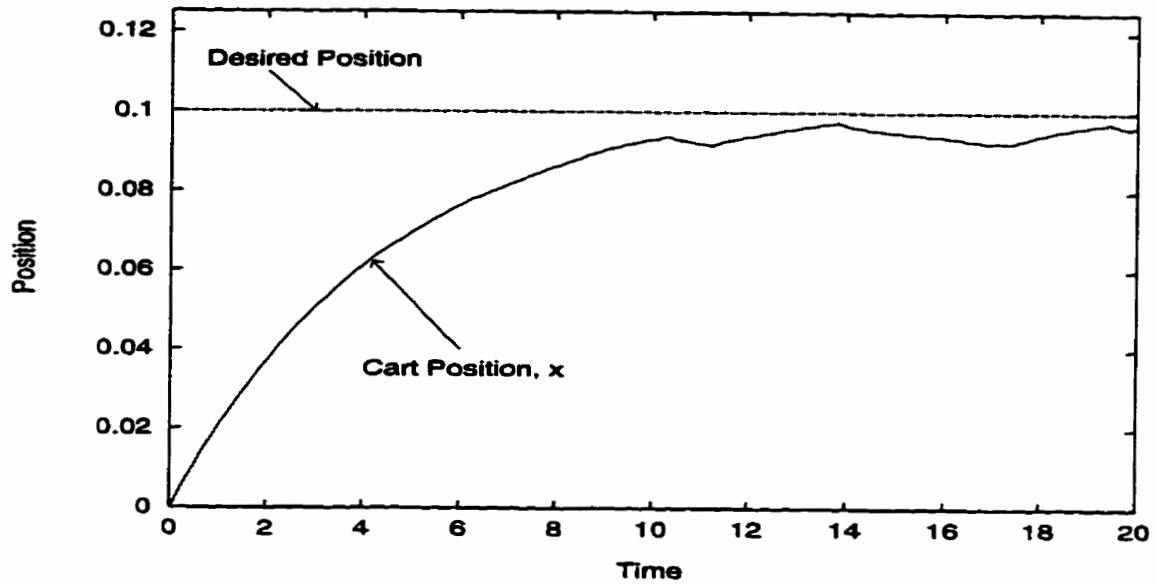
Figure 6.22: Position response of the C-O-A-L controller for $k_1 = 100 \ kg/s^2$, $k_2 = 450 \ kg/s$ to $x_d = 10 \ cm$
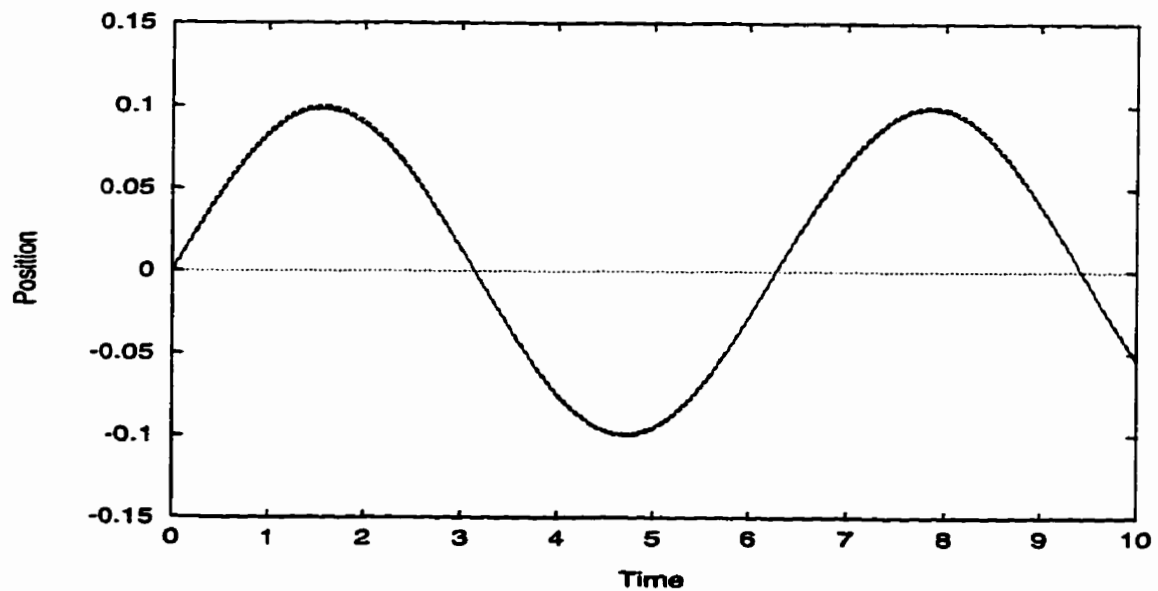
Figure 6.23: System response to tracking $x_d = 0.1sin(t) \ m$ using the C-O-A-L controller with $k_1 = 350 \ kg/s^2$, $k_2 = 450 \ kg/s$.
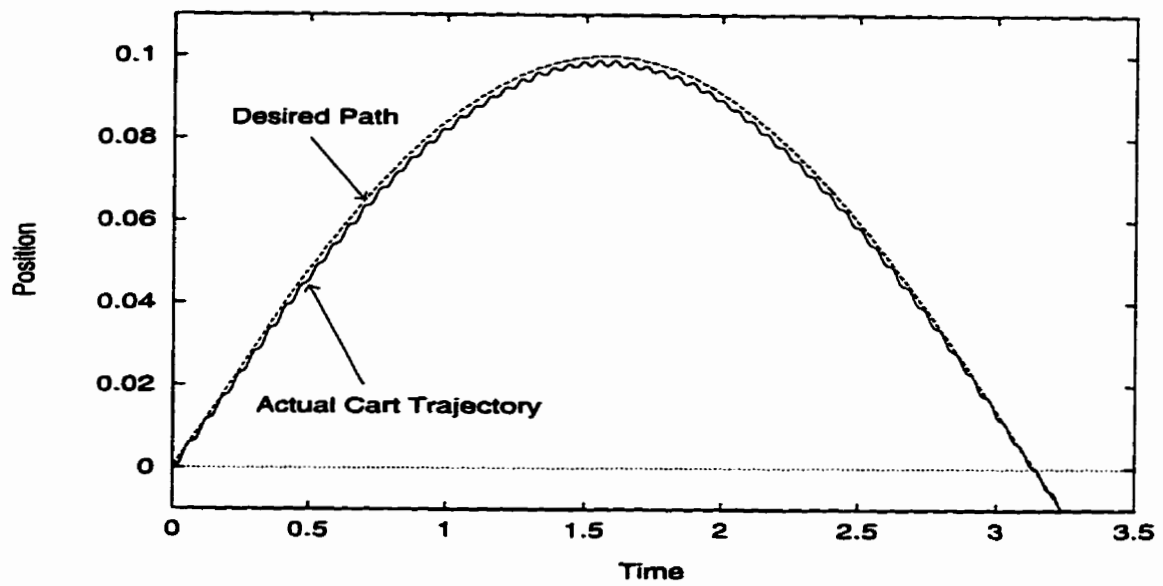
Figure 6.24: Segment of system response in figure 6.24. Tracking $x_d = 0.1sin(t)$ m with the C-O-A-L Controller

6.6 Summary

Restrictions placed on the proportional and derivative gains of the C-O-A-L control law pose experimental problems. Because of the need for a large derivative gain, damping is high and the response is slow in regulator tasks. When implemented on the servo motor-cart apparatus, large proportional gain results in voltage truncation, and vibration in the motion of the cart.

Moreover, the need for high frequency sampling introduces noise into the velocity estimate. This noise is amplified by feedback and can introduce error into the observer for the internal state z. A filter was required to smooth the velocity estimate.

For point-to-point positioning, a linear PD controller proved to be better than the C-O-A-L controller. Although PD controllers are less versatile, they are far simpler to implement and can be tuned to perform well for a particular positioning task.

For tracking a moving path, the PD controller encountered problems near zero-velocity. A linear friction model does not allow the PD to counter static friction effects. The C-O-A-L controller was capable of tracking a sinusoid with relatively high accuracy, but continued to exhibit undesirable high frequency vibrations.

In theory, the model-based friction compensation control law proposed by Canudas de Wit *et al.* [7] should perform tracking tasks better than a simple PD controller. However, the need for high gain feedback makes implementing the C-O-A-L controller difficult. One solution is to construct a different dynamic output feedback controller that allows the use of smaller proportional and derivative gains.

Chapter 7

A New Dynamic Feedback Controller and Nonlinear Observer

7.1 Introduction

Experiments with the C-O-A-L controller from Chapter 6 indicate that accuracy in positioning and tracking control can be improved via nonlinear friction compensation. However, a large derivative feedback gain is necessary with the C-O-A-L controller, resulting in excess damping, slow response, and noise amplification. Increasing the proportional gain achieves faster response, but can lead to control saturation. Hunting is also observed.

We need the freedom to choose smaller proportional and derivative feedback gains, so as not to exceed the practical limits of the mechanical system. In [20], Pomet, Hirschorn and Cebuhar construct a controller for systems where the unobserved states enter the system equations linearly. In [20] it is assumed that the output can be regulated by full state feedback. Here, the results of [20] are adapted to systems where some of the requirements of [20] are not satisfied. A Lyapunov-based dynamic controller is introduced that can be extended to a fairly large class of systems, although it applies to a less general class of systems than the strategy of [20]. Our adaptation allows a controller to be developed for the servo system, without explicitly constructing an observer for z first. This approach permits more freedom in choosing controller gains but results in a more complex observer, $\hat{z}$, whose state may not converge to z.

The general form of the adapted control strategy is presented in this chapter.

An explicit controller and friction observer are developed for the servo motor system for which stability is verified. Results using this new dynamic feedback controller are presented, and this controller is compared to a linear PD controller, and the C-O-A-L control law of Chapter 6.

7.2 The Generalized Formulation

Consider the dynamical system modeled by

$$
\begin{aligned}
\dot{x} &= a_1(x,u) + A_1(x,u)z, \\
\dot{z} &= a_2(x,u) + A_2(x,u)z, \\
y &= h(x) = x,
\end{aligned}
\tag{7.1}
$$

with input $u \in \mathbb{R}^m$ and output $y \in \mathbb{R}^k$. Here $x \in \mathbb{R}^k$, $z \in \mathbb{R}^l$ and $(x,z)^T \in \mathbb{R}^n$. The unobserved state, z, enters the system equations linearly. Under a prescribed set of assumptions, there exist a dynamic controller $u = u_{\mathrm{nom}}$ and an observer $\hat{z}$ such that the state $(x(t), z(t), \hat{z}(t))$ is bounded and $x(t) \to 0$. The first assumption requires that the unobserved state z be bounded. This is the first property of the bristle friction model of equations (4.1) and (4.2). More formally:

Assumption A1 : *There exists $a > 0$ such that for $\|z(t_0)\| \leq a$ every solution $(x(t), z(t))$ to (7.1) satisfies $\|z(t)\| \leq a \ \forall \, t \geq t_0$.*

Next, we assume that if z is available, it is possible to design a full state feedback controller, $u_{\mathrm{nom}}(x,z)$, which regulates the output. Assumption A2 allows us to conclude that y tends to zero by a Lyapunov-like analysis. It is closely related to Assumption A2 of [20] but is weaker in the sense that here, V need only be a proper function of x. In [20], V must be a proper function of both x and z, which cannot be satisfied for our system.

Assumption A2 : *There exists a continuously differentiable, positive semidefinite function V from $\mathbb{R}^k$ to $\mathbb{R}$, a positive definite $k \times k$ matrix W, and a map u_{nom} from $\mathbb{R}^n$ to $\mathbb{R}^m$ such that*

1. *The function V is proper (i.e., the preimage of a compact set is compact).*

2. *Defining the function ρ by*

$$
\rho(x,z) = -\frac{\partial V}{\partial x}(x) \left[a_1(x, u_{nom}(x,z)) + A_1(x, u_{nom}(x,z))z \right],
\tag{7.2}
$$

we have that

$$\rho(x,z) \geq x^T W x \qquad \forall\, (x,z) \in I\!\!R^n. \tag{7.3}$$

Now, we define the $n \times n$ matrix $E(x,z)$, and the $k \times n$ matrix H by

$$E(x,z) = \begin{pmatrix} 0 & A_1(x,u_{\text{nom}}(x,z)) \\ 0 & A_2(x,u_{\text{nom}}(x,z)) \end{pmatrix}, \quad H = (I_k\ \ 0).$$

The third assumption is a type of weak observability condition. If $E(x,z) = E$, i.e. is constant, then the system

$$\begin{pmatrix} \dot{x} \\ \dot{z} \end{pmatrix} = E \begin{pmatrix} x \\ z \end{pmatrix}, \tag{7.4}$$

$$y = H \begin{pmatrix} x \\ z \end{pmatrix}, \tag{7.5}$$

can be stabilized via output feedback and is, therefore, detectable. Note that observability implies detectability.

Assumption A3 : *There exist a constant positive definite $n \times n$ matrix Q and an $n \times k$ matrix $K(x,z)$ smoothly depending on (x,z) such that, for any (x,z),*

$$Q(E(x,z) - K(x,z)H) + (E(x,z) - K(x,z)H)^T Q \leq 0 \tag{7.6}$$

in the sense of symmetric matrices.

With the above assumptions, we will develop a theorem that yields a nonlinear dynamic feedback control law such that $x(t)$ converges to zero, even when z is unavailable. First define the notation that a hat over a symbol signifies that it has been evaluated with $\hat{z}$, i.e. $\hat{a}_1 = a_1(x,u_{\text{nom}}(x,\hat{z}))$, $\widehat{A}_1 = A_1(x,u_{\text{nom}}(x,\hat{z}))$ etc.; a tilde over a symbol signifies that it represents the observer error, i.e. $\tilde{z} = z - \hat{z}$.

The dynamic controller from [20] becomes

$$u = u_{\text{nom}}(x,\hat{z}), \tag{7.7}$$

$$\dot{\hat{x}} = \hat{a}_1 + \widehat{A}_1\hat{z} + \hat{K}_1\tilde{x} + P_1(x,\hat{z}), \tag{7.8}$$

$$\dot{\hat{z}} = \hat{a}_2 + \widehat{A}_2\hat{z} + \hat{K}_2\tilde{x} + P_2(x,\hat{z}), \tag{7.9}$$

with

$$P = \begin{pmatrix} P_1(x,\hat{z}) \\ p_2(x,\hat{z}) \end{pmatrix} = Q^{-1} \begin{pmatrix} 0 \\ \widehat{A}_1^T \left(\frac{\partial V}{\partial x}\right)^T \end{pmatrix} \tag{7.10}$$

and Q, $K = \begin{pmatrix} K_1 \\ K_2 \end{pmatrix}$ given by assumption A3. The following theorem is essentially Theorem 1 from [20].

Theorem 7.1 *Under assumptions A1, A2 and A3, the dynamic controller achieves the following property for the closed loop system: for any initial conditions, the state $(x(t), z(t), \hat{x}(t), \hat{z}(t))$ is bounded and $x(t) \to 0$.*

The proof of this theorem is based on the following lemma:

Lemma 7.1.1 *The derivative of the function*

$$U(x, \hat{x}, z, \hat{z}) = V(x)|\frac{1}{2}(\tilde{x}^T, \tilde{z}^T)Q(\tilde{x}, \tilde{z})^T \tag{7.11}$$

along the solutions of the closed-loop system obtained with the controller 7.7 is given by:

$$\dot{U} = -\rho(x, \hat{z}) + \frac{1}{2}(\tilde{x}^T, \tilde{z}^T)\left[Q(\widehat{E} - \hat{K}H) + (\widehat{E} - \hat{K}H)^T Q\right](\tilde{x}, \tilde{z})^T. \tag{7.12}$$

The proofs of the Theorem 7.1 and Lemma 7.1.1 can be found in [20].

In [20], a special case exists for Assumption A3 that results in a simplified, reduced-order controller. The special case is applicable to our servo motor system.

Assumption A3′ : *There exists a (constant) positive definite $\ell \times \ell$ matrix Q_2 such that, for any $(x, z) \in \mathbb{R}^n$,*

$$Q_2 A_2(x, u_{\text{nom}}(x, z)) + A_2(x, u_{\text{nom}}(x, z))^T Q_2 \leq 0. \tag{7.13}$$

The following theorem gives the reduced order controller for the case where assumption A3′ holds.

Theorem 7.2 *Under assumptions A1, A2 and A3′, the dynamic controller*

$$u = u_{\text{nom}}(x, \hat{z}) \tag{7.14}$$

$$\dot{\hat{z}} = \hat{a}_2 + \hat{A}_2\hat{z} + Q_2^{-1}\widetilde{A}_1^T(\frac{\partial V}{\partial x})^T \tag{7.15}$$

achieves the following property for the closed-loop system: for any initial conditions, the state $(x(t), z(t), \hat{z}(t))$ is bounded, and $x(t) \to 0$.

Proof:

Define a Lyapunov function candidate by $U(x, z, \hat{z}) = V + (1/2)\tilde{z}^T Q_2 \tilde{z}$, where V is the positive definite function defined in assumption A2; $Q_2 > 0$ and is defined in assumption A3'. Then, taking derivatives along the system trajectories, we will have

$$\dot{U}(x(t), z(t), \hat{z}(t)) = -\rho(x, \hat{z}) + \frac{1}{2}\tilde{z}^T[Q_2\hat{A}_2 + \hat{A}_2^T Q_2]\tilde{z}.$$

Using the dynamic feedback controller, $u_{\text{nom}}(x, \hat{z})$, yields the closed loop system

$$\begin{aligned}
\dot{x} &= \hat{a}_1 + \widehat{A}_1\hat{z}, \\
\dot{z} &= \hat{a}_2 + \widehat{A}_2 z, \\
\dot{\hat{z}} &= \hat{a}_2 + \widehat{A}_2\hat{z} + Q_2^{-1}\widehat{A}_1^T\left(\frac{\partial V}{\partial x}\right)^T.
\end{aligned} \tag{7.16}$$

For simplicity define

$$M(x, \hat{z}) = Q_2^{-1}\widehat{A}_1^T\left(\frac{\partial V}{\partial x}\right)^T.$$

The derivative of V is given by

$$\dot{V} = \frac{\partial V}{\partial x}(\hat{a}_1 + \widehat{A}_1 z). \tag{7.17}$$

From assumption A2,

$$\rho(x, \hat{z}) = -\frac{\partial \widehat{V}}{\partial x}(\hat{a}_1 + \widehat{A}_1\hat{z}).$$

If we add and subtract $\rho(x, \hat{z})$ from the equation for $\dot{V}$, it follows from (7.17) that

$$\begin{aligned}
\dot{V} &= -\rho(x, \hat{z}) - \frac{\partial \widehat{V}}{\partial x}(\hat{a}_1 + \widehat{A}_1\hat{z}) + \frac{\partial V}{\partial x}(\hat{a}_1 + \widehat{A}_1 z), \\
&= -\rho(x, \hat{z}) + \frac{\partial V}{\partial x}\widehat{A}_1\tilde{z} + \left(\frac{\partial V}{\partial x} - \frac{\partial \widehat{V}}{\partial x}\right)(\hat{a}_1 + \widehat{A}_1\hat{z}).
\end{aligned} \tag{7.18}$$

From assumption A2, we know that V is a function of x and not of z, so $\widehat{V} \equiv V$ and

$$\frac{\partial V}{\partial x} \equiv \frac{\partial \widehat{V}}{\partial x}.$$

Hence

$$\dot{V} = -\rho(x, \hat{z}) + \frac{\partial V}{\partial x}\widehat{A}_1\tilde{z}. \tag{7.19}$$

Taking the time derivative of U along solution curves of the closed loop system (7.16) yields

$$\dot{U} = \dot{V} + \tilde{z}^T Q_2(\dot{z} - \dot{\hat{z}}), \tag{7.20}$$

where

$$\dot{z} - \dot{\hat{z}} = \hat{a}_2 + \widehat{A}_2 z - \hat{a}_2 - \widehat{A}_2 \hat{z} - M(x, \hat{z}),$$

$$= \widehat{A}_2 \tilde{z} - M(x, \hat{z}). \tag{7.21}$$

Substituting (7.21) into (7.20) yields

$$\dot{U} = \dot{V} + \tilde{z}^T Q_2(\widehat{A}_2 \tilde{z} - M(x)),$$

$$= \dot{V} + (\frac{1}{2})\tilde{z}^T(Q_2\widehat{A}_2 + \widehat{A}_2^T Q_2)\tilde{z} - \tilde{z}^T Q_2 M(x), \tag{7.22}$$

$$= -\rho(x, \hat{z}) + \frac{\partial V}{\partial x}\widehat{A}_1 \tilde{z} + (\frac{1}{2})\tilde{z}^T(Q_2\widehat{A}_2 + \widehat{A}_2^T Q_2)\tilde{z} - \tilde{z}^T Q_2 M(x).$$

Recall that $M(x) = Q_2^{-1}\widehat{A}_1^T\left(\frac{\partial V}{\partial x}\right)^T$ by definition. Therefore,

$$\dot{U} = -\rho(x, \hat{z}) + (\frac{1}{2})\tilde{z}^T(Q_2\widehat{A}_2 + \widehat{A}_2^T Q_2)\tilde{z}. \tag{7.23}$$

Under assumption A3′, $Q_2\widehat{A}_2 + \widehat{A}_2^T Q_2 \leq 0$. Thus, by assumptions A2 and A3′, $\dot{U} \leq x^T W x$. Hence $x \to 0$ and $\tilde{z}$ is bounded. We know that z is bounded from assumption A1, so it is reasonable to conclude that $\hat{z} = z + \tilde{z}$ is also bounded. Therefore, under assumptions A1, A2 and A3′, it follows that $(x(t), z(t), \hat{z}(t))$ is bounded and $x(t) \to 0$.

7.3 The Servo-Motor Problem

Recall the model for the servo motor-cart system from equation (5.1), which is

$$m\ddot{x} = Ku - F.$$

Define

$$x_1 = x,$$
$$x_2 = \dot{x}, \tag{7.24}$$
$$p(x_2) = \frac{|x_2|}{g(x_2)}.$$

We know from Chapter 4 that $g(x_2) > 0$ for all x_2. Therefore, $p(x_2) > 0$. With the bristle friction model from equations (4.1) and (4.2), the open-loop system model can be written

$$\dot{x}_1 = x_2,$$
$$\dot{x}_2 = \left(\frac{1}{m}\right)(Ku - \sigma_0 z - \sigma_1 \dot{z} - \sigma_2 x_2),$$
$$= \left(\frac{1}{m}\right)(Ku - \sigma_0 z - \sigma_1(x_2 - p(x_2))z - \sigma_2 x_2), \tag{7.25}$$
$$\dot{z} = x_2 - p(x_2)z,$$

where the observed states are $x1 \in I\!R$, $x2 \in I\!R$, and the unobserved state, $z \in I\!R$, enters the equations linearly. Hence the above system of equations can be written in the form of (7.1);

$$\begin{aligned} \dot{x} &= a_1(x, u) + A_1(x)z \\ \dot{z} &= a_2(x) + A_2(x)z \end{aligned}$$

where

$$a_1 = \begin{pmatrix} x_2 \\ (\frac{1}{m})(Ku - (\sigma_1 + \sigma_2)x_2) \end{pmatrix}, \quad A_1 = \begin{pmatrix} 0 \\ (\frac{1}{m})(\sigma_1 p(x_2) - \sigma_0) \end{pmatrix}, \quad (7.26)$$

$$a_2 = (x_2), \quad A_2 = -p(x_2). \quad (7.27)$$

In order for Theorem 7.2 to apply, we require that assumptions A1, A2 and A3' hold. Assumption A1 requires that z be bounded for all time. The first property of the bristle model of equation (4.1) is finite bristle deflection, so A1 holds for $|z(t_0)|$ sufficiently small.

Assumption A2 allows us to conclude that if z is available, then there exists a feedback controller, $u_{\text{nom}}(x, z)$, such that for a positive definite function V, $\dot{V} \leq 0$ implies that $x(t) \to 0$. Suppose the control input, Ku, in the system (7.25) combines proportional and derivative feedback with nonlinear model-based friction compensation; let

$$u_{\text{nom}} = Ku = \alpha x_1 + \beta x_2 + (\sigma_1 + \sigma_2)x_2 + (\sigma_0 - \sigma_1 p(x_2))z. \quad (7.28)$$

Then the closed loop system becomes

$$\begin{aligned} \dot{x}_1 &= x_2, \\ \dot{x}_2 &= \left(\frac{1}{m}\right)(\alpha x_2 + \beta x_1), \quad (7.29) \\ \dot{z} &= x_2 - p(x_2)z. \end{aligned}$$

This can be written in the form

$$\begin{aligned} \dot{x} &= Ax \\ \dot{z} &= a_2(x) + A_2\tilde{z} \end{aligned}$$

where

$$A = \begin{pmatrix} 0 & 1 \\ \frac{\alpha}{m} & \frac{\beta}{m} \end{pmatrix}, \quad (7.30)$$

and a_2, A_2 are defined by (7.27).

If α and β in A are chosen so that the eigenvalues of A fall in the left half of the complex plane, then $\dot{x} = Ax$ is a stable system. Thus Lyapunov's equation can be solved; given $T > 0$, there exists a positive definite matrix $P > 0$ such that

$$PA + A^T P = -T \quad . \tag{7.31}$$

Let $V = x^T P x$. Let $\rho(x, z)$ be as defined in assumption A2, i.e.

$$\rho(x, z) = -\frac{\partial V}{\partial x}(x) \left[a_1(x, u_{\text{nom}}(x, z)) + A_1(x, u_{\text{nom}}(x, z))z \right]. \tag{7.32}$$

It follows from equation (7.32) that

$$\begin{aligned} \rho(x, z) &= -\frac{\partial V}{\partial x}(x) \begin{pmatrix} x_2 \\ \frac{\alpha x_2}{m} + \frac{\beta x_1}{m} \end{pmatrix}, \\ &= -\frac{\partial V}{\partial x}(x) Ax. \end{aligned}$$

Hence

$$\begin{aligned} \rho(x, z) &= -x^T (PA + A^T P)x, \\ &= x^T T x. \end{aligned}$$

Assumption A2 requires that $\rho(x, z) \geq x^T W x$. Thus, for $\|T\| \geq \|W\|$, assumption A2 holds.

Finally, define $Q_2 = \gamma$, where γ is a positive constant scalar. With $A_2 = -p(x_2)$ from (7.27) we have

$$Q_2 A_2 + A_2^T Q_2 = -2p(x_2)\gamma \leq 0. \tag{7.33}$$

Thus assumption A3$'$ holds. Hence for $Ku = u_{\text{nom}}(x, \hat{z})$, where

$$u_{\text{nom}}(x, \hat{z}) = \alpha x_1 + \beta x_2 + (\sigma_1 + \sigma_2)x_2 + (\sigma_0 - \sigma_1 p(x_2))\hat{z}, \tag{7.34}$$

we have

$$\dot{\hat{z}} = x_2 - p(x_2)\hat{z} + Q_2^{-1} \widehat{A}_1^T \left(\frac{\partial V}{\partial x}\right)^T, \tag{7.35}$$

$$= x_2 - p(x_2)\hat{z} + \frac{2\widehat{A}_1^T P}{\gamma} \begin{pmatrix} x_1 \\ x_2 \end{pmatrix}. \tag{7.36}$$

Therefore, $(x_1(t), x_2(t), z(t), \hat{z}(t))$ is bounded and $(x_1(t), x_2(t)) \to 0$ by Theorem 7.2.

The position error, $e = x - x_d$, and velocity error, $\dot{e} = \dot{x} - \dot{x}_d$, are used in the proportional and derivative feedback for tracking control. Define $e_1 = e$ and $e_2 = \dot{e}$. Then the appropriate dynamic feedback control law is given by

$$u_{\mathrm{nom}}(x, \hat{z}) = \alpha e_1 + \beta e_2 + (\sigma_1 + \sigma_2)x_2 + (\sigma_0 - \sigma_1 p(x_2))\hat{z} + m\ddot{x}_d, \qquad (7.37)$$

$$\dot{\hat{z}} = x_2 - p(x_2)\hat{z} + \frac{2\widehat{A}_1^T P}{\gamma}\begin{pmatrix} e_1 \\ e_2 \end{pmatrix}. \qquad (7.38)$$

The closed loop system becomes

$$\begin{aligned}
\dot{x}_1 &= x_2, \\
\dot{x}_2 &= \left(\frac{1}{m}\right)(\alpha e_1 + \beta e_2 + (\sigma_1 p(x_2) - \sigma_0)(z - \hat{z}) + \ddot{x}_d), \qquad (7.39) \\
\dot{z} &= x_2 - p(x_2)z, \\
\dot{\hat{z}} &= x_2 - p(x_2)\hat{z} + \frac{2\widehat{A}_1^T P}{\gamma}\begin{pmatrix} e_1 \\ e_2 \end{pmatrix}.
\end{aligned}$$

Alternatively,

$$\begin{aligned}
\dot{e}_1 &= e_2, \\
\dot{e}_2 &= \left(\frac{1}{m}\right)(\alpha e_1 + \beta e_2 + (\sigma_1 p(x_2) - \sigma_0)\tilde{z}), \qquad (7.40) \\
\dot{\tilde{z}} &= -p(x_2)\tilde{z} - \frac{2\widehat{A}_1^T P}{\gamma}\begin{pmatrix} e_1 \\ e_2 \end{pmatrix}.
\end{aligned}$$

The stability of the system given by (7.40) can be verified using Lyapunov's direct method.

Theorem 7.3 ([19]) **Lyapunov's Theorem** *Let E be a open subset of $\mathbb{R}^n$ containing x_0. Suppose that $f \in C^1(E)$ and that $f(x_0) = 0$. Suppose further that there exists a function $V \in C^1(E)$ satisfying $V(x_0) = 0$ and $V > 0$ if $x \neq x_0$. Then (a) if $\dot{V}(x) \leq 0$ for all $x \in E$, x is stable; (b) if $\dot{V}(x) < 0$ for all $x \in E$ except x_0, x_0 is asymptotically stable; (c) if $\dot{V}(x) > 0$ for all $x \in E$ except x_0, x_0 is unstable.*

A proof of Lyapunov's Theorem is available in [19].

Define a candidate for a Lyapunov function,

$$U(e, \tilde{z}) = V + (1/2)\tilde{z}^2 \gamma. \qquad (7.41)$$

Define $e = [e_1 \ e_2]^T$ and $V = e^T Pe$ where P solves equation (7.31). Note that $U \geq 0$ and $U = 0$ only if $(e, \tilde{z}) = (0, 0)$. Taking the derivative of U along trajectories of the system (7.40) yields

$$
\begin{aligned}
\dot{U}(e, \tilde{z}) &= -e^T T e + 2\widehat{A}_1^T Pe\tilde{z} + \gamma\tilde{z}(\dot{\tilde{z}}), \\
&= -e^T T e + 2\widehat{A}_1^T Pe\tilde{z} + \gamma\tilde{z}\left(-p(x_2)\tilde{z} - \frac{\widehat{A}_1^T Pe}{\gamma}\right), \\
&= -e^T T e - \gamma\tilde{z}^2 p(x_2).
\end{aligned}
\tag{7.42}
$$

Hence $\dot{U} \leq 0$ for all $(e, \tilde{z})$. By Lyapunov's Theorem, $(e, \tilde{z}) = (0, 0)$ is stable. Thus $(e, \tilde{z})$ is bounded. In addition, $\dot{U} = 0$ implies that $e = 0$, but does not imply that $\tilde{z} = 0$. Thus $e \rightarrow 0$ asymptotically and $\tilde{z}$ is bounded. Because both $\tilde{z}$ and z are bounded, we conclude that $\hat{z} = z + \tilde{z}$ is also bounded. Therefore, $(e(t), z(t), \hat{z}(t))$ is bounded for the closed loop system (7.39) and $e(t) \rightarrow 0$.

7.4 Experimental Procedure

In order to implement the new dynamic feedback controller, the differential equation for $\hat{z}$ must be explicitly defined for the servo system; the term $2\widehat{A}_1^T Pe/\gamma$ from equation (7.35) must be explicitly computed. Recall that P is solves Lyapunov's equation with A defined in (7.30) and $T > 0$, i.e.

$$
PA + A^T P = -T.
$$

We can choose scalars $h > 0$ and $l > 0$ so that

$$
T = \begin{pmatrix} h & 0 \\ 0 & l \end{pmatrix} > 0.
\tag{7.43}
$$

From (7.30), A is given by

$$
A = \begin{pmatrix} 0 & 1 \\ \frac{\alpha}{m} & \frac{\beta}{m} \end{pmatrix},
$$

and P can be determined by solving equation (7.31), which yields

$$
P = \begin{pmatrix} \frac{\beta^2 h + \alpha^2 l - \alpha m h}{2\alpha\beta} & -\frac{mh}{2\alpha} \\ -\frac{mh}{2\alpha} & -\frac{m(\alpha l - mh)}{2\alpha\beta} \end{pmatrix}.
$$

Given the vector $e = [e_1, e_2]^T$ and the matrix A_1 from (7.26)

$$\widehat{A}_1 = A_1 = \begin{pmatrix} 0 \\ -\frac{\sigma_0}{m} + \frac{\sigma_1 p(x_2)}{m} \end{pmatrix},$$

an explicit form of the observer $\hat{z}$ can be expressed in terms of α, β, γ, h, and l, namely

$$\dot{\hat{z}} = x_2 - p(x_2)\hat{z} + \frac{(-\sigma_0 + \sigma_1 p(x_2)) (he_1 \beta + e_2 \alpha l - e_2 mh)}{\gamma \alpha \beta}. \tag{7.44}$$

7.4.1 PD Control Parameters

The proportional and derivative gains, α and β of equation (7.37), are chosen to stabilize the linear system $\dot{x} = Ax$, where

$$A = \begin{pmatrix} 0 & 1 \\ \frac{\alpha}{m} & \frac{\beta}{m} \end{pmatrix}.$$

The eigenvalues of A are the roots of the characteristic equation, $det(Is - A) = 0$. The characteristic equation for A is given by

$$ms^2 - \beta s - \alpha = 0. \tag{7.45}$$

In order for A to be stable, we want the roots of equation (7.45) to be in $Re[s] < 0$. Let $s = -b_1 \pm b_2 i$, with $b_1 > 0$ and $b_2 > 0$, $b_1, b_2 \in R$. Thus the desired characteristic polynomial is

$$s^2 + 2b_1 s + b_1{}^2 + b_2{}^2 = 0. \tag{7.46}$$

Hence, from equations (7.45) and (7.46), A has stable eigenvalues for α and β given by

$$\beta = -2mb_1, \tag{7.47}$$

$$\alpha = -m(b_1{}^2 + b_2{}^2). \tag{7.48}$$

Therefore, for the new dynamic feedback control law of equation (7.37), we have the flexibility to use optimal gains of any magnitude for the linear feedback; the PD gains for (7.37) can be much smaller than those required for the C-O-A-L controller. Note that the linear system $\dot{x} = Ax$ captures no friction effects.

7.4.2 Observer Parameters

From equations (7.44), and (7.37), the dynamic feedback controller for the servo system is given by

$$
\begin{aligned}
u_{\text{nom}} &= \alpha e_1 + \beta e_2 + \sigma_0 \hat{z} + \sigma_1 (x_2 - p(x_2)\hat{z}) + \sigma_2 x_2 + \ddot{x}_d, \quad\quad (7.49)\\
\dot{\hat{z}} &= x_2 - p(x_2)\hat{z} + \frac{(-\sigma_0 + \sigma_1 \, p(x_2))\,(he_1 \,\beta + e_2\,\alpha l - e_2\, mh)}{\gamma \alpha \beta}.
\end{aligned}
$$

This is similar to the C-O-A-L controller from chapter 6, given by

$$
\begin{aligned}
u_{\text{nom}} &= -k_1 e_1 - k_2 e_2 + \sigma_0 \hat{z} + \sigma_1 (x_2 - p(x_2)\hat{z} - ke_1) + \sigma_2 x_2 + m\ddot{x}_d \quad\quad (7.50)\\
\dot{\hat{z}} &= x_2 - p(x_2)\hat{z} - ke_1.
\end{aligned}
$$

The two control schemes differ in the structure of the governing equation for $\hat{z}$. The observer of (7.50) includes a term that is proportional to the position error, ke_1. Thus an appropriate value for k must be chosen in order to implement the C-O-A-L; this was discussed in Chapter 6. The dynamic feedback of (7.49) is more complex and includes a term that is a function of both position error, and velocity error. Setting

$$
q(e) = \frac{(-\sigma_0 + \sigma_1 \, p(x_2))\,(he_1 \,\beta + e_2\,\alpha l - e_2\, mh)}{\gamma \alpha \beta}. \quad\quad (7.51)
$$

we have

$$
\dot{\hat{z}} = x_2 - p(x_2)\hat{z} - q(e). \quad\quad (7.52)
$$

To explicitly compute a value of $\hat{z}$ in (7.49), we must first determine suitable values for the parameters h, l and γ.

Choosing γ:

All three parameters appear in both the governing equation for $\hat{z}$, and in the derivative of the Lyapunov function U, defined in equation (7.41). The magnitude of $\dot{U}$, defined in (7.42), is directly related to the rate of convergence of the states of system (7.40) because closed-loop stability implies that $\dot{U} \leq 0$ along trajectories of the system. From equation (7.42), we note that the observer error, $\tilde{z}$, is scaled by γ in the same way that it is scaled by $1/k$ in equation (6.13). Theorem 7.2 does not guarantee that $\tilde{z}$ will converge to zero, but a large value for γ results in a small bound on $\tilde{z}$.

The magnitude of $\dot{\hat{z}}$ in equation (7.49) is influenced by γ in the same way that $\dot{\hat{z}}$ in equation (7.50) is affected by $1/k$. In Chapter 6 we noted that k should be kept small

so that $|\hat{z}|$ is comparable to $|z|$. By a similar argument, γ should be large so that $q(e)$ does not dominate the differential equation governing $\hat{z}$.

Finally, consider $q(e)$ for $e_2 = 0$ and $e_1 \neq 0$. This can occur in point-to-point positioning when the motion of the cart stops a distance e_1 from the reference point. From (7.51), it follows that

$$q(e) = \frac{-\sigma_0 h e_1}{\gamma \alpha},$$

and therefore

$$\dot{\hat{z}} = \frac{\sigma_0 h e_1}{\gamma \alpha}.$$

In this case, $u_{\text{nom}} = \alpha e_1 + \sigma_0 \hat{z}$, and the term $\sigma_0 \hat{z}$ behaves as integral action. The values of h and γ influence the effect of this integral action on the overall performance of the controller. Integral action is known to cause hunting in some cases [24], so we wish to keep the integral gain small. Thus a moderate value for h, and a large value for γ is desirable.

Simulations have shown that, ideally, there is no upper bound on γ. However, for finite but very large γ, $q(e)$ has no significant effect on $\hat{z}$; the observer error $\tilde{z}$ is assumed to be very small and converges almost immediately. This is unrealistic in practical situations. A value of $\gamma = \sigma_0(10^4)$ was used for all experiments.

Choosing h and l:

From equation (7.42),

$$\dot{U} = -e^T T e + \gamma \tilde{z}^2 p(x_2).$$

If U represents control energy, then h and l behave as cost coefficients for the states e_1 and e_2. If both are large, then both e_1 and e_2 should converge quickly. On the other hand, it is possible to weight the matrix T so that priority can be placed on reducing one or the other. Choosing a large h relative to l associates a high cost with position error; the controller will work to reduce e_1 quickly, thereby reducing controller energy.

Both l and h also arise in equation (7.49) via the term $q(e)$. We wish for h to be large relative to l, but not so large as to increase the impact of integral action on the system. Thus a small value for l is desirable. Simulations indicate that there is no lower bound on l. However, if l is too small, the controller associates almost no energy loss with a large velocity error.

It is difficult to find an optimal cost matrix T. Through simulation, values of $h = 20$ and $l = 0.1$, along with $\gamma = \sigma_0(10^4)$, proved to result in a well-behaved closed-loop response for the system (7.40). Thus $h = 20$ and $l = 0.1$ were adopted for experimental use. It should be noted that with $h = 20$ and $\gamma = \sigma_0(10^4)$, the integral gain $k_i = \sigma_0^2 h/\gamma\alpha$ for $e_2 = 0$, is $k_i = 200/\alpha$. With poles placed at $-4 \pm 4i$, $k_i \approx 6.3$. The magnitude of k_i decreases with larger gains. Thus $k_i \leq 6.3$, which is small compared to the PD gains employed.

7.4.3 Experimental Implementation

The experimental considerations for implementing friction compensation were discussed in Chapter 6. Similar issues arise in experiments using the new dynamic feedback controller of equation (7.49), with a few notable differences.

The governing equation for $\hat{z}$ here is (7.49), a more complex equation than (7.50). Furthermore, the freedom to choose complex pole placement to determine gains α and β for (7.49) results in a faster response of the cart, and faster rate of change of $\hat{z}$. The farther poles are placed from the imaginary axis along the 45 degree line, the faster the dynamics of $\hat{z}$. Thus, for experiments with the controller of (7.49), a sampling frequency of 5000 Hz was needed; this is higher than the sampling rate of 3000 Hz used with the C-O-A-L controller.

Using a sampling frequency of 5000 Hz increases the noise in the estimate for velocity. Velocity was estimated every 25 cycles for experiments with the new dynamic feedback controller; the rate used with the C-O-A-L controller was every 10 cycles. The velocity signal was smoothed at each step with the first order filter

$$x_{2smooth} = \delta t(ax_{2noisy} - ax_{2smooth}) + x_{2noisy}.$$

Here a was reduced from $a = 80$ to $a = 60$, to increase smoothing. It should be noted that at a sampling rate of 5000 Hz, noise in the velocity estimate cannot be completely filtered out. This does not pose problems at high velocities, but may introduce error at low velocities where sign changes are critical to $\hat{z}$.

With both the new dynamic feedback control law in equation (7.49) and the C-O-A-L controller, a steady state value for $\hat{z}$ of $\hat{z}_{ss} = g(v)sgn(v)$ was assigned for velocities greater than $0.1 \; m/s$. This reduced computation and observer error.
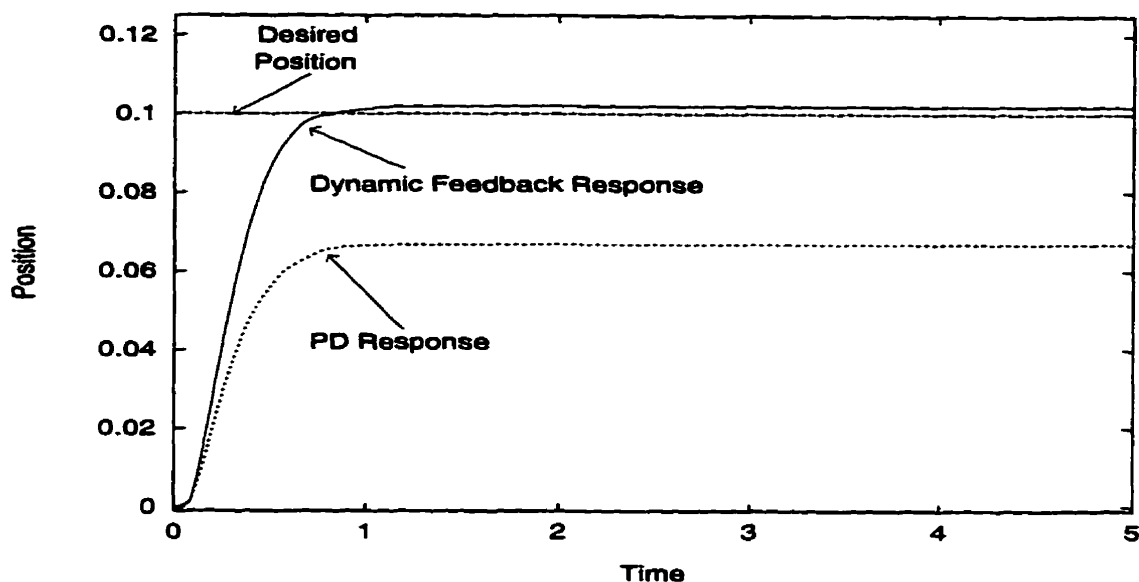
7.5 Experimental Results

Figure 7.1: Response of the new dynamic feedback control law with friction compensation and straight PD control to $x_d = 10\ cm$ with poles at $-4 \pm 4i$.

The new dynamic feedback control scheme was tested for both point-to-point positioning and tracking of a slow moving path. The results of the same tests, using the C-O-A-L controller, are discussed in Chapter 6. Because of the structure of our controller (equation (7.49)), it is natural to compare its performance to that of a linear PD controller. The comparison allows us to assess the value of friction compensation with optimal PD feedback gains. Control engineers usually include linear friction in the model of a mechanical system. Therefore, we include a viscous friction term in the system model used with PD feedback control. A viscous friction coefficient of 4.6 has been adopted for this purpose.

7.5.1 Comparison of Dynamic Feedback Control to PD: The Regulator

Figure 7.1 shows the response of both a PD controller and the new dynamic feedback controller to $x_d = 10\ cm$. The poles for both the linear component of the new dynamic feedback controller, and the PD controller are placed at $-4 \pm 4i$. The response of the PD controller exhibits high steady state error; it is approximately 35%. In this case the dynamic feedback control law responds more quickly than the linear PD. In addition, with friction
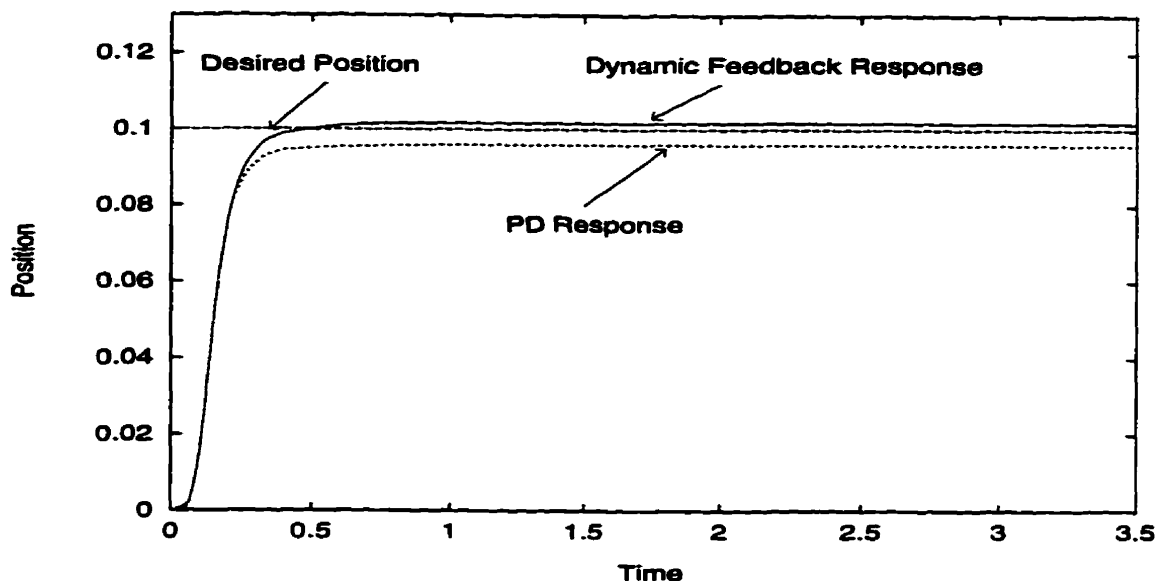
Figure 7.2: Response of the new dynamic feedback controller with friction compensation, compared to that of a PD controller to $x_d = 10$ cm with poles at $-10 \pm 10i$.

compensation, the steady state error is reduced to approximately 2%.

Figure 7.2 shows the position responses of both the linear PD controller and the dynamic feedback controller to $x_d = 10$ cm. The input is the same as in figure 7.1, but the poles have been pushed out to $-10 \pm 10i$. The controller with dynamic feedback, like the PD, responds more quickly with larger proportional and derivative gains. Both controllers respond quickly, but with added friction compensation, the steady state error of the PD controller is reduced from about 5% to 2%.

The new dynamic feedback controller is superior to a straight PD controller for this positioning task. Although both can achieve good performance with large feedback gains, the addition of friction compensation provides high accuracy positioning with small feedback gains.

It is also important to assess the merits of friction compensation for fine positioning. Figure 7.3 shows the performance of both the PD and the dynamic feedback controllers in response to $x_d = 1$ cm, with pole placement at $-10 \pm 10i$. Once again, it is clear that friction compensation significantly reduces steady state error. The steady state error of the dynamic feedback controller here is almost 10%. This is relatively large compared to the error in figure 7.2. However, the performance is much better than that of the PD controller;
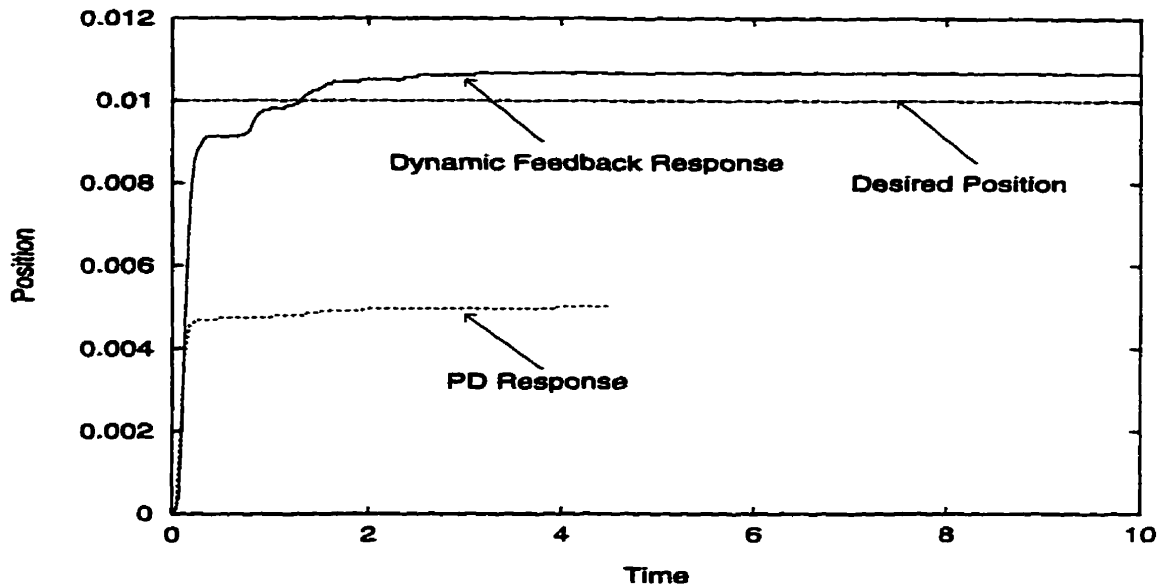
Figure 7.3: Response of the new dynamic feedback control law with friction compensation and straight PD control to $x_d = 1$ cm with poles at $-10 \pm 10i$.

there is little need for re-tuning.

We expect that reducing the proportional and derivative gains will hamper the performance of both controllers in fine positioning. The response of both controllers to $x_d = 1$ cm, with poles at $-4 \pm 4i$ is displayed in figure 7.4. The PD controller does not respond here, since the proportional gain, together with the small position error, is insufficient to overcome static friction. The dynamic feedback controller responds surprisingly well. However, the cart exhibits unsteady motion near the reference point, and slowly overshoots the desired position.

7.5.2 Comparison of Dynamic Feedback Controller to a PD: Tracking

The new dynamic feedback controller was used to track a slow moving path. Figure 7.5 shows the position response to $x_d = 0.1sin(t)$ m for both the dynamic feedback controller and a PD controller with poles at $-4 \pm 4i$. The straight PD controller encounters stiction effects at zero velocity, as well as exhibiting large steady state error. The steady state error is much lower in the system with friction compensation. However, static friction effects are present at velocity reversals.

The position response to the same sinusoidal input, of both the PD and the dy-
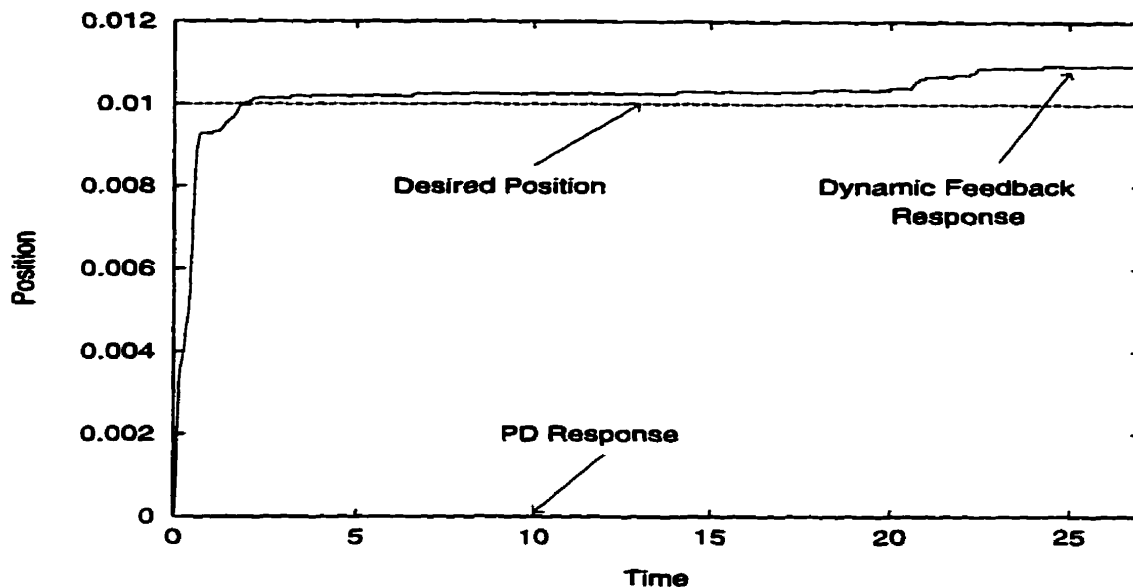
Figure 7.4: Response of the new dynamic feedback controller with friction compensation, compared to that of a PD controller to $x_d = 1\ cm$ with poles at $-4 \pm 4i$.

namic feedback controller with poles at $-10 \pm 10i$, is shown in figure 7.6. It is evident that the performance of both controllers has improved over that shown in figure 7.5, but the steady state error in the PD response has not been eliminated. The system with nonlinear friction compensation tracks very well, but exhibits small stiction effects at velocity reversals. On the other hand, if the stiction effects are viewed as a disturbance, the compensated controller corrects very quickly and returns to accurate tracking.

To truly test the tracking ability of the system with friction compensation, a more complex desired path was used. The path chosen contains a step, a ramp and a sinusoidal segment, with discontinuities. The response of the straight PD controller with pole placement at $-10 \pm 10i$ is displayed in figure 7.7; it exhibits steady state error on all segments of the path. The response of the controller with model-based friction compensation is displayed in figure 7.8. The proportional and derivative gains here also correspond to a pole placement of $-10 \pm 10i$. Comparing the results in figures 7.7 and 7.8 confirms that model-based friction compensation reduces the steady state error of a PD controller. However, small errors are present at velocity reversals.
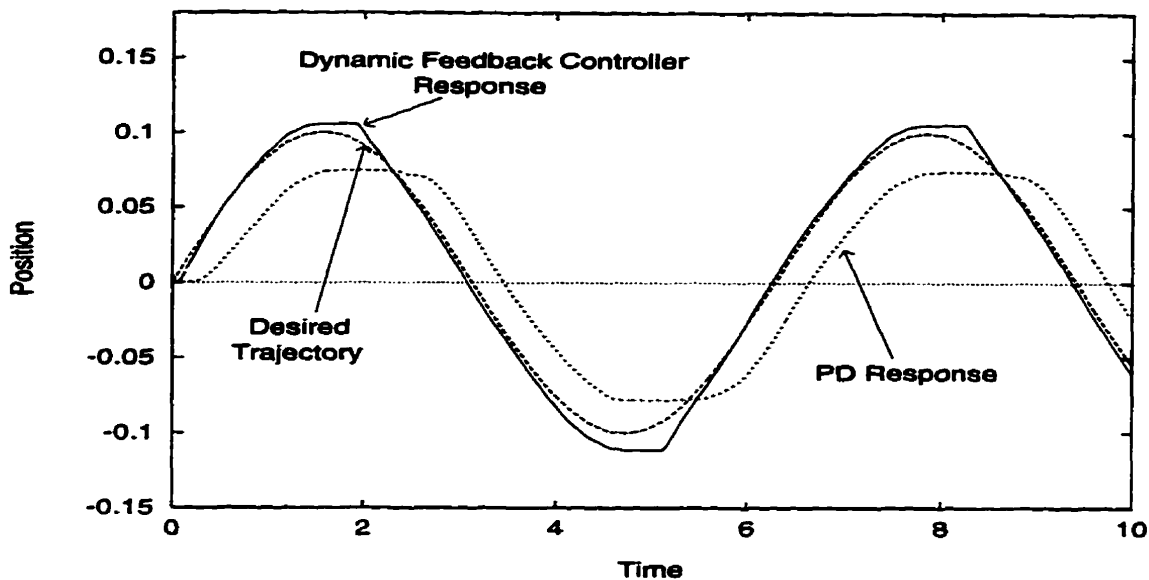
Figure 7.5: Response of both the dynamic feedback controller with friction compensation and a PD controller to $x_d = 0.1sin(t)$ m with poles at $-4 \pm 4i$.

7.5.3 Comparison of New Dynamic Feedback Controller with the C-O-A-L

Comparisons were also made between the new dynamic feedback controller and the C-O-A-L controller from Chapter 6. Figures 7.9, 7.10 and 7.11 display this comparison for $x_d = 10\ cm$, $x_d = 1\ cm$ and $x_d = 0.1sin(t)$ m respectively. It is clear from figure 7.9 that the new dynamic feedback controller responds more quickly than the C-O-A-L. The response of the new controller has slightly larger steady state error, but exhibits none of the hunting that is present in the response of the C-O-A-L controller.

Figure 7.10 shows that for fine positioning, the new dynamic feedback controller shows a marked improvement over the performance than the C-O-A-L. Despite the presence of model-based friction compensation in the C-O-A-L controller, it does not reduce steady state error as effectively as our new controller. In addition, the C-O-A-L response continues to exhibit hunting.

Finally figure 7.11, shows that both controllers track a sinusoidal path with comparable accuracy; the tracking error is slightly smaller using the new controller. There is small error due to stiction effects at velocity reversals in the response of our controller that are not present in the response of the C-O-A-L. However, the response of the C-O-A-L con-
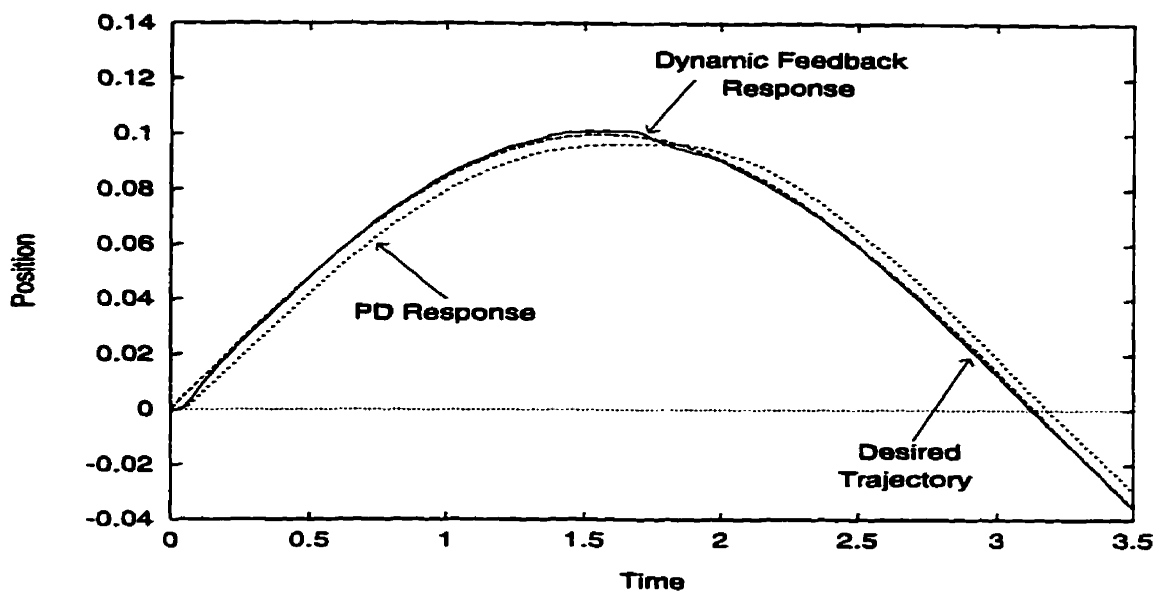
Figure 7.6: Response of both the new dynamic feedback controller with friction compensation and a linear PD to $x_d = 0.1sin(t)$ m with poles at $-10 \pm 10i$.

trolled system exhibits the effects of high gains, including vibration and unsteady motion. The response using our controller does not show this effect.

The freedom to choose small gains for the new controller eliminates the vibration and noise effects present in the C-O-A-L response. With the exception of small static friction effects at velocity reversals, the new dynamic feedback controller clearly performs much better than the C-O-A-L in both high precision positioning and tracking, at least on our test apparatus.

7.5.4 Discussion

Using the new dynamic feedback controller to track a slow path with velocity reversals reveals problems that can arise with this friction compensation scheme. When the cart slows to zero velocity, the observed bristle deflection is non-zero, which is consistent with simulated values for z. However, friction compensation continues to act in the direction of prior motion. A measured change in velocity is needed to alter the value of $\hat{z}$. There are two possible solutions to this problem. The first is to increase the magnitude of $q(e)$ in the friction observer, thereby increasing $\dot{\hat{z}}$ at zero velocity. The second option is to construct a model-based velocity estimate as input to the observer.
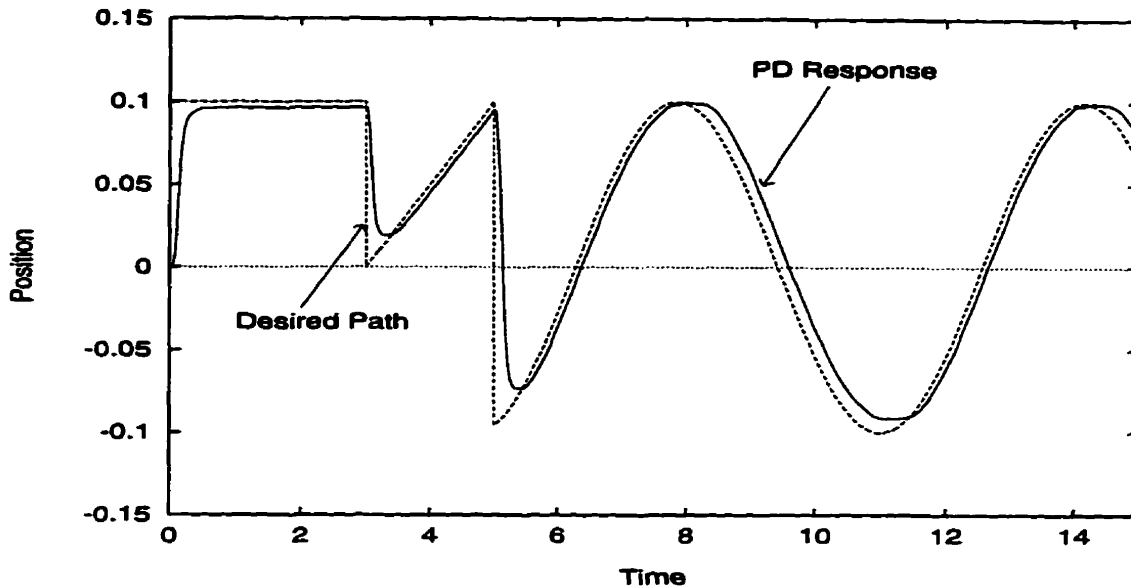
Figure 7.7: Response of a linear PD controller to tracking a discontinuous path x_d with poles at $-10 \pm 10i$

A similar situation arises in fine positioning, as shown in figure 7.4. Once the cart overshoots the reference point and slows, the observer-based friction compensation continues to push it away from the desired position. Proportional feedback must be great enough to counteract this effect for the cart to change directions. The overshoot can be increased by over-compensation for friction with an inexact model. Nevertheless, once the cart comes to rest, the observed bristle deflection is altered only by the term $q(e)$. After a long period of time, $\hat{z}$ will change sign. This can be explained by the fact that the estimation error, $\tilde{z}$, slowly approaches zero. In this case, a high value of $q(e)$ seems appropriate, but the increase of integral action in the controller could lead to hunting.

Static friction effects can be overcome by accurately modeling zero velocity friction forces. In theory, the control law presented here achieves this because friction is modeled as a function of displacement at zero velocity. Simulations show that when the macroscopic motion of the cart is zero, presliding displacement still occurs. Applying a force whose net direction is opposite to that of bristle deflection, will change the value of x_1, and decrease z. When this occurs, x_2 is non-zero, which alters the observed bristle deflection, $\hat{z}$. This, in turn, alters the friction compensation. However, presliding displacement is a very small quantity; our identified bristle model indicates that the bristles deflect to a maximum of
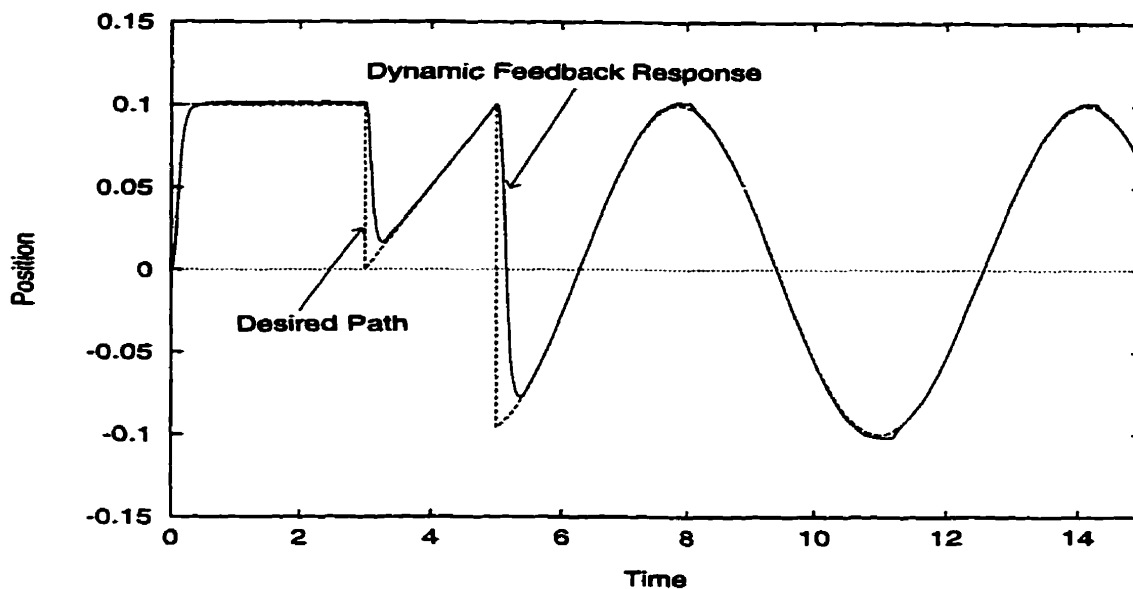
Figure 7.8: Response of the new dynamic feedback controller to tracking a discontinuous path x_d with poles at $-10 \pm 10i$

2.15×10^{-5} m. Some microscopic motion is not detected by the encoders in the real system. Hence there is no measured change in x_2, and no change in observed bristle deflection $\hat{z}$. For a real system, the position and velocity error must be high enough to induce measurable motion via PD feedback, before friction compensation can occur. Constructing an observer for velocity that predicts small position changes could improve the performance.

It should be noted that detecting presliding motion would not completely eliminate the problems associated with direction changes. Tests for presliding displacement, discussed in Chapter 5, showed motion is detected for small applied forces. However, the magnitude of the detected motion is much larger than the maximum bristle deflection. Thus small-scale sliding occurs in the servo system for applied forces less than the identified value for F_S; our model may over-estimate static friction, which can lead to overshoot [8]. In addition, the nonlinear nature of the model makes constructing a stable observer for velocity extremely difficult. For many applications, a small increase in controller gains can reduce the effects of stiction to an acceptable level.

Figure 7.9: A comparison of the responses of the new model-based dynamic feedback control law to the C-O-A-L controller with input $x_d = 10\ cm$. Here the poles for the new controller are at $-10 \pm 10i$ and the gains for the C-O-A-L are $k_1 = 350\ kg/s^2$ and $k_2 = 450\ kg/s$.

Figure 7.10: A comparison of the responses of the new model-based dynamic feedback control law to the C-O-A-L controller with input $x_d = 1\ cm$. Here the poles for the new controller are at $-10 \pm 10i$ and the gains for the C-O-A-L are $k_1 = 350\ kg/s^2$ and $k_2 = 450\ kg/s$.
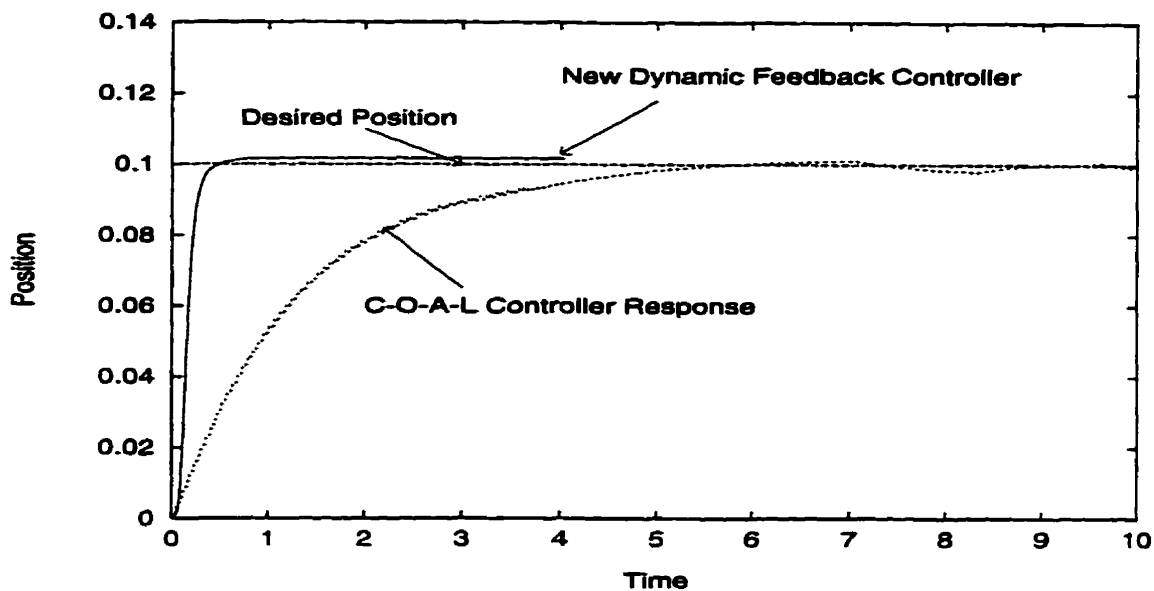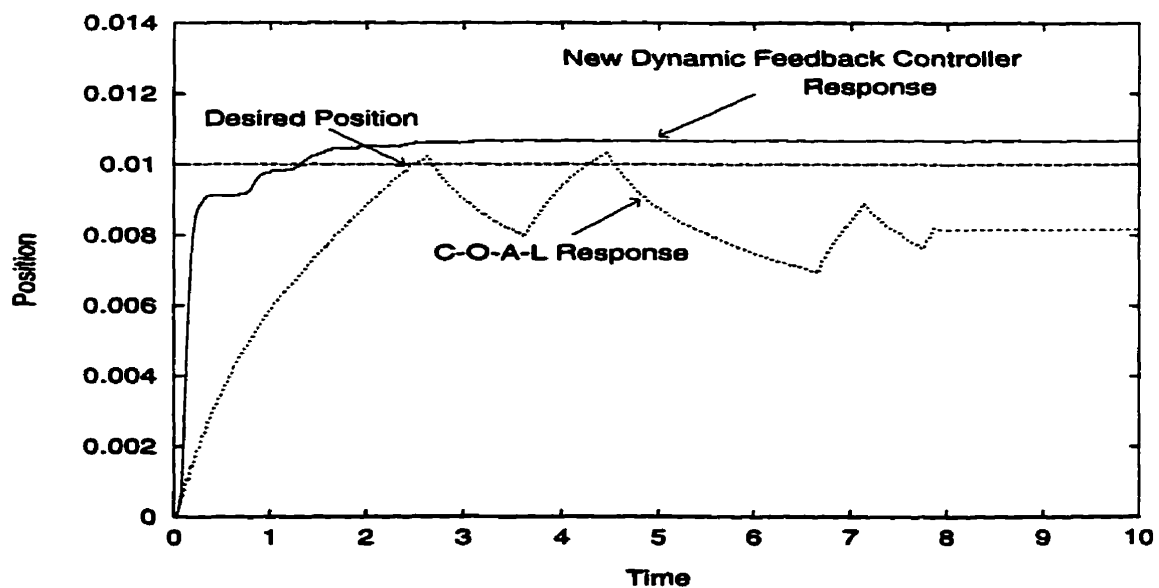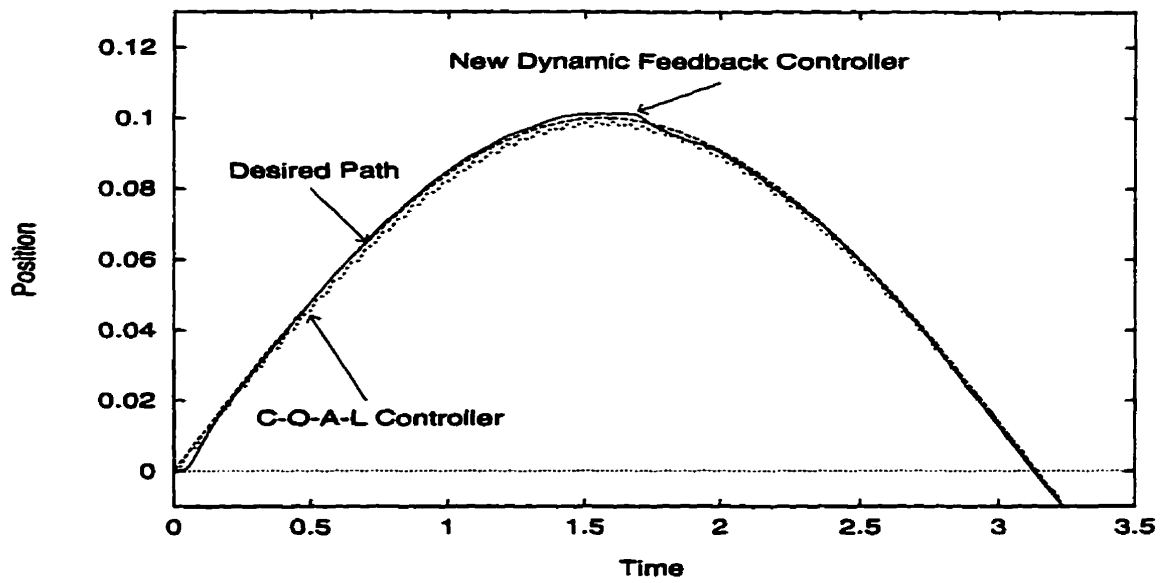
Figure 7.11: A comparison of the responses of the new model-based dynamic feedback control law to the C-O-A-L controller with input $x_d = 0.1sin(t)$ m. Once again, the poles for the new controller are at $-10 \pm 10i$ and the gains for the C-O-A-L are $k_1 = 350$ kg/s^2 and $k_2 = 450$ kg/s.

7.6 Summary

A new dynamic feedback control law has been introduced for the servo motor-cart apparatus. This control law combines proportional and derivative feedback with nonlinear model-based friction compensation using the bristle model of equations (4.1) and (4.2). Compensation is achieved via dynamic output feedback. With this controller, sensible proportional and derivative gains can be used.

The controller developed in this chapter was tested for point-to-point positioning and for low velocity tracking control. The results of these tests were compared to the response of a PD controller with only linear viscous friction included in the system model. Results indicate that the dynamic feedback controller outperforms the simpler PD. The speed of response for positioning is comparable. However, the accuracy improves significantly with the addition of model-based friction compensation. In addition, the dynamic feedback controller shows less need for re-tuning. In tracking control experiments, the PD controller response exhibits steady state error that is not present with model-based friction compensation. The dynamic feedback controller exhibits stiction effects at velocity reversals, which has been attributed to using sensory velocity data to compute the observed bristle deflection.

Finally, the new controller with friction compensation was compared to the C-O-A-L controller of Chapter 6. The accuracy achieved with the new controller is comparable to that of the C-O-A-L, but the response is much faster. The new controller does not induce vibration, which is observed using the C-O-A-L controller, nor does it exhibit hunting. Thus the new dynamic feedback controller is preferable to the C-O-A-L controller.

Chapter 8

Conclusions and Future Work

A study has been conducted to determine whether positioning and tracking control in a servo system can be improved through model-based friction compensation. The performance of two model-based friction compensation controllers was assessed experimentally, and compared to that of a PD feedback controller.

8.1 General Conclusions

The model adopted for friction compensation was the bristle model of equations (4.1) and (4.2), proposed in [7]. This state variable model was identified for our servo-cart system. Experiments and simulation indicate that our model captures known nonlinear friction behaviour. The predicted open-loop response to various inputs was compared to the actual system response. Our nonlinear model was found to reasonably predict the behaviour of the real system.

Both controllers tested are a combination of proportional and derivative feedback and dynamic output feedback friction compensation. The first controller tested was proposed by the authors that developed the bristle model [7]. The second controller was developed as a part of this thesis. The primary difference between the two arises in the nature of the nonlinear dynamic feedback. The C-O-A-L controller includes an observer for the internal state z that is a simple extension of the model for z; the estimated variable, $\hat{z}$, converges to z. However, the requirement that the transfer function between position error and observer error be SPR means that a large derivative gain is needed. The controller developed in Chapter 7 requires a more complex observer, whose state $\hat{z}$ may not converge

to z. However, with this scheme, optimal pole placement is possible.

A PD controller was introduced as a basis of comparison because of the structure of both controllers. Thus both dynamic feedback controllers were tested separately and their performance was compared to that of the PD controller. The C-O-A-L controller of Chapter 6 proved to be more accurate than a PD controller, but slower to respond. Experimental problems arose because of high gain feedback, resulting in an overdamped response, noise amplification, and control saturation. Thus for our servo system, the C-O-A-L controller is not the most practical option. Conversely, the dynamic feedback controller developed in Chapter 7 was found to have a comparable response time to a PD, with significantly increased accuracy for both positioning and tracking problems. It was also noted that adding friction compensation reduces the need for re-tuning that is encountered with PD control.

The two dynamic feedback controllers were also compared to one another. The controller of Chapter 7 responded much more quickly than the C-O-A-L controller, with similar accuracy, but no hunting. Despite the increased complexity of the dynamic feedback, the controller from Chapter 7 exhibits no serious practical problems, other than the requirement that sufficient speed of computation is needed for real-time implementation.

8.2   Future Work

We have determined that our model is not perfect. Some error arises due to asymmetric friction that is not captured by the model. Friction is also non-uniform; it varies with imperfections in the motor and track. Tests for presliding displacement in Chapter 4 indicate that the model may over-estimate static friction. Many of these problems arise due to using steady state data, obtained from motion in only one direction, in the least squares estimation. An adaptive identification method could to significantly improve the model identification. However, it might be useful to try a fixed model whose parameters change for different directions of motion.

It may also be useful to consider separate friction models for different components of the mechanical system and attempt to combine them into a single model. This would indicate how effectively the model captures the total friction in the system.

Other problems encountered arise because of the method used to estimate velocity. Significant noise was present in the velocity signal, despite filtering. A higher order

numerical method for integrating the friction observer could provide a more accurate estimate for bristle deflection and may allow us to reduce the sampling frequency. This could reduce noise in the velocity estimate. Nonetheless, the estimate for bristle deflection, $\hat{z}$, is very sensitive to noise because of its small magnitude and its fast dynamics. There is also a limit to encoder resolution and some small motions are undetected. In this case, the velocity is considered to be zero, and $\hat{z}$ remains constant. The nonlinear nature of the model would make constructing an observer for velocity extremely difficult. However, with such an observer, performance may be improved.

A more sophisticated controller may achieve higher accuracy. For example, it may be worthwhile to test a combination of optimal control and friction compensation.

Finally, the cart-motor servo system is an extremely simple apparatus, which was used so that friction effects could be easily studied. Extending the theory of Chapter 7 to higher order systems would have wider applications. This appears to be a difficult problem, but one worthy of consideration.

Bibliography

[1] Adams, J., Payandeh, S., "Methods for Low-Velocity Friction Compensation: Theory and Experimental Study" *Journal of Robotic Systems*, Vol. 13, No. 6, 1996.

[2] Alici, G., Daniel, R.W., "Static Friction Effects During Hard-on-Hard Contact Tasks and Their Implication for Manipulator Design", *The International Journal of Robotics Research*, Vol. 13, No. 6, Dec. 1996.

[3] Armstrong-Helouvry, B., *Control of Machines with Friction*, Boston, MA: Kluwer, 1991.

[4] Armstrong-Helouvry, B., Dupont, P., Canudas de Wit, C., "A Survey of Models, Analysis Tools and Compensation Methods for the Control of Machines with Friction", *Automatica*, Vol. 7, No. 9, 1994.

[5] Aström, K.J., and Wittenmark, B. *Adaptive Control*, Reading, MA: Addison-Wesley, 1989.

[6] Bona, B., Indri, M., "Force/Position Controlled Manipulators", *IEE Proceedings Control Theory Applications*, Vol. 142, No. 6, Nov. 1995.

[7] Canudas de Wit, C., Olsson, H., Aström, K.J., and Lischinsky, P., "A New Model for Control of Systems with Friction", *IEEE Transactions on Automatic Control*, Vol. 40, No. 3, March 1994.

[8] Canudas de Wit, C., Noél, P., Aubin, A., Brogliato, B., "Adaptive Friction Compensation in Robot Manipulators: Low Velocities", *International Journal of Robotics Research*, Vol. 10, No. 3, June 1991.

[9] Dupont, P.E., "Avoiding Stick-Slip Through PD Control", *IEEE Transactions on Automatic Control*, Vol. 39, No. 5, May 1994.

[10] Garvin, C., Mathew, A. "The Application of the Method of Simultaneous Stabilization to the Control of a Nonlinear Servo Valve", *IEEE Transactions on Control Systems Technology*, Vol. 4, No. 6, Nov. 1996.

[11] Haessig, Friedland, "On the Modeling and Simulation of Friction", *Transactions of the ASME*, Vol. 113, Sept 1991.

[12] Hess, Soom, "Friction as a Lubricated Line Contact Operating as Oscillating Sliding Velocities", *Journal of Tribology*, Vol. 112, Jan. 1990.

[13] Hirschorn, R.M., Miller G.M. "Control of Nonlinear Systems with Friction", *Manuscript for publication*, 1997.

[14] Howe, R.D, Cutosky, M.R., "Practical Force-Motion Models for Sliding Manipulation", *International Journal of Robotics Research*, Vol. 15, no. 6, Dec. 1996.

[15] Iezawa, M., Imagi, A., Tomisawa, M., "High-Precision Control of AC Servo Motor Positioning Systems by Friction Compensation", *JSME International Journal, Series C*, Vol. 39, No. 3. 1996.

[16] Karnopp, D., "Computer Simulation of Stick-Slip Friction in Mechanical Dynamic Systems", *Transactions of the ASME*, Vol. 107, Mar. 1985.

[17] Lee, H.S., Tomizuka, M. "Robust Motion Controller Design for High-Accuracy Positioning Systems", *IEEE Transactions on Industrial Electronics*, Vol. 43, No. 1, Feb 1996.

[18] Li, W. Cheng, X., "Adaptive High-Precision Control of Positioning Tables-Theory and Experiments", *IEEE Transactions on Control Systems Technology*, Vol. 2, No. 3, Sept. 1994.

[19] Perko, L. *Differential Equation and Dynamical Systems*, New York: Springer-Verlag 1993.

[20] Pomet, J.-B., Hirschorn, R.M., and Cebuhar, W., "Dynamic Output Feedback Regulation for a Class of Nonlinear Systems", *Math. Control Signals Systems*, 6:106-125, 1993.

[21] Rachoor, H., Harnoy, A., "Modeling of Dynamic Friction in Lubricated Line Contacts for Precise Motion Control", *Tribology Transactions*, Vol. 6, No. 2, 1996.

[22] Rice, J.R., and Ruina, A.L. "Stability of Stead Frictional Slipping", *Journal of Applied Mechanics*, Vol. 50, June 1983.

[23] Slotine, J.-J.E., Li, W., *Applied Nonlinear Control*, Englewood Cliffs, NJ: Prentice Hall, 1991.

[24] Tataryn, P.D., Sepehri, N. Strong, D., "Experimental Comparison of Some Compensation Techniques for the Control of Manipulators With Stick-Slip Friction", *Control Engineering Practice*, Vol. 4, No. 9, Sept. 1996

[25] Yang, S., Tomizuka, M., "Adaptive Pulse Width Control for Precise Positioning Under the Influence of Stiction and Coulomb Friction", *Journal of Dynamic Systems, Measurement, and Control*, Vol. 110, Sept. 1988.